Durham E-Theses

The scattering of solitons in classes of (1+1) dimensional models

BARON, HELEN,ELIZABETH

The scattering of solitons in classes of (1+1) dimensional models

Helen Elizabeth Baron

A Thesis presented for the degree of
Doctor of Philosophy

Centre for Particle Theory
Department of Mathematical Sciences
University of Durham
England

March 2016

Dedicated to

My patient husband.

The scattering of solitons in classes of (1+1) dimensional models

Helen Elizabeth Baron

Submitted for the degree of Doctor of Philosophy

March 2016

Abstract

We investigate the validity of the collective coordinate approximation to the scattering of two solitons in several classes of (1+1) dimensional field theory models. First we consider the collision of solitons in the integrable NLS model and compare the results of the collective coordinate approximation with results obtained using a full numerical simulation. We find that the approximation is accurate when the solitons are some distance apart and is reasonably good during their interaction.

We then consider a modification of the NLS model with a deformation parameter which changes the integrability properties of the model, either completely or partially (the model becomes quasi-integrable). As the collective coordinate approximation does not allow for the radiation of energy out of a system we pay particular attention to how the approximation fares when the model is quasi-integrable and therefore has asymptotically conserved charges (*i.e.* charges $Q(t)$ for which $Q(t \to -\infty) = Q(t \to \infty)$). We find that the approximation accurately reproduces the physical properties of the solitons, and even their anomalous charges, for a large range of initial values. The only time the approximation is not totally reliable is for the scatterings when the solitons come very close together (within one width of each other).

To determine whether these results hold in a model with topological solitons we then consider a modified sine-Gordon model. The deformation preserves the topology of the model but changes the integrability properties in a similar way

to the modified NLS model. In this model we find that the approximation is accurate when the model is either integrable or quasi-integrable, but the accuracy was much reduced when the model was completely non-integrable.

To further explore this link between the accuracy of the collective coordinate approximation in a modified sine-Gordon model and the integrability properties of the system, we then consider soliton scattering in a double sine-Gordon model. The double sine-Gordon model allows us to vary between two integrable sine-Gordon models, and when the model is not integrable it still possesses the additional symmetries necessary for quasi-integrability. We find that for all values of our deformation parameters the approximation is accurate and that, as expected, the anomalous charges are asymptotically conserved.

Declaration

The work in this thesis is based on research carried out at the Centre for Particle Theory, the Department of Mathematical Sciences, England. No part of this thesis has been submitted elsewhere for any other degree or qualification and it is all my own work unless referenced to the contrary in the text.

Acknowledgements

Contents

List of Figures

Chapter 1

Introduction

In this chapter we give an overview of various concepts which are intrinsic to this work. We discuss the links between integrability and solitons in (1+1) dimensions and briefly outline some useful results that can be obtained in integrable systems. We examine the concept of quasi-integrability and give some motivation for our choice of modified models that we investigate in later chapters. We discuss the collective coordinate approximation and give details on the numerics that we use in our simulations that we present throughout this work. The contents of this chapter are based on the work of others with the necessary references given throughout.

The term 'soliton' can mean various things depending on the context in which it is used. Topological solitons are particle-like solutions of non-linear field theories with a topology which is different from the vacuum. Topological solitons have smooth energy densities which are spatially finite and they are stable due to their topological distinctiveness, *i.e.* they can not simply decay into a topologically trivial field. Associated with topological solitons is an integer topological charge, N, which is the generalised winding number of the field and can be thought of as the particle number (so one soliton has $N = 1$). Examples of topological solitons exist in various dimensions and include kinks, monopoles, vortices and Skyrmions; for a review see [1].

Solitons can be defined in a slightly different sense as special localised solutions

of non-linear evolution equations that maintain their shape and energy as they propagate. They collide without radiating out any energy. The only difference a long time after they interact is a shift in the position of the soliton compared to where it would have been if no interaction had taken place. Non-linear partial differential equations have a sharpening non-linear term and a dispersive term, and the balancing of these terms results in solitons. Soliton solutions occur in integrable systems though commonly people also use the term soliton to refer to soliton-like solutions which can exist in non-integrable systems, as we do later. Topological solitons exist in theories which are generally non-integrable, with the exception of the sine-Gordon model which is an integrable model which possesses topological solitons.

In chapter 2 we present work based on the published paper [2]. Chapters 3 and 4 concern material relating to the preprint [3]. Chapter 5 relates to work that is currently ongoing.

Integrability and solitons

Integrable systems, *i.e.* non-linear differential equations which are exactly solvable, are incredibly important in mathematical physics. Although integrable systems are rare, integrability gives rise to interesting mathematics in many areas, from differential geometry to complex analysis, and there is a wide and varied background of research on integrability. Integrability is also central to many physical systems, for example solitons in integrable systems can be used to model information transfer in optical systems (NLS solitons) [4]; protein folding (sine-Gordon solitons) [5]; and shallow water waves (KdV solitons) [6]. In this work we focus on the behaviour of solitons in integrable (and, later, non-integrable) systems.

Integrable solitons often occur in (1+1) dimensional integrable systems, *i.e.* the equations of motion in these models can be rewritten as a zero curvature condition (also known as the Lax-Zakharov-Shabat equation) [7], [8]. When a system is integrable exact solutions can be constructed via the inverse scattering trans-

form. This was introduced by Gardner et al in 1967 for the KdV equation [9]. From the zero curvature condition an infinite number of conserved quantities can also be found [10], and the interesting behaviour of solitons is a result of these conserved charges constraining the soliton dynamics. The conserved charges can be constructed from the zero curvature condition by implementing the abelianization procedure [11] (also known as the Drinfeld-Sokolov reduction [12]), and we use this procedure to construct these quantities explicitly for the non-linear Schrödinger equation in chapter 2.

Quasi-integrability

While integrable systems possess interesting solutions and can be analysed using various mathematical techniques, most physical phenomena are well described by systems that are not integrable. However, lots of physical systems do demonstrate similar characteristics to integrable systems, such as soliton like solutions which preserve their physical properties when they interact. For example, in the scattering of particles at hight energies at CERN the elastic cross sections correspond to about 20% of the total cross section which is surprising considering the amount of energy available for the production of particles. But considered in terms of simple mathematical solitonic models particle production is described by energy radiation so this lack of particle production could be related to the almost integrability of the system. These observations have led to the development of the concept of 'quasi-integrability' [13] - [17]. Equations of motion in quasi-integrable systems can be rewritten in terms of an anomalous zero curvature connection. We demonstrate this explicitly in the case of a modified NLS model in chapter 3. This leads to solitons with an infinite number of charges $Q(t)$ which do vary in time but are the same a long time before and after any interaction, *i.e.* they possess an infinite number of asymptotically conserved charges $Q(t = -\infty) = Q(t = \infty)$. However, unlike in the integrable theories, the possession of these characteristics was shown to be dependent on the field configurations and only configurations with additional symmetries demonstrated these integrability-like properties. It was found

that these charges are asymptotically conserved in the scattering of two-soliton configurations when the fields are eigenstates of the space-time reflection around a point for some choice of (x_Δ, t_Δ), given by

$$P: \quad (\tilde{x}, \tilde{t}) \rightarrow (-\tilde{x}, -\tilde{t}), \qquad \text{with} \quad \tilde{x} = x - x_\Delta \;\; \text{and} \;\; \tilde{t} = t - t_\Delta. \quad (1.2.1)$$

The collective coordinate approximation

The idea of using collective coordinates to describe the main features of the scattering of solitons and other extended structures is quite old. An early work in this area was performed by Thiele [18] who suggested an equation which describes the dynamics of solitons. This was further generalised by Tretiakov and others [19] to a larger systems of variables (see also a recent paper [20] which uses such an approach to discuss perturbed NLS equations). In our work we use the approach of Manton [1], [21], which can be used to model the dynamics of solitons in a wide variety of systems and generally reproduces the results of the full simulations in such systems with good accuracy. Any collective coordinate approach reduces an infinite-dimensional problem to a finite dimensional system described by a set of ODEs and so is much quicker to implement than a full numerical simulation. However, the important issue here involves choosing the variables that describe, as accurately as possible, the full problem (see for example [22]). The main observation that helps here is the realisation that for a system that possesses free parameters a slow change of these parameters has only a minimal effect on the total energy of the full system and so may be a good approximation to its slow dynamics. Thus one starts with a static solution $\psi(x, q_1, ..., q_n)$. The energy of this solution is independent of the parameters but changing the field configuration can only increase the energy, so in the field space there are low energy valleys in the direction of the parameters of the solution. Consider now moving solitons. For small velocities of the solitons the motion requires the least amount of energy to move along the valleys described by the parameters of the static solution (as then the increase of the energy is only due to the kinetic energy associated with this change which, for very slow changes, is very small). Therefore, it makes

sense to approximate the dynamics of slow moving solitons by allowing these parameters to vary in time, *i.e.* $q_i = q_i(t)$, and assume that these parameters describe most of the solitons' dynamics.

The collective coordinate approximation is similar to the moduli space approximation [23]. The moduli space approximation requires theories to have a moduli space of exact multi-soliton static solutions. The low energy dynamics of the solitons is then assumed to be geodesic motion on the moduli space. The coordinates which span the moduli space are generally referred to as the collective coordinates.

The collective coordinate approximation neglects other modifications of the fields and, in particular, all radiative corrections to the solitons and so is valid only for very slow motions and when the solitons are well separated. When solitons interact with each other the approximation becomes less accurate as some radiation may be sent out and the solitons are mutually distorted. However, for many field theories of interest the radiative corrections are small and the collective coordinate approximation is a useful tool which has been studied in detail in many papers (see [24], [25] for the study of the sine-Gordon case).

To describe the dynamics of the collective coordinates we proceed as follows [1]. We start with an approximation ansatz whose form is based on the stationary solution with a suitable choice of parameters which become collective coordinates $q_i(t)$; these coordinates generally describe physical properties of the soliton such as position, height, *etc.* This ansatz is then substituted into the Lagrangian density of the system and the relevant spatial degrees of freedom (in our case x) are integrated out to obtain an effective Lagrangian for the collective coordinates. From the effective Lagrangian a coupled system of ODEs for the coordinates can be derived. Solving these ODEs describes the time evolution of the coordinates, which in turn tells us how the field evolves in time. In some cases, and sometimes with further simplifying assumptions, the equations of motion for the collective coordinates can be solved analytically; such is the case in [26]. In our work the equations of motion need to be solved numerically and for this we use a 4th order Runge-Kutta method.

General comments on the numerical approach

The work described in these chapters involves several different numerical techniques. They include performing 'full numerical simulations' and the calculations involving the collective coordinates. The two approaches are then compared to each other to assess the validity of the collective coordinate approximations.

There are many different numerical methods available for evolving nonlinear PDEs, each with their own advantages and disadvantages (a review of the various methods can be found here [27]). Symplectic methods preserve the invariant of a system, such as its energy and momentum, and have been shown to be effective for long time simulations [28] though it can be computationally expensive. The Runge-Kutta method is another numerical method which is often used to solve nonlinear PDEs, and because it does not specifically preserve the energy of a system it means that the conservation of energy during a simulation can be used as a check on the numerics. Throughout this work we use a 4th order Runge-Kutta method of simulating the time evolution. We chose this method as it has previously been successfully used to simulate solitons in [16] and [17], and because it is suitably efficient and accurate for our simulations. We were able to use the energy conservation as a check of our numerics and found that in the NLS case there is no change of energy at all during the simulations.

For the full simulations the implementations are different in the two classes of models (NLS and sine-Gordon) as the NLS equation involves only first derivatives with respect to time and the phase of the complex field ψ performs fast rotations with the increase of time, while the modified sine-Gordon model involves only a nonlinear wave motion.

Thus, in the NLS case we choose to perform the simulation in a rotating frame (*i.e.* we go to the frame in which the phase rotation involves only the additional dynamical variation relative to this global rotation). The global rotation is calculated at each value of time and the equation is transformed to that frame. Therefore, in this frame, the further phase variation is small and it is only due to the dynamics of the system of solitons. Consequently, for a given time and

position steps of the program, the changes of the derivatives of ψ are kept small.

Our approach is a standard procedure for such fields and more discussion of its use in the NLS case can be found in [16] where it is shown that it has worked very well in this case. The numerical errors are negligible and the results of our simulations are essentially the same when we tested the method by varying a little the parameters of our numerical approach. To obtain reliable simulations we experiment by using various lattice sizes, various numbers of points *etc.* until we are satisfied that we can 'trust' our results; *i.e.* when the numerical errors are very small and so are insignificant.

Then we perform many simulations as described in this work. In fact, most of the results we present here have been obtained on a lattice involving $N = 5001$ grid points with lattice spacing $dx = 0.01$. As in [16] the initial configurations involve two one soliton fields, with solitons placed at $x = \pm x_0$ (as discussed in chapter 2) and with the fields tied together at $x = 0$. Luckily, at small values of x the values of the fields are very close to each other and so the numerical errors due to this joining procedure are negligible (in fact we even smooth the fields there over 3 lattice points).

For our calculations, as the equations are first order in time derivative, we have to take a small time step. We have varied this too and found that we can trust our results when $dt = 0.00002$ or smaller. Most of our results that we report in this work are obtained with this value of dt. To determine whether the solution is stable for this value of dt we calculated a linearised stability bound for the NLS equation (*i.e.* treating the nonlinearity part of the NLS equation as a constant) for a 4th order Runge-Kutta method with our boundary conditions, as in [29], and find that we need $\frac{dt}{dx^2} < \frac{3\sqrt{2}}{8}$ to ensure stability. For our chosen values of dt and dx we are satisfied that the solution is stable.

In the modified sine-Gordon model the equations are of the wave type and so the numerical calculations are simpler than in the NLS case. We use the fixed boundary conditions with $N = 10001$ points, with the lattice spacing $dx = 0.01$ and $dt = 0.0001$. We absorb the energy at the boundaries by multiplying the fields there by a constant which varies from 1 to 0.9 over 10 points (with the

constant being 1 in the centre and 0.9 near the edge). This absorption makes very little difference because almost no energy ever reaches the boundaries as the scatterings are very elastic.

In the collective coordinate approximation the ODEs are solved numerically with $dt = 0.005$, (the simulations were also run with various values of dt to find a value for which the simulations are efficient and the results are accurate, and we are satisfied with the accuracy of the results using the values mentioned above).

In the modified models that we investigate we are required to integrate the effective Lagrangian density over x in order to obtain the effective Lagrangian, but in the integrable NLS model we were able to integrate the effective Lagrangian analytically using the residue theorem. This allowed us to check our numerical integration in the limiting case of the modified NLS where it reduces to the integrable NLS (*i.e.* when $\epsilon = 0$) by comparing our numerical integrations with the integrations performed analytically, and we were satisfied with the accuracy of the numerical integration for our chosen value of $dx = 0.01$. In the double sine-Gordon model that we consider the two deformation parameters, A_0 and λ_0, change the steepness of the fields, and we choose our values of dx for each simulation based on the values of A_0 and λ_0 by considering the initial soliton configuration.

Chapter 2

The nonlinear Schrödinger model

The nonlinear Schrödinger equation (NLS) is an important model in mathematical physics, with applications in many fields which includes nonlinear optics, plasma physics, biophysics and Bose-Einstein condensates (BECs) [30], [31], [32]. Interactions between NLS solitons are particularly important; for example in soliton-based optical communications the NLS equation describes information transfer in optical fibres [33], and soliton interactions fundamentally limit the capacity of these communication systems [34].

As the NLS equation is integrable its exact soliton solutions can be found analytically via the inverse scattering transform [8] (see *e.g.* [35]). However, given the rather involved nature of this approach, the complicated form of these solutions and the fact that they hold only for the exact form of the NLS equation it is useful to look at other approaches to this problem. This is particularly true if one wants to get a 'physical feeling' about the forces governing the scattering of solitons *i.e.* to see whether they are attractive or repulsive, how they depend on the various parameters of the solutions and how they respond to small perturbations of these solutions or the equation itself.

Hence, the equation has also been studied numerically [36] - [39] and an attempt has been made to introduce a collective coordinate approximation to a two soliton field configuration [26]. Several other papers have also looked at NLS solitons perturbed by external fields or in interaction with them [40], [41], [42], [22]

but though very interesting, these papers have not approximated the dynamics of the system of solitons by a full Lagrangian based collective coordinate model [23], which has recently been shown [1], [24], [43] (in relativistic models) to be a very good approximation for the investigation of soliton dynamics.

In their paper Zou and Yan [26] consider the scattering of two solitons in the NLS model. As this paper does not present many explicit results we have modified its approach a little and have looked at the interaction of two solitons in some detail. We have found that the collective coordinate approach, which is expected to describe the properties of the solitons when they are far apart from each other, works quite well even when the solitons are close together and so may be a somewhat unexpectedly good approximation to the description of the two soliton scattering at all times. Thus this chapter discusses this approximation and its validity for the integrable NLS model in (1+1) dimensions.

NLS model

The non-relativistic Lagrangian describing the dynamics of the NLS field $\psi(t, x)$ and its complex conjugate $\psi^*(t, x)$ is given by

$$\mathcal{L} = \int dx \, \frac{i}{2} \left(\psi^* \partial_t \psi - \psi \partial_t \psi^* \right) - \partial_x \psi^* \partial_x \psi - V \left(|\psi|^2 \right), \qquad (2.1.1)$$

with the NLS potential $V = V_{NLS} = \eta |\psi|^4$. Variation of this Lagrangian with respect to $\psi^*(t, x)$ gives us

$$i\partial_t \psi = -\partial_x^2 \psi + 2\eta |\psi|^2 \psi, \qquad (2.1.2)$$

which is the NLS equation for $\psi(t, x)$ (variation of the Lagrangian with respect to $\psi(t, x)$ gives the complex conjugate of (2.1.2) which is the NLS equation for $\psi^*(t, x)$).

Solutions to (2.1.2) with boundary conditions $|\psi|_{x=-\infty} = |\psi|_{x=\infty}$; $\partial_x \psi \to 0$ as $x \to \pm\infty$ have conserved Noether charges as a result of the symmetries of the action.

Thus the invariance of the action under time translations gives the energy conservation:

$$E = \int_{-\infty}^{\infty} dx \, \left(|\partial_x \psi|^2 + \eta |\psi|^4 \right). \tag{2.1.3}$$

Conservation of momentum results from the invariance of the action under space translations:

$$P = i \int_{-\infty}^{+\infty} dx \, \left(\psi^* \partial_x \psi - \psi \partial_x \psi^* \right). \tag{2.1.4}$$

And, finally, the internal $U(1)$ symmetry of the action, $\psi \to e^{i\alpha} \psi$ for a constant α, gives the conservation of the normalisation

$$N = \int_{-\infty}^{+\infty} dx \, |\psi|^2. \tag{2.1.5}$$

As is well known for $\eta < 0$, (2.1.2) has the one soliton solution (called 'bright soliton')

$$\psi = \frac{b}{\sqrt{|\eta|} \cosh \left[b \left(x - vt - x_0 \right) \right]} e^{i \left[\left(b^2 - \frac{v^2}{4} \right) t + \frac{v}{2} x \right]}, \tag{2.1.6}$$

where b, v and x_0 are real parameters of the solution. This solution is clearly defined up to an overall constant phase due to the $U(1)$ symmetry of (2.1.1). It describes a soliton moving with velocity v, which at $t = 0$ is positioned at x_0. The parameter b, which describes the 'height' and 'width' of the soliton, is related to N and so is, in fact, fixed.

Similarly, for $\eta > 0$ there exists the one soliton solution (called 'dark soliton')

$$\psi = \frac{b}{\sqrt{|\eta|}} \tanh \left[b \left(x - vt - x_0 \right) \right] e^{i \left[\frac{v}{2} x - \left(2b^2 + \frac{v^2}{4} \right) t \right]}. \tag{2.1.7}$$

Conserved charges for NLS

Here we demonstrate the construction of an infinite number of conserved quantities in the integrable NLS model, following the abelianization procedure used in [16].

The NLS equation of motion in (1+1) dimensions is given by (2.1.2). As this model is integrable the equation of motion can be expressed as a zero curvature

condition of the form

$$\partial_t A_x - \partial_x A_t + [A_x, A_t] = 0, \tag{2.2.1}$$

where the connection A_μ is given by

$$
\begin{aligned}
A_x &= -iT_3^1 + \gamma^* \psi^* T_+^0 + \gamma \psi T_-^0, \tag{2.2.2}\\
A_t &= iT_3^2 + i\frac{\delta V}{\delta |\psi|^2} T_3^0 - \left(\gamma^* \psi^* T_+^1 + \gamma \psi T_-^1\right) - i\left(\gamma^* \partial_x \psi^* T_+^0 - \gamma \partial_x \psi T_-^0\right),
\end{aligned}
$$

where the parameter γ is defined to be

$$\gamma = i\,\sigma\,\sqrt{|\eta|}\,e^{i\theta}, \qquad \text{with} \ \ \sigma = \text{sign}\,\eta \ \ \text{and} \ \ \theta \in \mathbb{R} \ \ \text{so} \ \ \gamma\gamma^* = \eta, \tag{2.2.3}$$

and T_j^n, $j = 3, +, -$ and $n = 0, 1, 2, ...,$ are generators which satisfy the $SL(2)$ loop algebra commutation relations

$$\left[T_3^m, T_\pm^n\right] = \pm T_\pm^{m+n}; \qquad \left[T_+^m, T_-^n\right] = 2T_3^{m+n}. \tag{2.2.4}$$

This can be represented by the finite $SL(2)$ loop algebra generators $T_j^n \equiv \lambda^n T_j$ where λ is the spectral parameter.

Thus the curvature is given by

$$
\begin{aligned}
\partial_t A_x - \partial_x A_t + [A_x, A_t] &= XT_3^0 \tag{2.2.5}\\
&+ i\,\gamma^* \left(-i\partial_t \psi^* + \partial_x^2 \psi^* - \psi^* \frac{\delta V}{\delta |\psi|^2}\right) T_+^0 \\
&- i\,\gamma \left(i\partial_t \psi + \partial_x^2 \psi - \psi \frac{\delta V}{\delta |\psi|^2}\right) T_-^0,
\end{aligned}
$$

where X is given by

$$X \equiv -i\partial_x \left(\frac{\delta V}{\delta |\psi|^2} - 2\eta\,|\psi|^2\right). \tag{2.2.6}$$

When the equations of motion (2.1.2) are satisfied the parts proportional to T_+^0 and T_-^0 vanish, and when the potential is taken to be the NLS potential V_{NLS} then X also vanishes. When both of these conditions are met then the curvature is equal to zero, and this vanishing of the curvature makes the NLS equation integrable.

In order to implement the abelianization procedure we first rewrite the wave function in terms of its modulus and phase

$$\psi \equiv \sqrt{R}e^{i\frac{\varphi}{2}}. \tag{2.2.7}$$

And we use a new basis of the $SL(2)$ loop algebra defined as

$$b_n = T_3^n, \qquad F_1^n = \frac{\sigma}{2}\left(T_+^n - T_-^n\right), \qquad F_2^n = \frac{\sigma}{2}\left(T_+^n + T_-^n\right), \qquad (2.2.8)$$

with commutation relations

$$[b_m, b_n] = 0; \qquad [b_n, F_1^m] = F_2^{n+m}; \qquad [b_n, F_2^m] = F_1^{n+m}; \qquad [F_1^n, F_2^m] = \sigma b_{n+m}. \qquad (2.2.9)$$

This basis splits the $SL(2)$ loop algebra $\mathcal{G}$ into the kernel and image of its adjoint action, with b_n a basis of the kernel and F_i^n, $i = 1, 2$, a basis of the image.

We perform the gauge transformation

$$A_\mu \to \tilde{A}_\mu \equiv \tilde{g}\, A_\mu\, \tilde{g}^{-1} + \partial_\mu \tilde{g}\, \tilde{g}^{-1}; \qquad \text{with} \quad \tilde{g} = e^{i\left(\frac{\varphi}{2} + \phi\right) b_0}, \qquad (2.2.10)$$

so the connection becomes

$$\partial_t \tilde{A}_x - \partial_x \tilde{A}_t + \left[\tilde{A}_x, \tilde{A}_t\right] = 0, \qquad (2.2.11)$$

with components

$$\begin{aligned}
\tilde{A}_x &= -i\, b_1 + \frac{i}{2}\, \partial_x \varphi\, b_0 - 2\, i\, \sqrt{|\eta|}\, \sqrt{R}\, F_1^0, \qquad &(2.2.12)\\
\tilde{A}_t &= i\, b_2 + \frac{i}{2}\, \partial_t \varphi\, b_0 + i\, \frac{\delta V}{\delta R}\, b_0 + 2\, i\, \sqrt{|\eta|}\, \sqrt{R}\, F_1^1 \\
&+ \sqrt{|\eta|}\, \sqrt{R}\, \left(-\frac{\partial_x R}{R}\, F_2^0 + i\, \partial_x \varphi\, F_1^0\right). \qquad &(2.2.13)
\end{aligned}$$

Now we perform the usual abelianization technique [11], [12], [15], by performing a further gauge transformation

$$\tilde{A}_\mu \to a_\mu = g\, \tilde{A}_\mu\, g^{-1} + \partial_\mu g\, g^{-1}; \qquad \text{with} \quad g = exp\left(\sum_{n=1}^{\infty} \mathcal{F}^{(-n)}\right), \qquad (2.2.14)$$

where

$$\mathcal{F}^{(-n)} \equiv \zeta_1^{(-n)}\, F_1^{-n} + \zeta_2^{(-n)}\, F_2^{-n}. \qquad (2.2.15)$$

The parameters $\zeta_{1,2}^{(-n)}$ are chosen such that a_x and a_t are rotated into an abelian subalgebra spanned by the generators b_n, as we will discuss below. Now we define the grading operator d as

$$d \equiv \lambda \frac{d}{d\lambda}, \qquad [d, b_n] = n\, b_n, \qquad [d, F_j^n] = n\, F_j^n. \qquad (2.2.16)$$

The generators in $\tilde{A}_x$ are grade 0 and 1, and the gauge transformation (2.2.14) is an exponential of negative grade operators, so the a_x component has grades ranging from 0 to $-\infty$. We can expand a_x in terms of its eigen-subspaces under the grading operator: $a_x = \sum_{n=-1}^{\infty} a_x^{(-n)}$, to get

$$a_x^{(1)} = -i\,b_1, \tag{2.2.17}$$

$$a_x^{(0)} = i\left[b_1\,,\,\mathcal{F}^{(-1)}\right] + \tilde{A}_x^{(0)},$$

$$a_x^{(-1)} = i\left[b_1\,,\,\mathcal{F}^{(-2)}\right] + \left[\mathcal{F}^{(-1)},\,\tilde{A}_x^{(0)}\right] - \frac{i}{2!}\left[\mathcal{F}^{(-1)},\,\left[\mathcal{F}^{(-1)},\,b_1\right]\right]$$

$$+ \partial_x\mathcal{F}^{(-1)},$$

$$a_x^{(-2)} = i\left[b_1\,,\,\mathcal{F}^{(-3)}\right] + \left[\mathcal{F}^{(-2)},\,\tilde{A}_x^{(0)}\right] - \frac{i}{2!}\left[\mathcal{F}^{(-2)},\,\left[\mathcal{F}^{(-1)},\,b_1\right]\right]$$

$$- \frac{i}{2!}\left[\mathcal{F}^{(-1)},\,\left[\mathcal{F}^{(-2)},\,b_1\right]\right] + \frac{1}{2!}\left[\mathcal{F}^{(-1)},\,\left[\mathcal{F}^{(-1)},\,\tilde{A}_x^{(0)}\right]\right]$$

$$- \frac{i}{3!}\left[\mathcal{F}^{(-1)},\,\left[\mathcal{F}^{(-1)},\,\left[\mathcal{F}^{(-1)},\,b_1\right]\right]\right] + \partial_x\mathcal{F}^{(-2)}$$

$$+ \frac{1}{2!}\left[\mathcal{F}^{(-1)},\,\partial_x\mathcal{F}^{(-1)}\right],$$

$$\vdots$$

where $\tilde{A}_x^{(0)} = \frac{i}{2}\,\partial_x\varphi\,b_0 - 2\,i\,\sqrt{|\eta|}\,\sqrt{R}\,F_1^0$ is the part of $\tilde{A}_x$ with grade zero operators.

Notice that $\mathcal{F}^{(-n)}$ first appears in the expansion of a_x in the a_x^{-n+1} component and in the form $\left[b_1\,,\,\mathcal{F}^{(-n)}\right]$. So the parameters $\zeta_{1,2}^{(-n)}$ can be chosen to cancel the image component of a_x^{-n+1} and this can be done recursively, therefore with appropriately chosen parameters (see appendix A.1.1 for the first few explicit expressions of $\zeta_{1,2}^{(-n)}$) the gauge transformation (2.2.14) can rotate the a_x component of the connection into the abelian subalgebra generated by the b_n's, *i.e.*

$$a_x = -i\,b_1 + \sum_{n=0}^{\infty} a_x^{(3,-n)}\,b_{-n}, \tag{2.2.18}$$

with the first few components of $a_x^{(3,-n)}$ given in appendix A.1.1.

$\tilde{A}_x$ depends on the fields R and $\partial_x\varphi$, so the components $a_x^{(3,-n)}$ are polynomials of these fields and their x derivatives and have no dependence on the potential V. $\tilde{A}_t$ depends on V, and for the NLS potential $V = V_{NLS}$ the gauge transformation (2.2.14), with the parameters $\zeta_{1,2}^{-n}$ we have determined, rotates $\tilde{A}_t$ into the abelian

subalgebra spanned by b_n, *i.e.*

$$a_t = i \, b_2 + \sum_{n=0}^{\infty} a_t^{(3,-n)} \, b_{-n}, \tag{2.2.19}$$

with the first few components of $a_t^{(3,-n)}$ given in appendix A.1.1.

Now it is clear that this gauge transformation gives

$$\partial_t a_x^{(3,-n)} - \partial_x a_t^{(3,-n)} = 0; \qquad n = 0, 1, 2, \dots \tag{2.2.20}$$

Integrating this over space gives us

$$\int_{-\infty}^{\infty} dx \, \partial_t a_x^{(3,-n)} - a_t^{(3,-n)}(x = \infty) + a_t^{(3,-n)}(x = -\infty) = 0; \qquad n = 0, 1, 2, \dots \tag{2.2.21}$$

and if $a_t^{(3,-n)}$ satisfies the boundary condition $a_t^{(3,-n)}(x = \infty) = a_t^{(3,-n)}(x = -\infty)$ then we have an infinite number of charges

$$Q^{(n)} = \int_{-\infty}^{\infty} dx \, a_x^{(3,-n)}, \tag{2.2.22}$$

and these charges are conserved, *i.e.*

$$\frac{dQ^{(n)}}{dt} = 0. \tag{2.2.23}$$

The two-soliton configuration for NLS

Here we construct a set of collective coordinates for the study of the scattering of two solitons in the NLS equation with $\eta = -1$. In the NLS case there exists an explicit expression for the two moving solitons. However, this expression is not very transparent and when the solitons are far apart it reduces to the superposition approximation ansatz which we detail below. Moreover, when we go beyond the pure NLS model (*i.e.* when we modify it slightly) we do not have explicit expressions for two solitons and we are obliged to start by constructing a sensible approximation ansatz, so our work also involves a check for the suitability of our approximation ansatz.

The motivations for our approximation ansatz is the observation that when the solitons are far away from each other each one of them is well described by the one soliton solution (2.1.6). The overlap between them is very small so we take the two soliton field in the form of a superposition of two independent solitons *i.e.* we take

$$\psi = \psi_1 + \psi_2. \tag{2.3.1}$$

Where ψ_1 and ψ_2 are solutions of (2.1.2) when they are far apart. Following from Zou and Yan, [26], we assume that the two solitons are of equal height, constant width, and move symmetrically around their centre of mass. So we take $\psi_1 = \varphi_1 e^{-i\theta_1}$ and $\psi_2 = \varphi_2 e^{i\theta_2}$ where

$$\varphi_1 = \frac{a(t)}{\cosh\left(b(x + \xi(t))\right)}, \qquad \theta_1 = \mu(t)\left(x + \xi(t)\right) - b^2 t - \lambda(t) - \delta_1, \tag{2.3.2}$$

$$\varphi_2 = \frac{a(t)}{\cosh\left(b(x - \xi(t))\right)}, \qquad \theta_2 = \mu(t)\left(x - \xi(t)\right) + b^2 t + \lambda(t) + \delta_2,$$

and then treat $a(t)$, $\xi(t)$, $\mu(t)$ and $\lambda(t)$ as our collective coordinates.

When $|\xi| \to \infty$ this approximation ansatz models two one solitons with positions $\pm\xi$, heights a, width parameter b, velocities $\pm v = \pm\frac{\mu}{2}$, phase parameter λ and relative phase $\delta = \delta_2 - \delta_1$. This can be seen in figure 2.1 where we present a plot of $|\psi|^2 \equiv |\psi_1 + \psi_2|^2$ at $t = 0$ with $\xi = 10$, $a = 1$, $b = 1$, $v = 0.05$, $\lambda = 0$ and $\delta_1 = \delta_2 = 0$.

Effective Lagrangian for our collective coordinates for NLS

To construct the effective Lagrangian for our collective coordinates we put our approximation ansatz (2.3.1) into our Lagrangian (2.1.1), this yields an effective Lagrangian density which can be written in terms of the non-interacting part $\mathcal{L}_0$ and the interacting part $\mathcal{L}_{12}$.
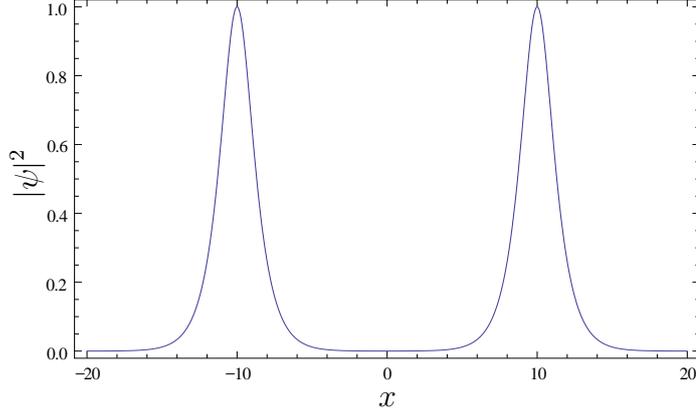
Figure 2.1: Plot of $|\psi|^2$ against x, for ψ the 2-soliton approximation of the NLS model.

Introducing $\omega_1 \equiv x + \xi$ and $\omega_2 \equiv x - \xi$, the non-interacting part becomes

$$
\begin{aligned}
\mathcal{L}_0 &= a^2 \left(\mu \dot{\xi} - b^2 - \dot{\lambda} - \mu^2 \right) \left(\frac{1}{\cosh^2(b\omega_1)} + \frac{1}{\cosh^2(b\omega_2)} \right) \\
&\quad - a^2 b^2 \left(\frac{\tanh^2(b\omega_1)}{\cosh^2(b\omega_1)} + \frac{\tanh^2(b\omega_2)}{\cosh^2(b\omega_2)} \right) \\
&\quad + a^4 \left(\frac{1}{\cosh^4(b\omega_1)} + \frac{1}{\cosh^4(b\omega_2)} \right) + a^2 \dot{\mu} \left(\frac{\omega_1}{\cosh^2(b\omega_1)} - \frac{\omega_2}{\cosh^2(b\omega_2)} \right),
\end{aligned}
\tag{2.3.3}
$$

where dot denotes the differential with respect to time. Integrating this over all space gives us the effective Lagrangian of free solitons

$$
L_0 = \frac{4a^2 \mu \dot{\xi}}{b} - \frac{16a^2 b}{3} - \frac{4a^2 \mu^2}{b} - \frac{4a^2 \dot{\lambda}}{b} + \frac{8a^4}{3b}.
\tag{2.3.4}
$$

Defining $\delta = \delta_2 - \delta_1$ and $\theta_1 + \theta_2 = \Delta$ and noting that $\Delta = 2\mu x + \delta$, the interacting Lagrangian density becomes

$$
\begin{aligned}
\mathcal{L}_{12} &= -a^2 b \left(\dot{\xi} + 2\mu \right) \left(\frac{\sinh(b\omega_1)}{\cosh(b\omega_2)\cosh^2(b\omega_1)} + \frac{\sinh(b\omega_2)}{\cosh(b\omega_1)\cosh^2(b\omega_2)} \right) \sin \Delta \\
&\quad + 2a^2 \left(\mu^2 + \dot{\mu}\xi + \mu\dot{\xi} - b^2 - \dot{\lambda} \right) \frac{\cos \Delta}{\cosh(b\omega_1)\cosh(b\omega_2)} \\
&\quad - 2a^2 b^2 \frac{\sinh(b\omega_1)\sinh(b\omega_2)}{\cosh^2(b\omega_1)\cosh^2(b\omega_2)} \cos \Delta \\
&\quad + 4a^4 \left(\frac{1}{\cosh^3(b\omega_1)\cosh(b\omega_2)} + \frac{1}{\cosh^3(b\omega_2)\cosh(b\omega_1)} \right) \cos \Delta \\
&\quad + \frac{2a^4}{\cosh^2(b\omega_1)\cosh^2(b\omega_2)} \cos(2\Delta) + \frac{4a^4}{\cosh^2(b\omega_1)\cosh^2(b\omega_2)},
\end{aligned}
\tag{2.3.5}
$$

which, when integrated over space, and after some rearranging yields

$$
\begin{aligned}
L_{12} \;=\;& \left(\dot{\mu}\xi - \mu^2 - \dot{\lambda} + \frac{4a^2\mu^2}{b^2} \right) \frac{4\pi a^2 \sin(2\mu\xi)\cos(\delta)}{b\sinh(\frac{\pi\mu}{b})\sinh(2b\xi)} \\
&+ \left(1 - \frac{2a^2}{b^2} \right) \frac{8\pi a^2 b \sin(2\mu\xi)\cos(\delta)}{\sinh(\frac{\pi\mu}{b})\sinh^3(2b\xi)} + 32a^4\xi\frac{\cosh(2b\xi)}{\sinh^3(2b\xi)} \\
&+ \left(\frac{2a^2}{b^2} - 1 \right) \frac{8\pi\mu a^2 \cos(2\mu\xi)\cosh(2b\xi)\cos(\delta)}{\sinh(\frac{\pi\mu}{b})\sinh^2(2b\xi)} - \frac{16a^4}{b\sinh^2(2b\xi)} \\
&+ \frac{8\pi a^4 \cosh(2b\xi)\sin(4\mu\xi)\cos(2\delta)}{b\sinh(\frac{2\pi\mu}{b})\sinh^3(2b\xi)} - \frac{16\pi a^4\mu\cos(4\mu\xi)\cos(2\delta)}{b^2\sinh(\frac{2\pi\mu}{b})\sinh^2(2b\xi)}.
\end{aligned}
\tag{2.3.6}
$$

The integrals given here have been evaluated using the residue theorem; some of these calculations are presented in detail in appendix A.2.

Equations of motion for NLS

Next we determine the equations for our collective coordinates. First we note that the total Lagrangian is given by

$$
\begin{aligned}
L \;=\;& \frac{4a^2}{b}\left(\mu\dot{\xi} - \frac{4b^2}{3} - \mu^2 - \dot{\lambda} + \frac{2a^2}{3} \right) + \left(1 - \frac{2a^2}{b^2} \right) \frac{8\pi a^2 b \sin(2\mu\xi)\cos(\delta)}{\sinh(\frac{\pi\mu}{b})\sinh^3(2b\xi)} \\
&+ \left(\dot{\mu}\xi - \mu^2 - \dot{\lambda} + \frac{4a^2\mu^2}{b^2} \right) \frac{4\pi a^2 \sin(2\mu\xi)\cos(\delta)}{b\sinh(\frac{\pi\mu}{b})\sinh(2b\xi)} + 32a^4\xi\frac{\cosh(2b\xi)}{\sinh^3(2b\xi)} \\
&+ \left(\frac{2a^2}{b^2} - 1 \right) \frac{8\pi\mu a^2 \cos(2\mu\xi)\cosh(2b\xi)\cos(\delta)}{\sinh(\frac{\pi\mu}{b})\sinh^2(2b\xi)} - \frac{16a^4}{b\sinh^2(2b\xi)} \\
&+ \frac{8\pi a^4 \cosh(2b\xi)\sin(4\mu\xi)\cos(2\delta)}{b\sinh(\frac{2\pi\mu}{b})\sinh^3(2b\xi)} \\
&- \frac{16\pi a^4\mu\cos(4\mu\xi)\cos(2\delta)}{b^2\sinh(\frac{2\pi\mu}{b})\sinh^2(2b\xi)}.
\end{aligned}
\tag{2.3.7}
$$

This expression agrees with the Lagrangian given in Zou and Yan's paper [26] if we take their approximation by neglecting higher order terms of μ, λ and their time derivatives.

From our full Lagrangian we can calculate the Euler-Lagrange equations for our collective coordinates $a(t)$, $\xi(t)$, $\mu(t)$ and $\lambda(t)$.

For λ we have

$$
\frac{d}{dt}\frac{\partial L}{\partial \dot{\lambda}} - \frac{\partial L}{\partial \lambda} = 0 \rightarrow \frac{d}{dt}\left(\frac{4a^2}{b}\left(1 + \frac{\pi\sin(2\mu\xi)\cos(\delta)}{\sinh(\frac{\pi\mu}{b})\sinh(2b\xi)} \right) \right) = 0,
\tag{2.3.8}
$$

which implies that

$$\frac{4a^2}{b}\left(1+\frac{\pi \sin(2\mu\xi)\cos(\delta)}{\sinh(\frac{\pi\mu}{b})\sinh(2b\xi)}\right) = \text{constant}, \tag{2.3.9}$$

is a conserved quantity corresponding to the normalisation N. So we can write

$$N = \int_{-\infty}^{+\infty} dx\, |\psi|^2 = \frac{4a^2}{b}\left(1+\frac{\pi \sin(2\mu\xi)\cos(\delta)}{\sinh(\frac{\pi\mu}{b})\sinh(2b\xi)}\right) \equiv N_0 + N_{12}, \tag{2.3.10}$$

where N has been split into interacting and non-interacting parts.

Next we fix N, which is conserved and so does not depend on t, by putting solitons initially far apart, *i.e.* taking x_0 very large. In our two soliton approximation ψ_1 and ψ_2 are one soliton solutions for the solitons far apart, if we compare this to the one soliton solution (2.1.6) we see that for our solitons initially far apart $\mu \approx -\frac{v}{2}$, $\xi \approx x_0 - vt$ and $a \approx b$, and therefore $N_{12} \approx 0$, $N_0 \approx 4b$.

Then we have

$$a^2 = \frac{b^2}{1 + \frac{\pi \sin(2\mu\xi)\cos(\delta)}{\sinh(\frac{\pi\mu}{b})\sinh(2b\xi)}} \equiv \frac{b^2}{1+\omega}, \tag{2.3.11}$$

where we have defined $\omega \equiv \frac{\pi \sin(2\mu\xi)\cos(\delta)}{\sinh(\frac{\pi\mu}{b})\sinh(2b\xi)}$ for convenience.

Equation (2.3.9) can be used to eliminate $a(t)$ from the equations of motion for $\mu(t)$ and $\xi(t)$, giving a system of coupled first order equations involving μ, ξ, their derivatives and $\dot{\lambda}$. The dependence in $\dot{\lambda}$ can be eliminated if we use the equation of motion for $a(t)$, leaving us with

$$F_1(\mu,\xi)\dot{\mu} + G_1(\mu,\xi)\dot{\xi} + H_1(\mu,\xi) = 0, \tag{2.3.12}$$
$$F_2(\mu,\xi)\dot{\mu} + G_2(\mu,\xi)\dot{\xi} + H_2(\mu,\xi) = 0.$$

Explicit expressions for $F_{1,2}, G_{1,2}$ and $H_{1,2}$ are given in appendix A.3. Finally we solve these to derive the system of equations

$$\dot{\mu} = \frac{G_1 H_2 - G_2 H_1}{F_1 G_2 - F_2 G_1}, \qquad \dot{\xi} = \frac{F_2 H_1 - F_1 H_2}{F_1 G_2 - F_2 G_1}. \tag{2.3.13}$$

We can rewrite the equation for $\dot{\mu}$ in the form of a conservation equation by setting $\ddot{\mu} = \dot{P}$ and integrating over time to get

$$\frac{\dot{\mu}^2}{2} = \frac{P^2}{2} + \mathcal{E}, \tag{2.3.14}$$

where $\mathcal{E}$ is an integration constant determined by the initial conditions. Similarly we can do this for the expression for $\dot{\xi}$ by setting $\ddot{\xi} = P$ and integrating to get

$$\frac{\dot{\xi}^2}{2} = \frac{P^2}{2} + \tilde{\mathcal{E}}, \tag{2.3.15}$$

so we have two energy-like conservation formulas. If we consider $\frac{\dot{\xi}^2}{2}$ to be like kinetic energy, $-\frac{P^2}{2}$ to be like a potential and $\tilde{\mathcal{E}}$ to be like total energy then we can plot potential curves as $-P^2$ up to a constant (we take this constant to be the square of the initial velocity), see figure 2.7.

Results for NLS

In our work we have used a fourth-order Runge-Kutta method to solve numerically our system of equations (2.3.13), (see section 1.4 for details on the numerics). Each one soliton configuration, ψ_1 and ψ_2, possesses a $U(1)$ symmetry so we can choose each phase arbitrarily and consider the dependence on their phase difference δ. In our analysis we have considered only small values of velocity ($\dot{\xi}(0)$) describing the initial motion of the solitons towards each other, as the collective coordinate approximation is a good approximation for slowly moving solitons. Throughout we have taken $b = 1$ and $a(0) = 1$, we have chosen these values in order to compare our results with those of Zou and Yan in [26].

Our simulations of the collective coordinate approximation have shown that the interaction between the solitons depends on their initial phase difference and their velocity at the time of interaction. Solitons with the same initial phase ($\delta = 0$) attract each other the most and, if their velocity is sufficiently small, they become trapped and oscillate around each other with constant frequency. Solitons with the opposite initial phase ($\delta = \pi$) are in the repulsive channel and so they repel each other. The attractive/repulsive forces vary continuously between $\delta = 0, \pi$ with complex interactions taking place around $\delta = \frac{\pi}{2}$ where the solitons experience an initial attraction and so come together, then repel and move away from each other with a constant velocity. The range of interactions can be seen in figure 2.2 where the relative position between the solitons is plotted as a function of time, for a simulation with the initial position $\xi = -5$, initial

velocity $v = -0.01$ so that they are sent towards each other, and for $\delta = 0$, $\frac{\pi}{4}$, $\frac{\pi}{2}$, $\frac{3\pi}{4}$ and π.
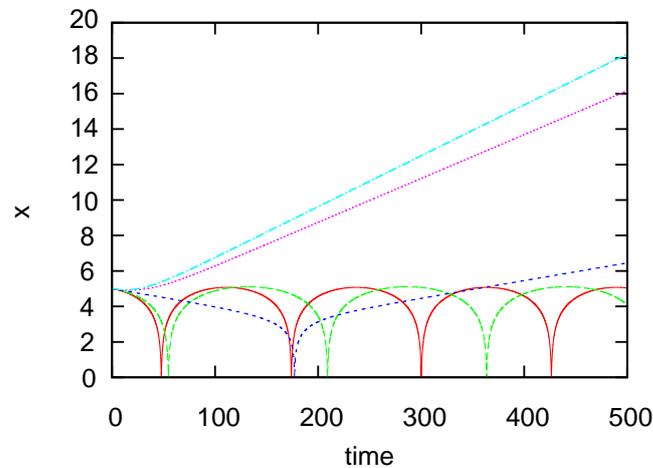
Figure 2.2: The distance of a soliton from the centre of mass of a system with time. The system consists of two solitons initially placed at ± 5 each with an initial velocity of $v = -0.01$ towards the centre of mass. The initial phase difference between the two solitons is: $\delta = 0$ (red line), $\delta = \frac{\pi}{4}$ (green line), $\delta = \frac{\pi}{2}$ (dark blue line), $\delta = \frac{3\pi}{4}$ (pink line) and $\delta = \pi$ (light blue line).
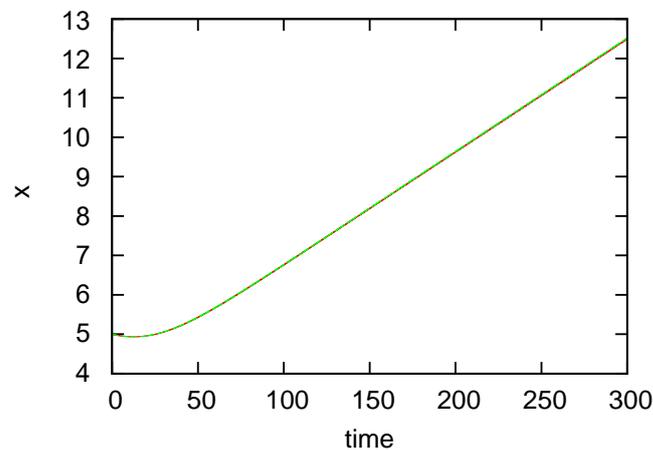
Figure 2.3: The distance of a soliton from the centre of mass of a system with time. The system consists of two solitons initially placed at ± 5 each with an initial velocity of $v = -0.01$ towards the centre of mass and initial phase difference $\delta = \pi$; results of the full simulation is the dashed line (green) and the approximation is the solid line (red).
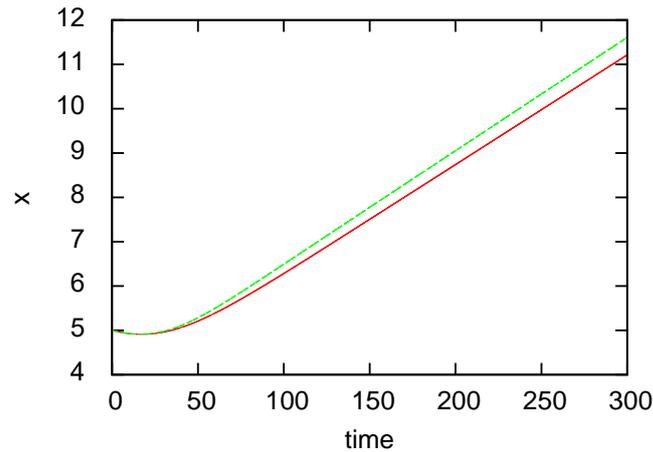
Figure 2.4: The distance of a soliton from the centre of mass of a system with time. The system consists of two solitons initially placed at ± 5 each with an initial velocity of $v = -0.01$ towards the centre of mass and initial phase difference $\delta = \frac{3\pi}{4}$; results of the full simulation is the dashed line (green) and the approximation is the solid line (red).
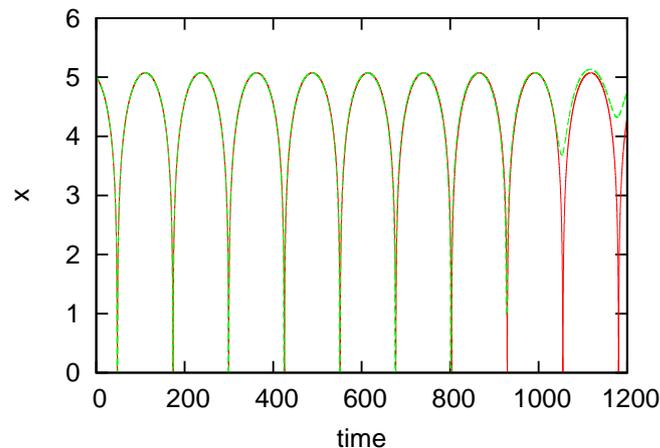
Figure 2.5: The distance of a soliton from the centre of mass of a system with time. The system consists of two solitons initially placed at ± 5 each with an initial velocity of $v = -0.01$ towards the centre of mass and initial phase difference $\delta = 0$; results of the full simulation is the dashed line (green) and the approximation is the solid line (red).

Comparison of the approximation with the full simulation confirms the observed dependence of the soliton scattering on the initial phase difference between the solitons, δ, and shows that the approximation describes the dynamics of the
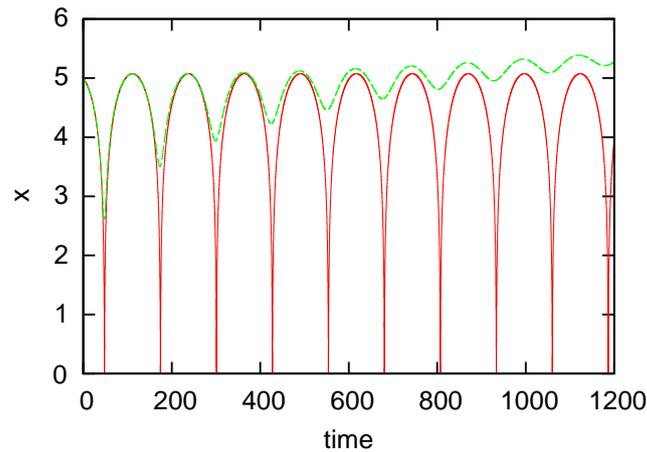
Figure 2.6: The distance of a soliton from the centre of mass of a system with time. The system consists of two solitons initially placed at ± 5 each with an initial velocity of $v = -0.01$ towards the centre of mass and initial phase difference $\delta = \frac{\pi}{32}$; results of the full simulation is the dashed line (green) and the approximation is the solid line (red).

soliton scattering with varying levels of accuracy for different values of δ. For $\delta = \pi$ the approximation is very accurate, this can be seen in figure 2.3 where the results of the full simulation and the approximation are both plotted for solitons initially at $\xi = -5$ and with an initial velocity $v = -0.01$ (so that they are sent towards each other), and with relative phase $\delta = \pi$. In the repulsive cases, $\delta \gtrsim \frac{\pi}{2}$, the results for the full simulation and the approximation are very close, see figure 2.4 where the full simulation and approximation results are compared for $\delta = \frac{3\pi}{4}$, and initial $\xi = -5$, $v = -0.01$ as before.

However, for values of $\delta \lesssim \frac{\pi}{2}$ our collective coordinate approximation does not fully capture the soliton dynamics. For small values of δ in the full simulation the solitons initially attract and oscillate as in the approximation, but over time the oscillations weaken and the solitons start to repel each other. For small non zero values of δ the decay starts immediately and the approximation does not match the full simulation as well, though it does give a close approximation for the period of the oscillations, this can be seen in figure 2.6 where the results are compared for $\delta = \frac{\pi}{32}$. For values of δ closer to $\frac{\pi}{2}$ the attraction is so weak that the solitons only move towards each other for a short period of time before repelling
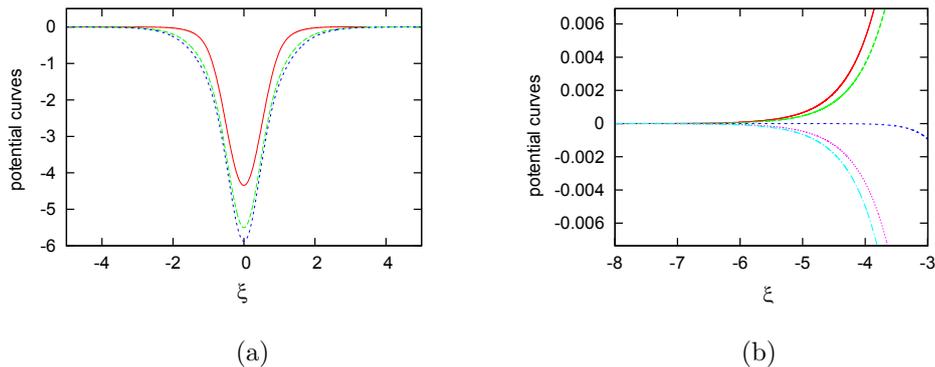
Figure 2.7: Potential curves for solitons initially at $\xi = -10$ and $v = -0.1$ with a) from top to bottom $\delta = \frac{\pi}{2}$, $\frac{\pi}{4}$, 0, and b) from top to bottom $\delta = \pi$, $\frac{3\pi}{4}$, $\frac{\pi}{2}$, $\frac{\pi}{4}$, 0

away. This is different to the results of the approximation where the solitons move together slowly and come on top of each other before slowly oscillating (or eventually repelling if initial velocity is too high). These differences could be due to the phase difference being a constant in our collective coordinate approximation but free to vary in time in the full simulation, therefore allowing solitons initially in an attractive channel to end up in a repulsive channel. This is explored in chapter 3 by changing the choice of collective coordinates to allow the solitons' phases to vary separately in time.

For $\delta = 0$ the approximation remains accurate for a long time as the oscillations only start to decay at around $t = 900$, see figure 2.5. We consider the exact two soliton solution of the NLS equation to see whether the oscillation decay that occurs in the full simulation is a real or numerical effect. In [38] Gordon considers the exact two soliton solution to the NLS equation and from this solution derives an approximate expression for the two soliton solution when the separation of the solitons is large. From this approximate expression Gordon demonstrates analytically that two in-phase solitons with equal velocities execute periodic motion. We see this periodic motion for in-phase solitons indefinitely in the collective coordinate approximation (compared to an eventual separation of the solitons in the full simulation), so it is possible that in this case the collective coordinate approximation provides more accurate results.

We have confirmed our observations by considering the conserved quantity
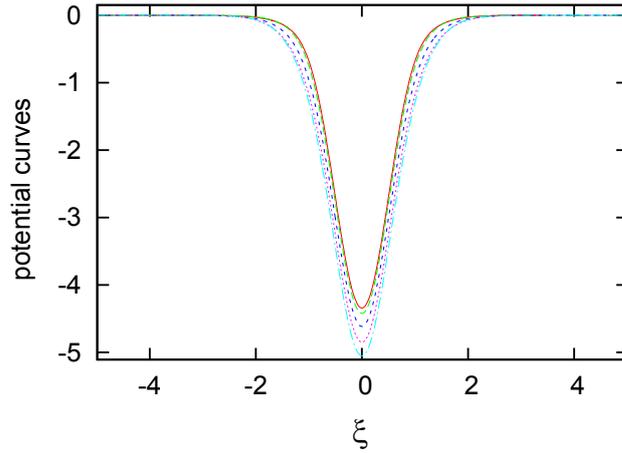
Figure 2.8: Potential curves for solitons initially at $\xi = -10$, $\delta = \frac{\pi}{2}$ and from top to bottom $v = -0.000001, -0.5, -1, -1.5, -2$

resulting from our expression for $\dot{\xi}$. This we have done by interpreting (2.3.15) as an energy conservation formula. This means that the movement of each soliton is like the motion of a unit mass particle moving in a potential $-\frac{P^2}{2}$. We calculate the potential $-\frac{P^2}{2}$ in simulations with various initial values and plot it against ξ to get potential curves. We do this so that we may directly compare our results with those of Zou and Yan in [26] (as they primarily evaluate their results using the potential curves that they calculate).

In figure 2.7 we have plotted the potential curves for initial velocity $v = -0.1$, initial position $\xi = -10$, and various values of δ. Note that in figure 2.7(b) the lines for $\delta = \pi$ and $\delta = \frac{3\pi}{4}$ are only plotted up to about $\xi = -3.8$ because for the simulations with initial phase difference $\delta = \pi$ and $\delta = \frac{3\pi}{4}$ the solitons do not come any closer together (see figures 2.3 and 2.4) so the potential could not be calculated for any smaller values of $|\xi|$.

If we consider figure 2.7 we see that $\delta = 0, \pi$ do indeed correspond to the attractive and repulsive potentials, respectively. Our potential curves are similar to those in Zou and Yan's results in [26] but with a few differences as we have not made any approximations in our calculations. Firstly, our potential curves have a dependence on the initial velocity which is demonstrated in figure 2.8 by plotting potential curves for $\delta = \frac{\pi}{2}$, initial position $\xi = -10$ and various values of initial velocity. Secondly our potential curves are more symmetric about $\delta = \frac{\pi}{2}$,

i.e. in our results solitons with $\delta = \pi$ / $\delta = 0$ feel repulsion/attraction at the same relative distance, whereas in Zou and Yan's results solitons with $\delta = \pi$ feel repulsion whilst further apart than solitons with $\delta = 0$ feel attraction. Finally, our potential curve for $\delta = \frac{\pi}{2}$ is much more attractive than theirs for all values of the initial velocity (see figure 2.7(a)).

Comments and conclusions for NLS

In this chapter we have presented a collective coordinate approximation (based on a modification of the approach of Zou and Yan [26]) for the study of the dynamics of two interacting bright solitons in a NLS model and then we have used it to investigate these dynamics in some detail. We have observed that the initial relative phase between the solitons determines whether they feel an attractive or repulsive force towards each other, and for a small enough velocity the solitons can form a bound state and continue to oscillate around each other indefinitely. In comparing our results to those of full numerical simulations we had good agreement in most cases, suggesting that our collective coordinate approximation can be used to reproduced the dynamics of the solitons even when the solitons are close together. We have also observed some discrepancies for small values of relative phase which we resolve in later chapters by adjusting our choice of collective coordinates.

Chapter 3

The modified NLS model

In the previous chapter we found that the collective coordinate approximation works well in the integrable NLS model, and here we consider the NLS model with a modified potential that breaks the integrability of the system. We do this to assess how the integrability properties of the system effects the usefulness of the approximation, and as a chance to consider the effects of using an improved collective coordinate ansatz in the limit where the modified model reduces to the integrable NLS model. We choose to consider a particular modification of the NLS model for which the integrability properties have already been studied in [16].

Modified NLS model

We consider the Lagrangian and equation of motion given in the previous chapter (2.1.1), (2.1.2) but now with a general potential V (that retains the η parameter). The equation of motion with this general potential admits an anomalous zero curvature representation (2.2.5) with the connection given by (2.2.2). When the wave function ψ is a solution to the equation of motion then the terms on the right hand side of the curvature equation proportional to T_+^0 and T_-^0 vanish, and all that remains is the term XT_3^0 with X given by (2.2.6). For the NLS potential X is equal zero and the theory is integrable, but this is not true for a general

potential.

For a general potential we can carry out the abelianization technique of the integrable field theories like in section 1.1. This calculation is performed in [16] and we give a short overview here. We start as before by rewriting the connection components in terms of a new basis of the $SL(2)$ loop algebra described in 2.2.8 and in terms of the R and φ fields defined as $\psi \equiv \sqrt{R} e^{i\frac{\varphi}{2}}$. We then perform the gauge transformation (2.2.10) and the anomalous zero curvature condition becomes

$$\partial_t \tilde{A}_x - \partial_x \tilde{A}_t + \left[\tilde{A}_x, \tilde{A}_t\right] = X b_0, \tag{3.1.1}$$

with connection components $\tilde{A}_\mu$ given in (2.2.12).

Now when we perform the gauge transformation as in (2.2.14) the a_x components can still be transformed into the abelian subalgebra as $\tilde{A}_x$ is independent of the choice of potential. $\tilde{A}_t$ is dependent on the potential, and with a general choice of potential under the gauge transformation (2.2.14) the a_t components are

$$a_t = i\, b_2 + \sum_{n=0}^{\infty} \left(a_t^{(3,-n)} b_{-n} + a_t^{(1,-n)} F_1^{-n} + a_t^{(2,-n)} F_2^{-n}\right). \tag{3.1.2}$$

Note that a_t has no b_1 component because the coefficient of F_1^0 in $\tilde{A}_x$ and the coefficient of F_1^1 in $\tilde{A}_t$ are the same up to a sign, (see (2.2.12)). The curvature becomes

$$\partial_t a_x - \partial_x a_t = X\, g\, b_0\, g^{-1}, \tag{3.1.3}$$

where we can write

$$g\, b_0\, g^{-1} = \sum_{n=0}^{\infty} \left(\alpha^{(3,-n)} b_{-n} + \alpha^{(1,-n)} F_1^{-n} + \alpha^{(2,-n)} F_2^{-n}\right). \tag{3.1.4}$$

Since a_x lies in the kernel of b_1 the commutator $[a_t, a_x]$ has components only in the image of b_1, and from (3.1.3) and (3.1.4) we get

$$\partial_t a_x^{(3,-n)} - \partial_x a_t^{(3,-n)} = X\alpha^{(3,-n)}; \qquad n = 0, 1, 2, ... \tag{3.1.5}$$

Explicit expressions for the first few expressions of $\alpha^{(3,-n)}$ are given in appendix A.1.1. Now we integrate (3.1.5) over space to get

$$\int_{-\infty}^{\infty} dx\, \partial_t a_x^{(3,-n)} - a_t^{(3,-n)}(x = \infty) + a_t^{(3,-n)}(x = -\infty) = \int_{-\infty}^{\infty} dx\, X\alpha^{(3,-n)}, \tag{3.1.6}$$

for $n = 0, 1, 2, ...$ When $a_t^{(3,-n)}$ satisfies the boundary condition $a_t^{(3,-n)}(x = \infty) = a_t^{(3,-n)}(x = -\infty)$ we have an infinite number of anomalous charges

$$Q^{(n)} = \int_{-\infty}^{\infty} dx \, a_x^{(3,-n)}. \tag{3.1.7}$$

This gives us an infinite number of anomalous conservation laws:

$$\frac{dQ^{(n)}}{dt} = \beta_n; \qquad \text{with} \quad \beta_n = \int_{-\infty}^{\infty} dx \, X \, \alpha^{(3,-n)} \tag{3.1.8}$$

for $n = 0, 1, 2, ...$ It is clear that when the potential corresponds to the NLS potential, i.e. $V_{\text{NLS}} = \eta \, |\psi|^4$, the anomaly X given in (2.2.6) vanishes and so do the integrals β_n. Therefore, the theory with the potential V_{NLS} is integrable as it has an infinite number of conserved charges $Q^{(n)}$.

In our modified model we use a perturbation of the NLS potential as in [16]

$$V = \frac{2}{2 + \epsilon} \eta \left(|\psi|^2 \right)^{2 + \epsilon}, \tag{3.1.9}$$

note that it becomes the unperturbed NLS potential in the case $\epsilon = 0$.

As shown in [16], for $\eta < 0$, this model has a one-soliton solution given by

$$\Psi = \left(\sqrt{\frac{2 + \epsilon}{2 \, |\eta|}} \frac{b}{\cosh \left[(1 + \epsilon) \, b \, (x - vt - x_0) \right]} \right)^{\frac{1}{1+\epsilon}} e^{i \left[\left(b^2 - \frac{v^2}{4} \right) t + \frac{v}{2} x \right] + i\phi}, \tag{3.1.10}$$

where b, ϕ, v and x_0 are real parameters of the solution.

For two interacting solitons, as argued in [17], we can take

$$\psi = \psi_1 + \psi_2, \tag{3.1.11}$$

where $\psi_1 = \Psi(x, t, x_0, v, \phi_1)$ and $\psi_2 = \Psi(x, t, -x_0, -v, \phi_2)$. Such fields describe well two solitons (each at $\pm x_0$ with velocity $\pm v$ and their phase difference of $(\phi_1 - \phi_2)$) when they are far apart as then, for any point in x, there is a significant contribution from (at most) one ψ_i due to the localised nature of the one soliton solution. Such a field configuration was successfully used in [17] as an initial configuration for the numerical investigations of two soliton scatterings, and so we use it here too.

It was shown in [17] that if the field of (3.1.11) $\psi = \psi_1 + \psi_2 \equiv \sqrt{R} e^{i\frac{\varphi}{2}}$ transforms under the parity

$$P: \quad (\tilde{x}, \tilde{t}) \to (-\tilde{x}, -\tilde{t}), \qquad \text{with} \quad \tilde{x} = x - x_\Delta \quad \text{and} \quad \tilde{t} = t - t_\Delta, \tag{3.1.12}$$

as

$$P: \qquad R \to R; \qquad \varphi \to -\varphi + \text{constant}, \tag{3.1.13}$$

then X (2.2.6) is odd under P and $\alpha^{(3,-n)}$ is even under P (see appendix A.1.1). And, for field configurations which transform as in (3.1.13) we have

$$\int_{-\tilde{t}_0}^{\tilde{t}_0} dt \int_{-\tilde{x}_0}^{\tilde{x}_0} dx \, X \, \alpha^{(3,-n)} = 0, \tag{3.1.14}$$

where $\tilde{t}_0$ and $\tilde{x}_0$ are given fixed values of the shifted time and space coordinates in (3.1.12).

Note that (3.1.8) shows that $Q^{(n)}(t_2) = Q^{(n)}(t_1) + \int_{t_1}^{t_2} \beta_n(t')dt'$ where we have already taken $\tilde{x}_0 \to \infty$. Taking t_1 and t_2 appropriately we find that we have non-conserved charges (3.1.8) that vary in time but are symmetric with respect to $t = t_\Delta$. Taking further $\tilde{t}_0 \to \infty$ we find that the system has an infinite number of asymptotically conserved charges, *i.e.*

$$Q^{(n)}(t = +\infty) = Q^{(n)}(t = -\infty). \tag{3.1.15}$$

This all assumes that the symmetry, which was shown to hold for the initial configuration (3.1.11) holds at all times, but the studies in [17] did show that the initial approximation is very good at all times and the charges are asymptotically conserved. Of course, the question then still arises whether this is also true in the collective coordinate approximation. This is what we discuss in the next section.

The two-soliton configuration for modified NLS

Here we construct a set of collective coordinates for the study of the scattering of two solitons with $\eta = -1$ in the NLS system with our modified potential. Guided by the ideas of [17] we use a natural extension of our approximation ansatz in [2], and so we take our approximation ansatz for two solitons in the modified NLS system also in the form of the sum of two one soliton fields similar to (3.1.11). Therefore we use an ansatz of the form

$$\psi = \psi_1 + \psi_2 = \varphi_1 e^{i\theta_1} + \varphi_2 e^{i\theta_2}, \tag{3.2.1}$$

where

$$\varphi_1 = \left(\sqrt{\frac{2+\epsilon}{2}} \frac{a_1(t)}{\cosh\left[(1+\epsilon)\,a_1(t)\,(x+\xi_1(t))\right]} \right)^{\frac{1}{1+\epsilon}},$$

$$\theta_1 = -\frac{\mu_1(t)}{2}\left(x + \frac{\xi_1(t)}{2}\right) + a_1^2(t)\,t + \lambda_1(t),$$

$$\varphi_2 = \left(\sqrt{\frac{2+\epsilon}{2}} \frac{a_2(t)}{\cosh\left[(1+\epsilon)\,a_2(t)\,(x+\xi_2(t))\right]} \right)^{\frac{1}{1+\epsilon}},$$

$$\theta_2 = -\frac{\mu_2(t)}{2}\left(x + \frac{\xi_2(t)}{2}\right) + a_2^2(t)\,t + \lambda_2(t), \quad (3.2.2)$$

and $a_i(t)$, $\xi_i(t)$, $\mu_i(t)$ and $\lambda_i(t)$ for $i = 1, 2$ are our collective coordinates. Note that, as is clear from (3.1.10), $\xi_i(t) = (-1)^i\,(vt + x_0)$ when the solitons are far away from each other. So velocity is given by $\mu_i(t)$ and is also contained in $\xi_i(t)$. This approximation ansatz models two lumps which, when they are far apart, resemble two one-soliton solutions akin to (3.1.10) with heights $a_i(t)$, positions $\xi_i(t)$, velocities $\mu_i(t)$ and phases $\lambda_i(t)$.

In the case $\epsilon = 0$ the system is integrable and this ansatz is similar to the one we used in [2] with the additional features of a time dependence in the width of the solitons. Also the height, position, velocity and phase of each soliton are allowed to vary independently (whereas previously we insisted that $a_1(t) = a_2(t)$, $\xi_1(t) = -\xi_2(t)$, $\mu_1(t) = -\mu_2(t)$ and $\lambda_1(t) = \lambda_2(t)$). In particular this allows a previously static parameter, the phase difference between the solitons $\delta \equiv \lambda_1 - \lambda_2$, to vary in time. These changes have been made based on our observations in [2], and we have later found that this improved approximation ansatz gives more accurate results for the NLS solitons when we compare them with our results in [2]. For $\epsilon = 0$ the ansatz (3.2.1) is invariant under the parity defined in (3.1.12).

For $\epsilon \neq 0$ and $\delta = n\pi$, where $n \in \mathbb{Z}$, the approximation ansatz (3.2.1) transforms under the parity defined in (3.1.12) as in (3.1.13). Thus the field configuration possesses the additional symmetries mentioned before that are necessary for the system to be quasi-integrable. Therefore, for these values of δ the system has asymptotically conserved charges.

For $\epsilon \neq 0$ and $\delta \neq n\pi$ the approximation ansatz does not transform under the parity defined in (3.1.12) as required for quasi-integrability, and so the system appears to be non-integrable and there are no constraints on the charges.

Implementing the approximation in modified NLS

In order to proceed with the collective coordinate approximation we insert our approximation ansatz (3.2.1) into the Lagrangian (2.1.1) to obtain an effective Lagrangian:

$$\mathcal{L} = I_{a_1}\dot{a}_1 + I_{a_2}\dot{a}_2 + I_{\xi_1}\dot{\xi}_1 + I_{\xi_2}\dot{\xi}_2 + I_{\mu_1}\dot{\mu}_1 + I_{\mu_2}\dot{\mu}_2 + I_{\lambda_1}\dot{\lambda}_1 + I_{\lambda_2}\dot{\lambda}_2 - V, \quad (3.2.3)$$

where the dot denotes differentiation with respect to time; and the I's and V are functions of $a_{1,2}(t)$, $\xi_{1,2}(t)$, $\mu_{1,2}(t)$, $\lambda_{1,2}(t)$ and t. These functions are fully described in appendix A.3.

From this effective Lagrangian we derive equations of motion as a set of coupled ODEs of the form:

$$\dot{I}_q - \dot{a}_1\frac{\partial I_{a_1}}{\partial q} - \dot{a}_2\frac{\partial I_{a_2}}{\partial q} - \dot{\xi}_1\frac{\partial I_{\xi_1}}{\partial q} - \dot{\xi}_2\frac{\partial I_{\xi_2}}{\partial q} - \dot{\mu}_1\frac{\partial I_{\mu_1}}{\partial q} - \dot{\mu}_2\frac{\partial I_{\mu_2}}{\partial q} - \dot{\lambda}_1\frac{\partial I_{\lambda_1}}{\partial q} - \dot{\lambda}_2\frac{\partial I_{\lambda_2}}{\partial q} + \frac{\partial V}{\partial q} = 0,$$
$$(3.2.4)$$

where q denotes the collective coordinates $q = a_1, a_2, \xi_1, \xi_2, \mu_1, \mu_2, \lambda_1, \lambda_2$. We decouple these equations, and solve them using a 4th order Runge-Kutta method (for details on the numerics see section 1.4).

Results for NLS ($\epsilon = 0$)

Here we describe the results of our analysis of the scattering of two solitons for the cases when $\epsilon = 0$ which correspond to the non-perturbed, integrable NLS. We consider the results of our collective coordinate approximation for a range of initial values of the collective coordinates, and compare them against those given by a full numerical simulation. This allows us to determine the effective range of parameters for our choice of the approximation ansatz. In all our studies we use $\eta = -1$ and take our initial height/width parameter to be $a_1 = a_2 = 1$. We start our solitons from initial positions $\xi_1 = -5$, $\xi_2 = 5$ (*i.e.* far enough apart not to

affect one another initially) and send each one of them towards the other with some initial velocity $v = \mu_1 = -\mu_2$.

As shown in our previous work [2] the solitons' scattering is highly dependent on the relative phase between them, *i.e.* $\delta \equiv \lambda_1 - \lambda_2$; so initially we compare the solitons' dynamics between the collective coordinate approximation and full numerical simulation for a range of δ. In each case only the trajectory of the right hand soliton has been plotted, calculated by each method, in order to keep the plots clearer. Figure 3.1 compares the trajectories for solitons with initial velocity $v = 0.01$ and initial phase difference $\delta = 0, \frac{\pi}{4}, \frac{\pi}{2}, \frac{3\pi}{4}, \pi$ (the results are symmetric around π and periodic in 2π). This figure shows that for most values of δ (whenever $\delta \neq 0$) both approaches produce almost identical trajectories, *i.e.* it is difficult to see the difference between the lines in plots 3.1(b) - (e). To quantify the agreement between the two methods we calculated a percentage difference in the trajectories a significant time after the solitons' collision (in this case at $t = 250$), and we found a percentage difference of 0.53% for $\delta = \frac{\pi}{4}$; 0.026% for $\delta = \frac{\pi}{2}$; 0.0067% for $\delta = \frac{3\pi}{4}$; and 0.0039% for $\delta = \pi$. It is evident from these values that the earlier the solitons repel the more accurate the approximation is.

In the case of $\delta = 0$ both results show excellent qualitative agreement for the first 3 oscillations, but the solitons in the collective coordinate approximation break away from oscillating around each other much earlier than in the full simulation. However, the qualitative results remain the same, and one possible cause for any disagreement between the collective coordinate approximation and full simulation is because in the full simulation the solitons deform one another away from the form given by (3.2.1) when they are in close proximity and the collective coordinate approximation does not allow such a deformation.

We can see how much the solitons deform each other as they come together by considering the difference between the collective coordinate ansatz and the soliton solution used in the full simulation, both at the beginning of the simulation and some time later (after the solitons have interacted). We do this by calculating the difference between $|\psi|^2$ for the collective coordinate, $|\psi_{cc}|^2$, and $|\psi|^2$ for the

full simulation, $|\psi_{fs}|^2$, at a set time and integrate it over space, *i.e.*

$$\text{difference} = \int_{-\infty}^{\infty} ||\psi_{cc}(x)|^2 - |\psi_{fs}(x)|^2|dx. \qquad (3.3.5)$$

Calculating this at the beginning of the simulation, with $\epsilon = 0$ and initial values $\delta = 0$, $v = 0.01$, $\xi_{1,2} = \pm 5$, $a_{1,2} = 1$, we found a difference of 2.6×10^{-6}. This demonstrates that the wave functions are very similar at the beginning of the simulation. After the solitons collide (when they are positioned at ± 3.8) we find a difference of 7.0×10^{-5}. So we see a slight deformation from the ansatz form in the full simulation after the solitons collide, but they still have a very similar shape.

The usefulness of the collective coordinate approximation for $\epsilon = 0$ is further explored by comparing the heights of the solitons as they collide, calculated using the collective coordinate approximation and using the full numerical simulation, for a variety of initial values of phase difference δ. Figure 3.2 compares the heights of the solitons during collision, calculated by each method, for solitons with initial velocity $v = 0.01$ and initial phase difference $\delta = \frac{\pi}{4}, \frac{\pi}{2}$. It is clear that in the cases where the trajectories show excellent qualitative agreement, *i.e.* when $\delta = \frac{\pi}{4}$, $\frac{\pi}{2}$, the heights of the solitons also show excellent qualitative agreement. This can be seen from figure 3.2 where the plotted lines are essentially coincident, to quantify this the percentage difference in the heights of the solitons as calculated by each method, at $t = 250$, is of the order $10^{-3}\%$ (comparing the right and left hand solitons separately). Figure 3.3 is similar to figure 3.2 but with initial phase difference $\delta = 0$, and only the heights of the right hand solitons have been plotted to maintain clarity (the results for the heights of the left hand solitons are similar). In this case the heights of the solitons peak when the solitons come together in a similar way in both the approximation and the full simulation; the heights of the solitons in the approximation cease peaking when the solitons cease to oscillate around each other which happens earlier in the collective coordinate approximation than in the full simulation (for the trajectories see figure 3.1(a)). These observations support those drawn when comparing the trajectories of the solitons.

We also consider the phase difference between the solitons as they collide to

Figure 3.1: The distance of a soliton from the centre of mass of a system as a function of time. The system consists of two solitons initially placed at ± 5 and sent towards their centre of mass with an initial velocity $v = 0.01$. Initial height/width parameter of each soliton is 1 and the initial phase difference between them is: (a) $\delta = 0$, (b) $\delta = \frac{\pi}{4}$, (c) $\delta = \frac{\pi}{2}$, (d) $\delta = \frac{3\pi}{4}$,(e) $\delta = \pi$. For each plot the solid line (red) has been obtained using the collective coordinate approximation and the dashed line (green) is the result of the full simulation (these may be indistinguishable).

(a)   (b)
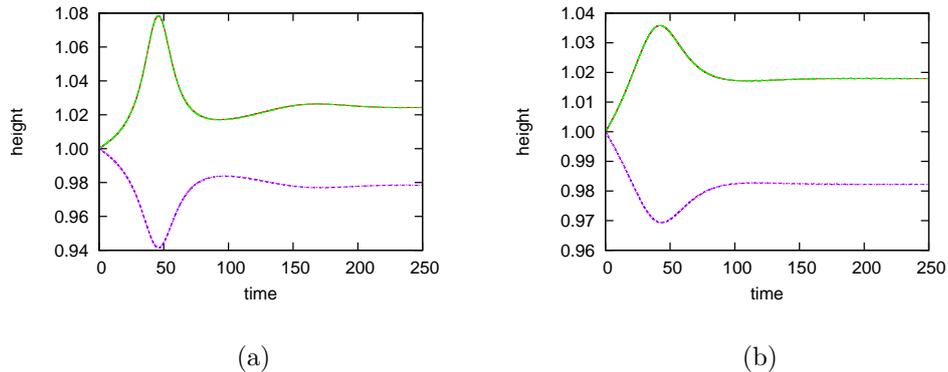
Figure 3.2: The heights of colliding solitons as a function of time. The system consists of two solitons initially placed at ± 5 and sent towards their centre of mass with an initial velocity $v = 0.01$. Initial height/width parameter of each soliton is 1 and the initial phase difference between them is: (a) $\delta = \frac{\pi}{4}$, (b) $\delta = \frac{\pi}{2}$. For each plot the increasing lines are the results for the right hand solitons for the collective coordinate approximation (red solid line) and the full simulation (green long dashed line), these are very similar. The decreasing lines are results for the left hand soliton for the collective coordinate approximation (purple short dashed line) and the full simulation (pink dotted line), these are also very similar.
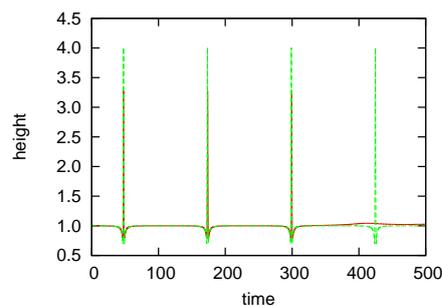
Figure 3.3: The heights of colliding solitons as a function of time. The system consists of two solitons initially placed at ± 5 and sent towards their centre of mass with an initial velocity $v = 0.01$. Initial height/width parameter of each soliton is 1 and the initial phase difference between them is $\delta = 0$. The solid line (red) has been obtained using the collective coordinate approximation and the dashed line (green) is the result of the full simulation (for t up to 350 these are difficult to distinguish).
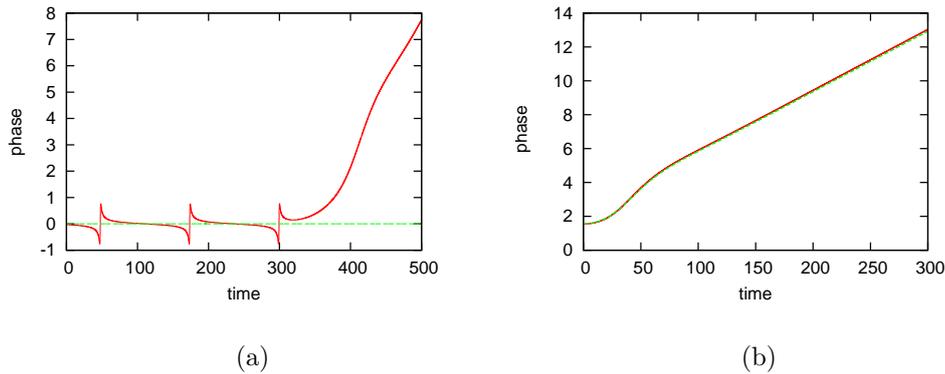
Figure 3.4: The phase difference between solitons as a function of time. The system consists of two solitons initially placed at ± 5 and sent towards their centre of mass with an initial velocity $v = 0.01$. Initial height/width parameter of each soliton is 1 and the initial phase difference between them is: (a) $\delta = 0$ and (b) $\delta = \frac{\pi}{2}$. For each plot the solid line (red) has been obtained using the collective coordinate approximation and the dashed line (green) is the result of the full simulation (these may be indistinguishable).

gain more information. Figure 3.4 compares the phase difference between the solitons during collision, as calculated by each method, for solitons with initial velocity $v = 0.01$ and initial phase differences $\delta = 0$, $\frac{\pi}{2}$. This figure shows excellent agreement in the case $\delta = \frac{\pi}{2}$, the percentage difference in the results at $t = 250$ is 0.87%. When $\delta = 0$ the phase difference between the solitons in the collective coordinate approximation varies around zero between $\pm \frac{\pi}{4}$ as the solitons come together then increases as the solitons repel (for the trajectory see figure 2.5), in the full numerical simulation the phase difference varies when the solitons come together but only by $\pm 5 \times 10^{-5}$. The dissimilarity between the phase difference in the two methods for solitons starting in the most attractive channel ($\delta = 0$) suggests that the approximation struggles to model exactly how the phase difference changes as the solitons come close together. This may explain the small differences in the physical properties of the solitons that have been noted in the $\delta = 0$ case.

Next we consider the effect of the initial velocity on the accuracy of the col-

lective coordinate approximation. Figure 3.5 compares the trajectories given by the collective coordinate approximation and those given by the full numerical simulation for solitons with initial phase difference $\delta = \frac{\pi}{4}$ and initial velocity $v = 0.1$ and $v = 0.2$. Although we expect the collective coordinate approximation to be better at smaller velocities, as mentioned in section 1.3, the total effect of the initial velocity on the accuracy of the collective coordinate approximation is difficult to gauge in full generality. This is because, when the initial velocity is changed, the amount of time the solitons spend close together during their interaction changes which, as we have already surmised, affects the accuracy of the approximation. Figure 3.5 shows that, as expected, increasing initial velocity decreases the accuracy of the approximation slightly. To be able to compare the agreement between the two methods for various initial velocities we calculated the percentage difference in position of the solitons a significant time after their collision for the different initial values and found a percentage difference of 1.3% for initial velocity $v = 0.1$ (at $t = 100$) and a percentage difference 3.9% for initial velocity $v = 0.2$ (at $t = 50$). This shows that for solitons which do not spend much time close together during their interaction the approximation is still very good up to an initial velocity of at least $v = 0.2$. As the collective coordinate approximation assumes slow moving solitons (see section 1.3) our results show that the approximation is extremely reliable for low velocity and for higher velocities it is more reliable than could have been reasonably expected. As the collective coordinate approximation neglects any radiative corrections to the solitons, this agreement for velocities of up to $v = 0.2$ suggests that the radiative corrections are small for these initial values. This is confirmed by considering how the energy of the system varies with time in the full numerical simulation. In simulations with $\epsilon = 0$ there is no change at all to the energy during the simulations (as we mentioned in section 1.4). When $\epsilon \neq 0$ the energy change is minute when the solitons do not come close together (of the order of 10^{-6}%) and is very small when they do come together (~ 1% for $\epsilon = 0.06$, $\delta = 0$ and $v = 0.01$).

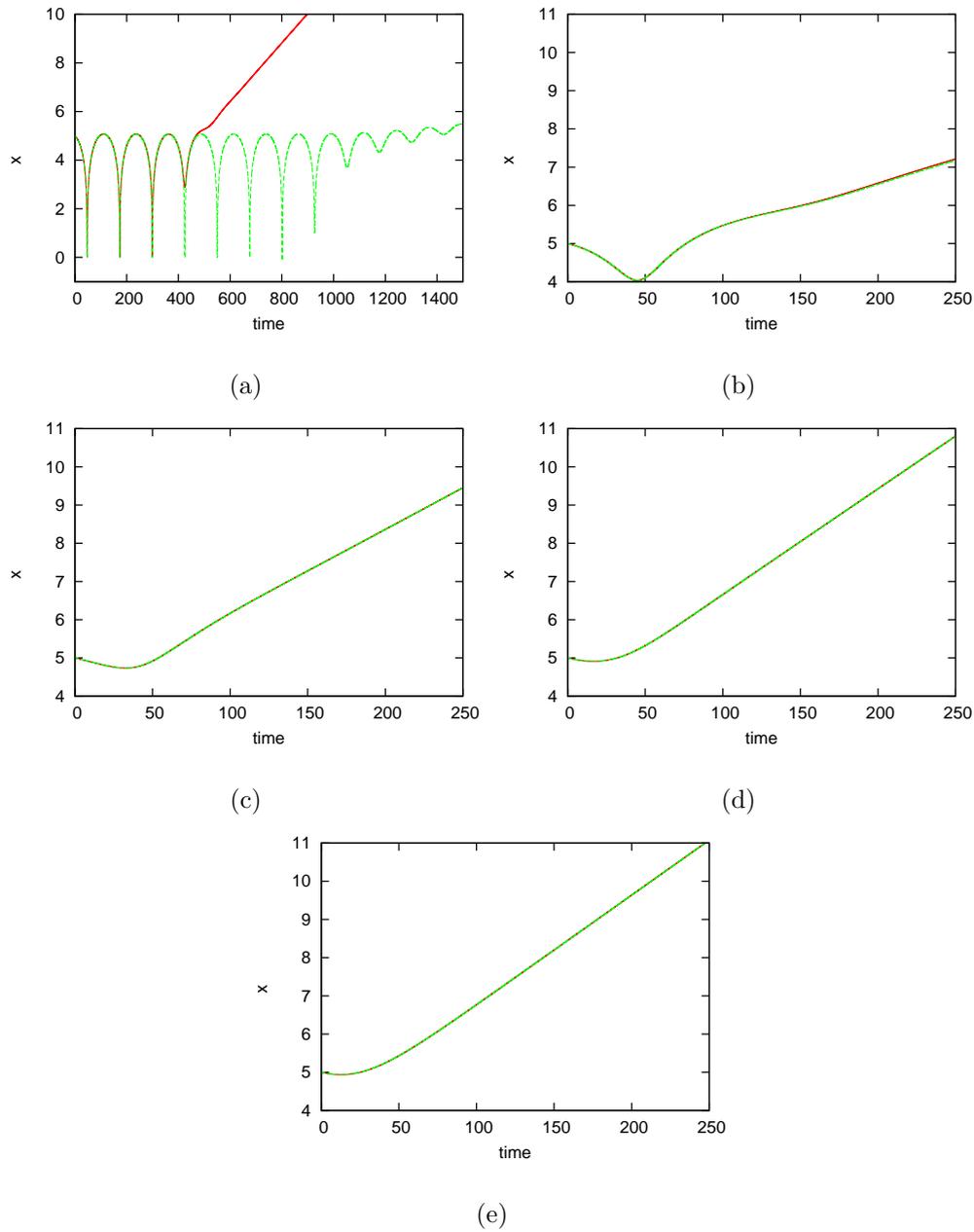(a)   (b)
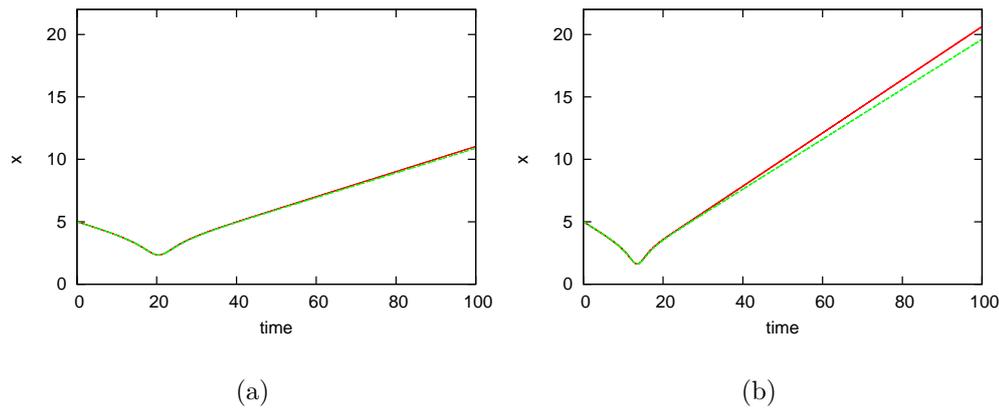
Figure 3.5: The distance of a soliton from the centre of mass of a system as a function of time. The system consists of two solitons initially placed at ± 5, with initial height/width parameter of 1 and the initial phase difference between them of $\delta = \frac{\pi}{4}$. The solitons move towards the centre of mass with initial velocity (a) $v = 0.1$, and (b) $v = 0.2$. For each plot the solid line (red) describes the outcome obtained in the collective coordinate approximation and the dashed line (green) shows the result of the full simulation (these may be indistinguishable).

Results for modified NLS

In the case $\epsilon \neq 0$ the modified NLS system of two solitons is no longer integrable; this means that the system no longer has an infinite number of conserved quantities and so some energy can be lost as radiation during soliton interactions. As before each simulation starts with solitons with initial positions $\xi_1 = -5$, $\xi_2 = 5$, initial height/width parameter $a_1 = a_2 = 1$, and various initial phase differences and velocities towards each other. As in the $\epsilon = 0$ case we find that the accuracy of the approximation depends on the amount of time the solitons spend in close proximity of each other during their interaction. This can be seen in figure 3.6 which compares the trajectories of solitons with initial velocities $v = 0.01$, $\epsilon = \pm 0.06$ and $\delta = 0, \frac{\pi}{4}, \frac{\pi}{2}$ (plots for $\delta = \frac{3\pi}{4}, \pi$ show excellent agreement so are not included). We note that for $\epsilon = \pm 0.06$ and $\delta \neq 0$ the results of the collective coordinate approximation show excellent qualitative agreement with the results of the full numerical simulation. As before we calculate the percentage difference

in the positions of the solitons at a significant time after the collision to quantify the agreement of the two methods. For an initial phase difference $\delta = \frac{\pi}{4}$ the percentage difference is 9.4% for $\epsilon = 0.06$ (at $t = 400$) and 0.29% for $\epsilon = -0.06$ (at $t = 250$); the percentage difference in the positions of the solitons for initial phase difference $\delta = \frac{\pi}{2}$ is 0.034% for $\epsilon = 0.06$ (at $t = 250$) and 0.041% for $\epsilon = -0.06$ (at $t = 250$). Though the percentage difference for $\delta = \frac{\pi}{4}$ and $\epsilon = -0.06$ is by far the largest, the trajectory for these initial values is the most complicated and the collective coordinate approximation captures that complexity well.

However, for $\epsilon = \pm 0.06$ and $\delta = 0$ the differences between the approximation and full simulation are more pronounced than in the $\epsilon = 0$ case: the collective coordinate approximation accurately describes the initial coming together of the solitons, but it does not capture the decreasing amplitude and increasing frequency of the oscillations demonstrated by the full simulation before the solitons eventually repel. This increased difference is probably because, for the $\epsilon \neq 0$ case, the solitons deform each other to a greater extent as they approach each other.

We can test this as we did before (in the $\epsilon = 0$ case) by calculating the difference between $|\psi|^2$ for the collective coordinate approximation and the full simulation. The difference (3.3.5) at the beginning of the simulation, with $\epsilon = 0.06$ and initial values $\delta = 0$, $v = 0.01$, $\xi_{1,2} = \pm 5$, $a_{1,2} = 1$, was found to be 5.9×10^{-4}. Calculating the difference after the solitons collide, with the solitons positioned at ± 2.9, we found a difference of 1.1×10^{-3}. This shows that during their collision the solitons do deform slightly in the full simulation from the ansatz form assumed in the collective coordinate approximation. Comparing this to the difference values found in the $\epsilon = 0$ case we see that the differences are overall larger for $\epsilon = 0.06$, but the proportional variation in the difference during the simulation is comparable.

Another possible reason that the two methods give different results for $\epsilon = \pm 0.06$ and $\delta = 0$ is that, when $\epsilon \neq 0$, some energy is radiated out which is not accounted for in the approximation. The amount of energy lost by the solitons in the full simulation is shown in figure 3.7 where we plot the energy of the system during a scattering for $\epsilon = 0.06$, and $\delta = 0, \frac{\pi}{4}, \frac{\pi}{2}$ and for the same initial conditions

Figure 3.6: The distance of a soliton from the centre of mass of a system as a function of time. The system consists of two solitons initially placed at ± 5 each with an initial velocity of $v = 0.01$ towards the centre of mass. Initial height/width parameter of each soliton is 1 with $\delta = 0$ and (a) $\epsilon = 0.06$, (b) $\epsilon = -0.06$; $\delta = \frac{\pi}{4}$ and (c) $\epsilon = 0.06$, (d) $\epsilon = -0.06$; $\delta = \frac{\pi}{2}$ and (e) $\epsilon = 0.06$, (f) $\epsilon = -0.06$. For each plot the solid line (red) is result of the collective coordinate approximation and the dashed line (green) is the result of the full simulation (these may be indistinguishable).
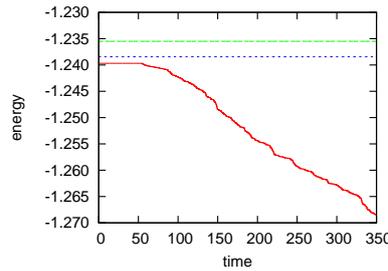
Figure 3.7: The time dependency of the energy of the solitons for $\epsilon = 0.06$ placed initially at ± 5. Each soliton is of initial height/width parameter of 1 and is sent towards the centre of mass with initial velocity $v = 0.01$. $\delta = 0$ corresponds to the solid line (red), $\delta = \frac{\pi}{4}$ the dotted line (blue) and $\delta = \frac{\pi}{2}$ the dashed line (green).

as those used in the trajectory plots (plots for $\epsilon = -0.06$ are very similar), and we do not plot the results of the collective coordinate approximation as this approximation does not allow the loss of energy. Over time the cases $\delta = \frac{\pi}{4}, \frac{\pi}{2}$ demonstrate an incredibly small energy change; when $t = 300$ (*i.e.* at a significant time after any collisions) they both have a percentage energy loss of $1.4 \times 10^{-6}\%$. In the case $\delta = 0$ the energy is constant until the solitons come together at which point some energy is radiated out. The system then evolves as two separate solitons and emits some small energy waves which we absorb as they reach the boundary so we see that the total energy of the soliton decreases. The percentage energy loss in this case is 1.1%.

As in the $\epsilon = 0$ case we consider the phase difference between the solitons as they collide. Figure 3.8 compares the phase difference between the solitons during collision, as calculated by each method, for solitons with $\epsilon = 0.06$, initial velocity $v = 0.01$ and initial phase difference $\delta = 0$. This figure resembles the one for the $\epsilon = 0$ case: the phase difference calculated using the approximation peaks when the solitons come together and steadily increases when the solitons cease oscillating around each other, the phase difference calculated using the full simulation has very small peaks when the solitons come together and also steadily increases when the solitons repel. Comparing this figure to figure 3.4 shows that the change in ϵ has no obvious effect on the how well the collective coordinate
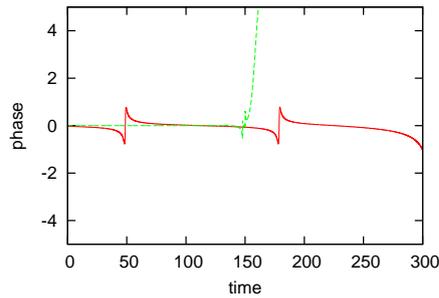
Figure 3.8: The phase difference between solitons as a function of time. The system consists of two solitons initially placed at ± 5 and sent towards their centre of mass with an initial velocity $v = 0.01$. Initial height/width parameter of the soliton is 1 and the initial phase difference between them is $\delta = 0$. The solid line (red) has been obtained using the collective coordinate approximation and the dashed line (green) is the result of the full simulation.

approximation models the time dependence of the phase difference.

We also consider the effect of the initial velocity on the accuracy of the collective coordinate approximation when $\epsilon = 0.06$. Figure 3.9 compares the trajectories obtained in the collective coordinate approximation and those found by the full numerical simulation for solitons with initial values as in figure 3.5 but with $\epsilon = 0.06$. These results show that the accuracy of the approximation is still quite good up to $v = 0.2$, with percentage difference in position of the solitons of 4.4% for $v = 0.1$ (at $t = 100$) and 9.2% for $v = 0.2$ (at $t = 50$). The trajectories of the solitons for these initial values show slightly less agreement than in the equivalent simulations with $\epsilon = 0$ (this can be seen by comparing figures 3.9 and 3.5).

Next we increase the parameter ϵ to investigate its effect on the accuracy of the approximation. Figure 3.10 presents the plots of the trajectories derived in the collective coordinate approximation and the full numerical simulation for solitons with initial phase difference $\delta = \frac{\pi}{4}$, and various values of ϵ and initial velocity. This figure also shows that, for solitons which do not spend much time in close proximity of each other, increasing the value of ϵ reduces the accuracy of the approximation very slightly with excellent qualitative agreement up to at least $\epsilon = 0.3$, the percentage difference in the positions of the solitons is 0.51%

(a) (b)
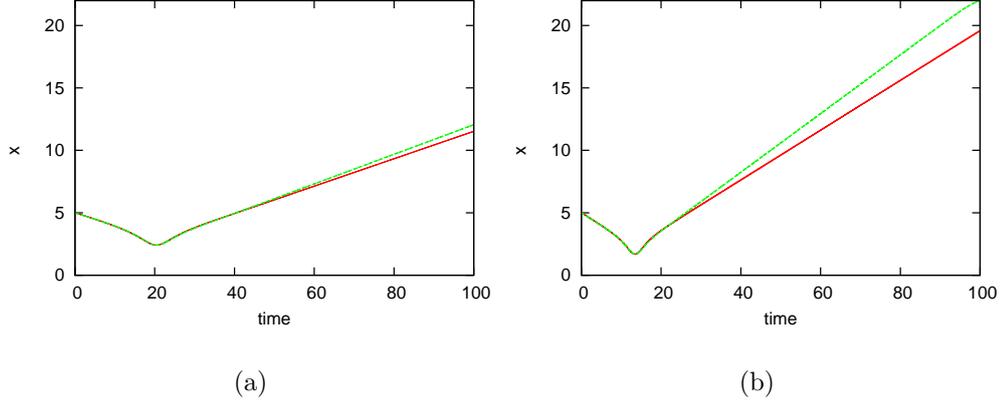
Figure 3.9: The distance of a soliton from the centre of mass of a system as a function of time with $\epsilon = 0.06$. The system consists of two solitons initially placed at ± 5, with initial height/width parameter of 1 and the initial phase difference between them of $\delta = \frac{\pi}{4}$. The solitons move towards the centre of mass with initial velocity (a) $v = 0.1$, and (b) $v = 0.2$. For each plot the solid line (red) is result of the collective coordinate approximation and the dashed line (green) is the result of the full simulation.

for $\epsilon = 0.1, v = 0.01$ at $t = 250$, and 1.4% for $\epsilon = 0.3, v = 0.1$ at $t = 100$.

In our numerical simulations we calculate and compare the quasi-conservation of the first non-trivial charge beyond the energy and momentum, *i.e.* the charge $Q^{(4)}$ defined in (3.1.8). We do this by computing the corresponding anomaly β_4, defined in (3.1.8) (X is defined in (2.2.6) and an explicit expression for $\alpha^{(3,-4)}$ is given in appendix A.1.1), and by integrating it over time to get the integrated anomaly:

$$
\chi^{(4)}(t) \equiv \int_{-\infty}^{t} dt' \, \beta_4 = \int_{-\infty}^{t} dt' \int_{-\infty}^{\infty} dx \, X \alpha^{(3,-4)} \tag{3.4.6}
$$

$$
= -2i \int_{-\infty}^{t} dt' \int_{-\infty}^{\infty} dx \left((\epsilon + 1) R^\epsilon - 1 \right) \partial_x R \times \tag{3.4.7}
$$

$$
\left[-6R^2 + \frac{3}{2} \left(\partial_x \varphi \right)^2 R - 2 \partial_x^2 R + \frac{3}{2} \frac{\left(\partial_x R \right)^2}{R} \right].
$$

This is written in terms of the fields R and φ which are defined by writing each soliton field ψ in the form $\psi \equiv \sqrt{R} e^{i\frac{\varphi}{2}}$. We calculate the time-integrated anomaly at each point in time during the simulations using the equation (3.4.8).
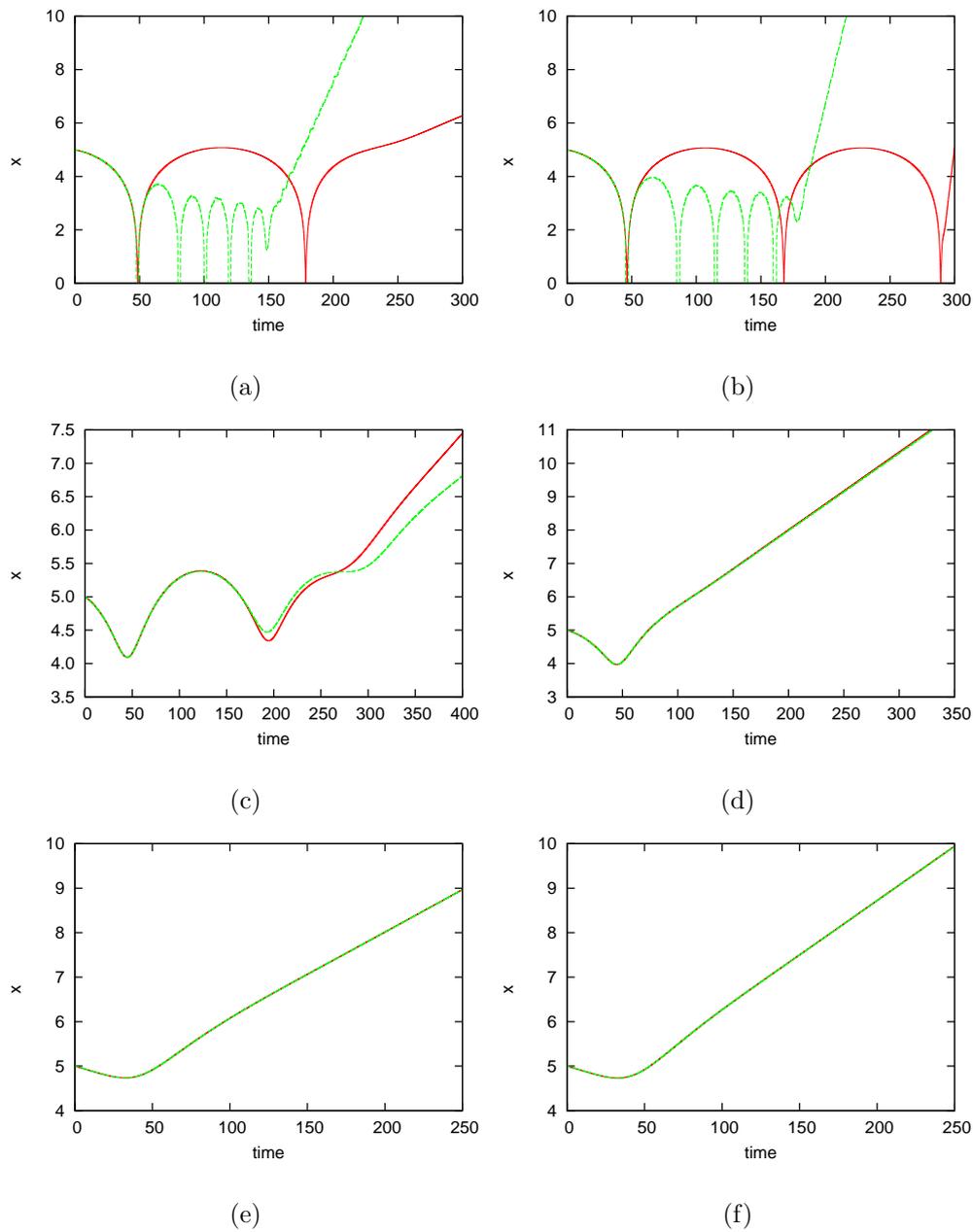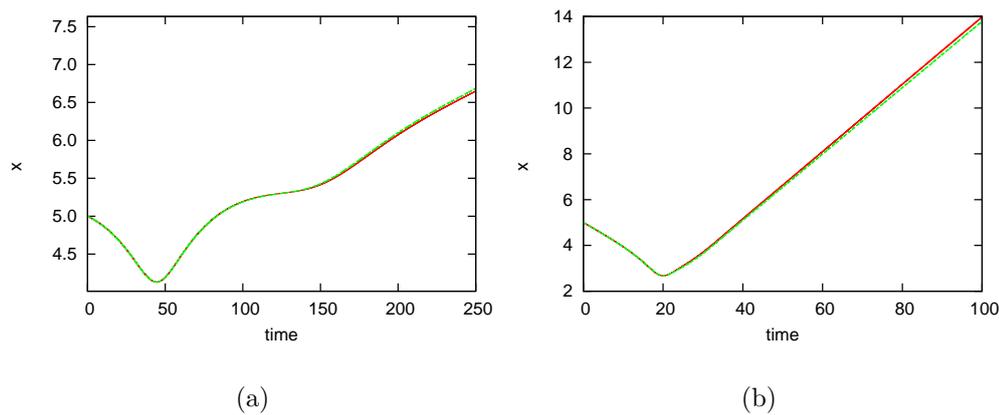
Figure 3.10: The distance of a soliton from the centre of mass of a system as a function of time. The system consists of two solitons initially placed at ± 5, with initial height/width parameter of 1 and the initial phase difference between them of $\delta = \frac{\pi}{4}$. For (a) the solitons have initial velocity $v = 0.01$ and $\epsilon = 0.1$, and for (b) the solitons have initial velocity $v = 0.1$ and $\epsilon = 0.3$. For each plot the solid line (red) is result of the collective coordinate approximation and the dashed line (green) is the result of the full simulation.

In figure 3.11 we present the plots of the time-integrated anomaly for each of the trajectories shown in figure 3.6. We note that the results are very similar for each method although not as exact as some of the trajectories. The time integrated anomalies are most different in the case $\delta = 0$ as the collective coordinate approximation shows a distinct peak when the solitons come together when compared to the results seen in the full simulation which displays only a minute deviation from zero at these points (of the order 10^{-7}). However, when the solitons are far apart the time-integrated anomaly does return to zero as predicted in [16] when δ is an integer value of π, as this corresponds to the case when the parity symmetry described in (3.1.13) is present. When δ is not an integer multiple of π this symmetry is not present and the integrated anomalies do not return to zero, and the collective coordinate method shows similar time-integrated anomalies to those found in the full simulation. This shows that, in addition to the trajectories, the collective coordinate approximation also does reproduce quite well the results for the anomalies obtained using the full numerical

method.

Conclusions for the modified NLS

In this chapter we have considered the applicability of the collective coordinate approximation to the description of the scattering of solitons in a deformation of the NLS model. The deformation of this model moves it away from being integrable, either completely or partially (the model becomes quasi-integrable for $\delta = n\pi$, $n \in \mathbb{Z}$). We considered a modified NLS for which the trajectories were already known from full simulations studied in [16]. Moreover, in [16], it was also suggested that quasi-integrability could be related to a particular symmetry of the field configurations (for configurations possessing the necessary symmetry the anomaly terms could vanish and so lead to quasi-integrability), so we looked at these properties using the collective coordinate approximation.

In the modified NLS the approximation works very well in the majority of cases and for a good range of initial conditions with a well chosen approximation ansatz. Comparing the results in the limit where the modified model reduces to the integrable NLS model, *i.e.* when $\epsilon = 0$, to the results we gained in chapter 2 we find that the improved ansatz (3.2.1) is indeed superior to the ansatz we used previously (2.3.1). Allowing the coordinates of each soliton to vary independently (which particularly allowed the phase difference between the two solitons to vary with time) lead to better agreement between the two methods for all initial conditions when $\epsilon = 0$.

The predominant influence on the accuracy of the approximation is the time the two solitons spend in close proximity of each other during their interaction; and for simulations where the solitons do not come closer together than the width of one soliton the collective coordinate approximation accurately reproduces the scattering of the solitons and their anomaly even for values of initial velocity up to $v = 0.2$. In these cases the trajectories, heights and phase difference of the solitons during their scattering, calculated using the collective coordinate approximation, are often indistinguishable from the those calculated using a full
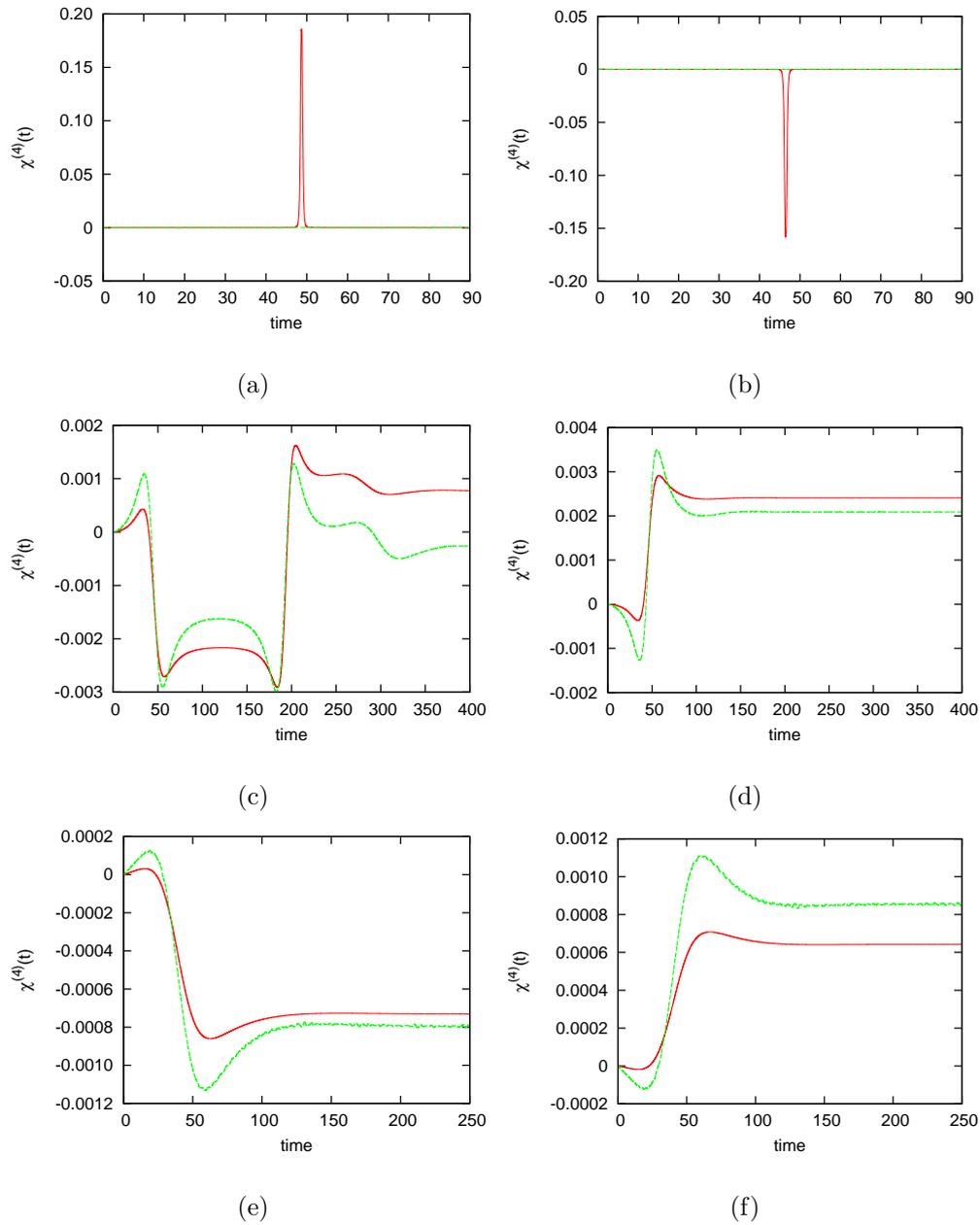
Figure 3.11: The time-integrated anomaly, $\chi^{(4)}(t)$, for the soliton interactions shown in figure 3.6 with $\delta = 0$ and (a) $\epsilon = 0.06$, (b) $\epsilon = -0.06$; $\delta = \frac{\pi}{4}$ and (c) $\epsilon = 0.06$, (d) $\epsilon = -0.06$; $\delta = \frac{\pi}{2}$ and (e) $\epsilon = 0.06$, (f) $\epsilon = -0.06$. For each plot the solid line (red) is result of the collective coordinate approximation and the dashed line (green) is the result of the full simulation.

numerical method. Moving the system away from integrability, *i.e.* increasing the deformation parameter ϵ, reduces the accuracy only slightly when the solitons stay far enough apart during their scattering and the results are very good for ϵ up to at least $\epsilon = 0.3$. For the vast majority of initial conditions the solitons maintain enough distance from each other during their interaction to ensure the accuracy of the approximation, and even show good qualitative agreement for the time-integrated anomalies.

When the solitons come closer together than the width of one soliton during their interaction the general behaviour of the solitons (trajectory, height and anomaly) is still reproduced but the accuracy of the approximation is reduced. We think this is probably because in the full simulation the solitons deform one another away from the form given by (3.2.1) when they are in close proximity. We have compared the waveforms given by the approximation and the full simulation when the solitons are far apart and when they come together, and have found that there is indeed some slight deformation as the solitons approach each other.

Another possible reason for the reduced accuracy is that, for $\epsilon \neq 0$, the full simulation can radiate out energy and the collective coordinate approximation does not allow this to happen. The collective coordinate ansatz can be adjusted to allow for the radiation of energy, see for example [44] and [45]. In order to model the radiation using the collective coordinate method a specific form for the radiation must be assumed, and the necessary computing time would be increased. Since we see a very small energy loss in most of our simulations the additional effort of modelling radiation using collective coordinates is unlikely to be worth the potential increase in the accuracy of the approximation.

These effects are exacerbated as the system moves away from integrability because the radiation/deformation effect increases with increasing ϵ.

The effect of quasi-integrability in the modified NLS is difficult to assess fully, as the collective coordinate approximation is incredibly reliable in the quasi-integrable case *i.e.* for the initial phase difference of $\delta = n\pi$ where n are odd integers. However, for the remaining initial values of the phase difference where the system is quasi-integrable ($\delta = n\pi$ for n even integers) the effect of the prox-

imity of the solitons (as discussed above) eclipses any effect of quasi-integrability on the accuracy of the approximation.

Chapter 4

The modified sine-Gordon model

So far we have looked at the scattering of solitons in modified NLS models, *i.e.* models in which the solitons are non-topological, and we have demonstrated the usefulness of using the collective coordinate approximation as a tool to investigate their properties. But one may ask if this is also the case for models which involve topological solitons; this is what we consider in this section. We base our discussion on the example of a modified sine-Gordon model previously studied in [17].

Modified sine-Gordon model

We consider the Lagrangian given by

$$L = \int dx \, \frac{1}{2} \left((\partial_t \psi)^2 - (\partial_x \psi)^2 \right) - V(\psi). \tag{4.1.1}$$

For the sine-Gordon potential $V = V_{SG} = \frac{1}{8} \sin^2(2\psi)$ there are static one-soliton solutions of the form

$$\psi = \arctan\left(e^{\pm(x-x_0)}\right). \tag{4.1.2}$$

A modification on this model was suggested in [17] by taking a change of variable $\psi \to \phi$ given by

$$\psi(\phi) = \frac{c\phi}{\sqrt{1 + \epsilon\phi(\phi - 2\gamma)}}, \tag{4.1.3}$$

which has two free parameters ϵ and γ, and the parameter c chosen to be

$$c = \sqrt{1 + \epsilon\pi\left(\frac{\pi}{4} - \gamma\right)}, \tag{4.1.4}$$

such that $\phi(\psi = 0) = 0$ and $\phi(\psi = \frac{\pi}{2}) = \frac{\pi}{2}$. The parameters ϵ and γ must be chosen such that $1 + \epsilon\pi\left(\frac{\pi}{4} - \gamma\right) > 0$ and $1 + \epsilon\phi\left(\phi - 2\gamma\right) > 0$. To ensure $\psi(\phi)$ is monotonous for $\phi \leqslant \frac{\pi}{2}$ we choose ϵ and γ such that $\epsilon\gamma < \frac{2}{\pi}$. The domain of (4.1.3) that we are interested in is $\psi = [-\frac{\pi}{2}, \frac{\pi}{2}]$. For our choice of ϵ and γ the range of (4.1.3) is $\phi = (-\infty, \frac{\pi}{2}]$.

Then ϕ, obtained by calculating $\phi = \phi(\psi)$ from (4.1.3) and using ψ given by (4.1.2), is a solution of the static Euler-Lagrangian equation associated to (4.1.1) with the potential

$$V(\phi) = \left(\frac{d\phi}{d\psi}\right)^2 V_{SG} = \frac{1}{8} \frac{(1 + \epsilon\phi\left(\phi - 2\gamma\right))^3}{c^2\left(1 - \epsilon\gamma\phi\right)^2} \sin^2\left(2\psi(\phi)\right). \tag{4.1.5}$$

In the case $\epsilon = 0$ the parameter γ becomes irrelevant and the potential (4.1.5) returns to the unperturbed sine-Gordon potential and $\phi = \psi$. For $\epsilon \neq 0$ and $\gamma = 0$ the model has the symmetry $\phi = -\phi$, while for $\epsilon, \gamma \neq 0$ there is no symmetry. This can be seen in figure 4.1 where we plot the potential as a function of ϕ for $\epsilon = 0.05$ and $\gamma = 0$ and $\gamma = 1$. By varying the parameters ϵ and γ the effects of this symmetry on the theory can be seen. Note that the topological charge of $\phi(\psi)$, for ψ given by (4.1.2), is conserved for any value of ϵ and γ within the constraints we have described. The construction of this modified model uses the procedure discussed in [46] which is a generalisation of the procedure discussed in [47].

The sine-Gordon model is an integrable model, and in a similar manner to the NLS case the equations of motion can be rewritten in terms of a zero curvature condition

$$\partial_+ A_- - \partial_- A_+ + [A_+, A_-] = 0, \tag{4.1.6}$$

with connection components

$$\begin{aligned} A_- &= \frac{1}{2}b_{-1} - \frac{i\omega}{2}\partial_-\phi F_0, \\ A_+ &= \frac{1}{2}\left(\omega^2 V - m\right)b_1 - i\omega\frac{dV}{d\phi}F_1, \end{aligned} \tag{4.1.7}$$
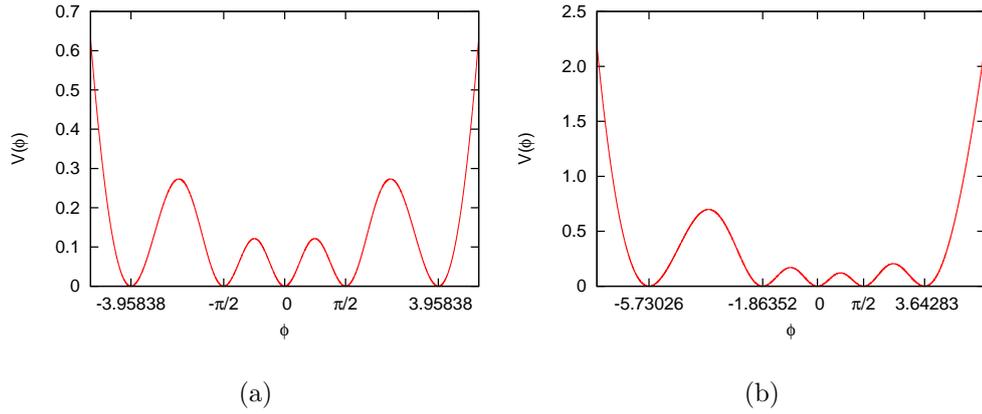
Figure 4.1: The modified potential $V(\phi)$ against ϕ for $\epsilon = 0.05$ and (a) $\gamma = 0$, (b) $\gamma = 1$.

for real parameters ω and m, and where the $SL(2)$ loop algebra generators b_n and F_n have commutation relations

$$\left[b_{2m+1}, F_{2n+1}\right] = -2F_{2(m+n+1)}, \qquad \left[b_{2m+1}, F_{2n}\right] = -2F_{2(m+n)+1},$$

$$\left[F_{2m+1}, F_{2n}\right] = -2b_{2(m+n)+1}.$$

Here we have used light-cone coordinates

$$x_{\pm} = \frac{1}{2}(t \pm x) \quad \text{with} \quad \partial_{\pm} = \partial_t \pm \partial_x \quad \text{and} \quad \partial_+\partial_- = \partial_t^2 - \partial_x^2 \equiv \partial^2. \qquad (4.1.8)$$

From the zero curvature condition an infinite number of conserved quantities can be derived via the abelianization procedure, similar to the NLS integrable model.

For the sine-Gordon model with a general potential there is an anomalous zero curvature condition

$$\partial_+ A_- - \partial_- A_+ + [A_+, A_-] = \tilde{X}F_1 - \frac{i\omega}{2}\left(\partial^2\phi + \frac{\partial V}{\partial \phi}\right)F_0, \qquad (4.1.9)$$

with the connection components as in (4.1.7) and $\tilde{X}$ equal to

$$\tilde{X} = \frac{i\,\omega}{2}\partial_-\phi\left[\frac{d^2V}{d\phi^2} + \omega^2 V - m\right]. \qquad (4.1.10)$$

When the equation of motion is satisfied the right hand side of the anomalous zero curvature condition proportional to F_0 vanishes, and when the potential is taken to be the sine-Gordon potential $\tilde{X}$ also vanishes for the choice of parameters

$\omega = 4$ and $m = 1$, and the system is integrable. With a general potential we can apply the abelianization procedure as in [17], gauge transforming the anomalous zero curvature condition and making use of the grading operator of the algebra, to obtain equations of the form

$$\partial_t \tilde{a}_x^{(2n+1)} - \partial_x \tilde{a}_t^{(2n+1)} = \tilde{X} \tilde{\alpha}^{(2n+1)} \qquad n = 0, 1, 2, ..., \qquad (4.1.11)$$

(the first few expressions of $\tilde{\alpha}^{(2n+1)}$ are given in appendix A.1.2). Integrating over space gives

$$\int_{-\infty}^{\infty} dx \, \partial_t \tilde{a}_x^{(2n+1)} - \tilde{a}_t^{(2n+1)}(x = \infty) + \tilde{a}^{(2n+1)}(x = -\infty) = \int_{-\infty}^{\infty} dx \, \tilde{X} \tilde{\alpha}^{(2n+1)},$$
$$(4.1.12)$$

for $n = 0, 1, 2, ...$. When $\tilde{a}_t^{(2n+1)}$ satisfies the boundary conditions $\tilde{a}_t^{(2n+1)}(x = \infty) = \tilde{a}_t^{(2n+1)}(x = -\infty)$ we have an infinite number of anomalous charges

$$\tilde{Q}^{(2n+1)} = \int_{-\infty}^{\infty} dx \, \tilde{a}_x^{(2n+1)}, \qquad (4.1.13)$$

which gives us an infinite number of anomalous conservation laws

$$\frac{d\tilde{Q}^{(2n+1)}}{dt} = \tilde{\beta}^{2n+1}; \qquad \text{with} \quad \tilde{\beta}^{(2n+1)} = \int_{-\infty}^{\infty} dx \, \tilde{X} \, \tilde{\alpha}^{(2n+1)}. \qquad (4.1.14)$$

When the potential is taken to be the sine-Gordon potential $\tilde{X}$ is zero, and we have an infinite number of conserved charges.

If the field configuration transforms under the parity defined in (1.2.1) as

$$P(\phi) = -\phi + \text{const.}, \qquad (4.1.15)$$

and if the potential evaluated on such a solution is even under the parity, *i.e.*

$$P(V) = V, \qquad (4.1.16)$$

then it follows that

$$\int_{-\tilde{t}_0}^{\tilde{t}_0} dt \int_{-\tilde{x}_0}^{\tilde{x}_0} dx \, \tilde{X} \tilde{\alpha}^{(2n+1)} = 0, \qquad (4.1.17)$$

where $\tilde{t}_0$ and $\tilde{x}_0$ are given fixed values of the shifted time and space coordinates $\tilde{t}$, $\tilde{x}$ introduced in (1.2.1). Taking $\tilde{x}_0 \to \infty$ the anomalous charges satisfy the following time-symmetry around the point t_Δ

$$Q^{(2n+1)}(t = \tilde{t}_0 + t_\Delta) = Q^{(2n+1)}(t = -\tilde{t}_0 + t_\Delta) \qquad n = 0, 1, 2, ... \qquad (4.1.18)$$

Now taking $\tilde{t}_0 \to \infty$ we have an infinite set of conserved quantities which are conserved asymptotically, *i.e.*

$$Q^{(2n+1)}(t = +\infty) = Q^{(2n+1)}(t = -\infty). \qquad (4.1.19)$$

To summarise: this modified model, when $\epsilon = 0$, becomes the sine-Gordon model, therefore the system is integrable and has an infinite number of conserved quantities. When $\epsilon \neq 0$ and $\gamma = 0$ then the field configuration and potential transform under the parity described in (1.2.1) as in (4.1.15) and (4.1.16); therefore the system is quasi-integrable and possesses an infinite number of asymptotically conserved charges. When $\epsilon \neq 0$ and $\gamma \neq 0$ then the symmetries necessary for quasi-integrability are not present; the system is non-integrable and there are no constraints on the charges.

The two-soliton configuration for modified sine-Gordon

As in the NLS case we construct an appropriate two-soliton ansatz for the sine-Gordon in the collective coordinate approximation by patching together two one-kink solutions. We do this in the following way:

$$\tan(\psi) = e^{(x-a)} - e^{-(x+a)} = 2\sinh(x)\, e^{-a}, \qquad (4.2.1)$$

where a is our collective coordinate. When a is large (4.2.1) represents two well separated kinks; one placed at $-a$ whose field varies between $[-\frac{\pi}{2}, 0]$ and one placed at a which varies between $[0, \frac{\pi}{2}]$. For energetic reasons it must be that $a > 0$ for all times. This ansatz was used in [24] to test the collective coordinate approximation for the scattering of sine-Gordon kinks and was found to work remarkably well, so our ansatz for our modified sine-Gordon model will be based on a generalisation of this ansatz.

To construct a modified approximation ansatz we perform the change of vari-

able as in (4.1.3), for ψ given by (4.2.1), to get

$$\phi = \frac{\psi^2 \epsilon \gamma + \sqrt{\psi^2 c^2 + \psi^4 \epsilon \left(-1 + \gamma^2 \epsilon\right)}}{\psi^2 \epsilon - c^2} \qquad \text{for } x < 0, \qquad (4.2.2)$$

$$\phi = \frac{\psi^2 \epsilon \gamma - \sqrt{\psi^2 c^2 + \psi^4 \epsilon \left(-1 + \gamma^2 \epsilon\right)}}{\psi^2 \epsilon - c^2} \qquad \text{for } x > 0,$$

and take this as our two soliton ansatz for the Euler-Lagrange equation associated to (4.1.1) with the potential given by (4.1.5). This ansatz returns to the ansatz for the unmodified sine-Gordon in the case $\epsilon = 0$. For $\epsilon \neq 0, \gamma = 0$ the kinks are altered but the potential retains the symmetry $V(\phi) = V(-\phi)$, whereas for $\epsilon \neq 0, \gamma \neq 0$ this symmetry is lost due to the shift in the vacua which can be seen in figure 4.1(b).

Implementing the approximation in modified sine-Gordon

We substitute our approximation ansatz (4.2.2) into the Lagrangian (4.1.1) (with the change of variable (4.1.3) and modified potential (4.1.5)) to find our effective Lagrangian:

$$L = \frac{g(a)}{2} \dot{a}^2 - V(a), \qquad (4.2.3)$$

where the dot refers to a differentiation with respect to time. The expression for $g(a)$ is given by (remembering the definition of c given by (4.1.4))

$$g(a) = 4e^{2a} c^4 \int_{\infty}^{\infty} dx \frac{A(x,a)}{B(x,a)}, \qquad (4.2.4)$$

where

$$A(x,a) = \sinh^2(x) \left(-2c^2 \epsilon \tan^{-1} \left(2e^{-a} \sinh(x)\right)^2 \left(\alpha \left(1 - 4\gamma^2 \epsilon\right) + 2\gamma c^2\right)\right.$$

$$+ \epsilon^2 \tan^{-1} \left(2e^{-a} \sinh(x)\right)^4 \left(\alpha \left(8\gamma^2 \epsilon \left(\gamma^2 \epsilon - 1\right) + 1\right) + 4\gamma c^2 \left(2 - 3\gamma^2 \epsilon\right)\right)$$

$$\left. - 4\gamma \epsilon^3 \left(\gamma^2 \epsilon \left(2\gamma^2 \epsilon - 3\right) + 1\right) \tan^{-1} \left(2e^{-a} \sinh(x)\right)^6 + \alpha c^4\right), \quad (4.2.5)$$

$$B(x,a) = \alpha \left(e^{2a} + 4\sinh^2(x)\right)^2 \left(c^2 - \epsilon \tan^{-1} \left(2e^{-a} \sinh(x)\right)^2\right)^4$$

$$\times \left(\epsilon \left(\gamma^2 \epsilon - 1\right) \tan^{-1} \left(2e^{-a} \sinh(x)\right)^2 + c^2\right). \quad (4.2.6)$$

Moreover, $V(a)$ is:

$$V(a) = 2e^{2a}c^4 \int_\infty^\infty dx \frac{C(x,a)}{D(x,a)}, \qquad (4.2.7)$$

where $C(x,a)$ and $D(x,a)$ are given by:

$$C(x,a) = \cosh(2x) \left(c^2 \tan^{-1}\left(2e^{-a}\sinh(x) \right)^2 \left(4\alpha\gamma\epsilon \left(3 - 8\gamma^2\epsilon \right) + 3c^2 \left(6\gamma^2\epsilon - 1 \right) \right) \right.$$
$$+\epsilon \left(\epsilon \tan^{-1}\left(2e^{-a}\sinh(x) \right)^4 \left(c^2 \left(12\gamma^2\epsilon(4\gamma^2\epsilon - 3) + 3 \right) - 2\alpha\gamma\epsilon \left(4\gamma^2\epsilon - 3 \right) \left(4\gamma^2\epsilon - 1 \right) \right) \right.$$
$$\left. \left. +\epsilon^2 \left(2\gamma^2\epsilon - 1 \right) \left(16\gamma^2\epsilon \left(\gamma^2\epsilon - 1 \right) + 1 \right) \tan^{-1}\left(2e^{-a}\sinh(x) \right)^6 - 6\alpha c^4\gamma \right) + c^6 \right),$$

$$(4.2.8)$$

$$D(x,a) = \left(e^{2a} + 4\sinh^2(x) \right)^2 \left(c^2 - \epsilon \tan^{-1}\left(2e^{-a}\sinh(x) \right)^2 \right)^4 \left(-\alpha\gamma\epsilon \right.$$
$$\left. +\epsilon \left(\gamma^2\epsilon - 1 \right) \tan^{-1}\left(2e^{-a}\sinh(x) \right)^2 + c^2 \right)^2. \quad (4.2.9)$$

For the clarity of the expressions we have introduced and defined α to be:

$$\alpha \equiv \sqrt{c^2 \tan^{-1}\left(2e^{-a}\sinh(x) \right)^2 + \epsilon \left(\gamma^2\epsilon - 1 \right) \tan^{-1}\left(2e^{-a}\sinh(x) \right)^4}. \qquad (4.2.10)$$

When $\epsilon = 0$ and $\gamma = 0$ the expressions for $g(a), V(a)$ revert to those given in [24].

From the Lagrangian (4.2.3) we derive the equation of motion

$$g\ddot{a} + \frac{1}{2}\frac{dg}{da}\dot{a}^2 + \frac{dV}{da} = 0, \qquad (4.2.11)$$

which we solve using a 4th order Runge-Kutta method (for details on the numerics see section 1.4).

Results for sine-Gordon

First we analyse the scattering of our two kinks for the case $\epsilon = 0$ which corresponds to the integrable sine-Gordon model. We compare the trajectories of the kinks as determined using the collective coordinate approximation and using the full numerical simulation for a range of initial velocities $v = \dot{a}(0)$ in order to determine the effective range of validity of our choice of approximation ansatz.

In figure 4.2 we compare the trajectories of the kinks initially placed at $a = 10$ and with initial approach velocities of $v = 0.3$ and $v = 0.6$ (note that the speed

Figure 4.2: The distance of a soliton from the centre of mass of a system as a function of time. The system consists of two solitons initially with $a = 10$ and $\epsilon = 0$, with an initial velocity towards the centre of mass of (a) $v = 0.3$ and (b) $v = 0.6$. For each plot the solid line (red) is result of the collective coordinate approximation and the dashed line (green) is the result of the full simulation (these may be indistinguishable).

of light is $c = 1$). We see that in the integrable system the collective coordinate approximation with our choice of ansatz gives excellent qualitative agreement with the full numerical simulation up to a high velocity, with percentage difference in soliton positions after collision of 0.21% for $v = 0.3$ at $t = 100$ and 0.44% for $v = 0.6$ at $t = 50$. This gives us confidence in our modified approximation ansatz as applied to our modified model.

Results for modified sine-Gordon

Now we consider the scattering of solitons when the system is no longer integrable, *i.e.* for $\epsilon \neq 0$, and analyse the scattering of the two kinks for various values of the parameters ϵ and γ (within the constraints described in section 4.1). For each set of values we compare the trajectories of the solitons calculated using the collective coordinate approximation with those using the full numerical simulation, and in each simulation we take the initial positions of the solitons corresponding to $a(0) = 10$. In the collective coordinate approximation the positions of the kinks are equivalent to $\pm a$ when $\epsilon = 0$, but when $\epsilon \neq 0$ the two are no longer equivalent. The location can be taken to be the position of the maximum of the energy peak,

though when the solitons come close together this is not always well defined. Alternatively, the location can be determined by the position where the soliton takes half of its maximum value. We compare the location determined by both of these definitions and find that they coincide where they are both well defined. Therefore we take the position of the soliton to be where it takes half of its maximum value.

In figure 4.3 we present a series of plots of trajectories for solitons sent together with an initial velocity of $v = 0.3$ for different values of ϵ and γ. From these plots we can see that the two approaches show excellent agreement when the symmetry necessary for quasi-integrability is present, *i.e.* when $\epsilon \neq 0$ and $\gamma = 0$, and the percentage difference in soliton positions at $t = 100$ is 0.21% for $\epsilon = -0.2$, 0.43% for $\epsilon = 0.4$, and 0.78% for $\epsilon = 1$. However, when the system moves away from quasi-integrability, *i.e.* $\epsilon \neq 0$ and $\gamma \neq 0$, the two methods show good agreement as the solitons approach each other but the solitons scatter at slightly different distances and with different velocities (though these differences are fairly small). This suggests that quasi-integrability is a sufficient condition for the collective coordinate approximation to accurately model trajectories of kinks in modified sine-Gordon systems.

We also consider the quasi-conservation of the first non-trivial charge beyond the energy itself, namely, $\tilde{Q}^{(3)}(t)$ defined in (4.1.14) by calculating both the anomaly $\tilde{\beta}^{(3)}$ and the time integrated anomaly which is given by:

$$\tilde{\chi}^{(3)} = -\frac{1}{2} \int_{t_0}^{t} dt'\, \tilde{\beta}^{(3)} = 4 \int_{t_0}^{t} dt' \int_{-\infty}^{\infty} dx\, \partial_- \phi\, \partial_-^2 \phi \left[\frac{d^2 V}{d\phi^2} + 16V - 1 \right], \quad (4.4.12)$$

where $\partial_- = \partial_t - \partial_x$ and t_0 is the initial time of the simulation which is usually taken to be zero.

Figure 4.4 is the plot of the time-integrated anomaly as a function of time for solitons placed at $a = 20$ with initial velocity $v = 0.05$, with $\epsilon = 0.000001$ and various values of γ. Notice that in the full simulation the time-integrated anomaly is always slowly increasing prior to the scattering of the solitons and slowly decreasing after the scattering; this is due to slight fluctuations away from zero in the anomaly which by itself is probably a result of numerical errors rather than any physical effect. This error increases as ϵ increases and so it becomes
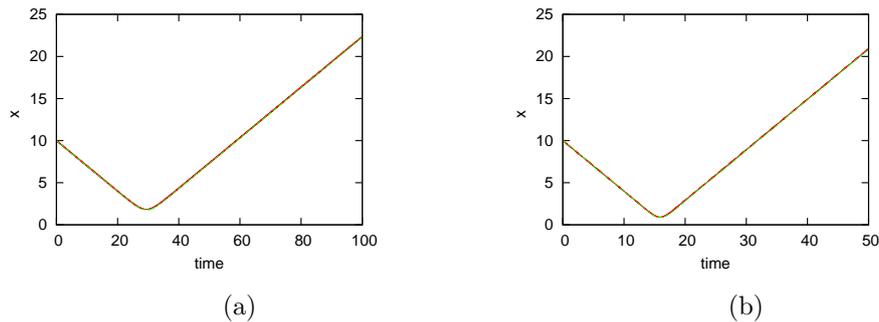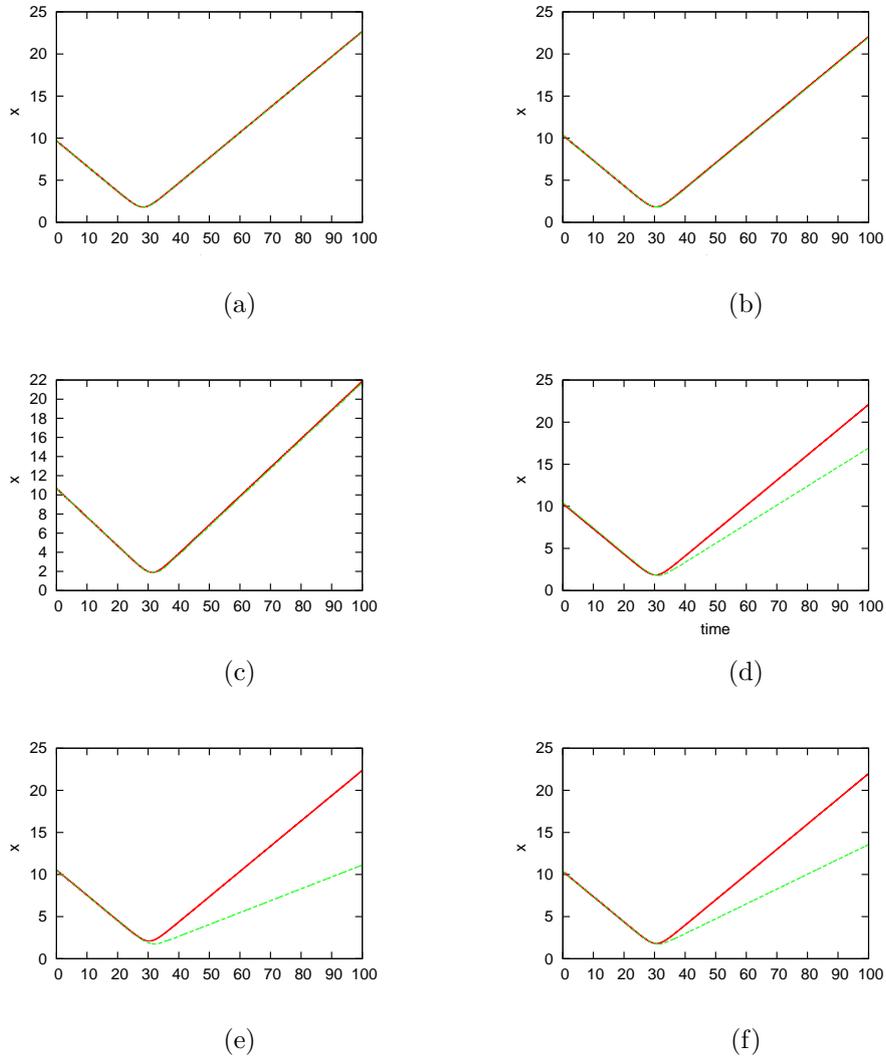
Figure 4.3: The distance of a soliton from the centre of mass of a system as a function of time. The system consists of two solitons initially with $a = 10$, each with an initial velocity of 0.3 towards the centre of mass. Initial parameter are (a) $\epsilon = -0.2$, $\gamma = 0$; (b) $\epsilon = 0.4$, $\gamma = 0$; (c) $\epsilon = 1$, $\gamma = 0$; (d) $\epsilon = 0.4$, $\gamma = 0.1$; (e) $\epsilon = 0.4$, $\gamma = 0.2$; and (f) $\epsilon = 0.4$, $\gamma = -0.2$. For each plot the solid line (red) is result of the collective coordinate approximation and the dashed line (green) is the result of the full simulation (for (a), (b) and (c) these are indistinguishable).

difficult to compare the results, this is why we present plots only for a small value of ϵ. We see that when γ is small the collective coordinate approximation and the full simulation are in excellent agreement, and far away from the scattering the time-integrated anomaly is close to zero, as expected, when γ is small and the model is close to the symmetry described in (4.1.15) and (4.1.16). When γ is taken further from zero we move from a model with approximate symmetry to a model where this symmetry is broken. This is confirmed by our results as seen in figure 4.4 which show that the further γ is from zero the further the time-integrated anomaly is from zero after the scattering of the solitons. Moreover, the figures 4.4(b) and 4.4(e) show that the symmetry can be broken in either direction depending on the sign of γ, with the time-integrated anomaly (calculated using the approximation) being close to $\tilde{\chi}^{(3)} \mp 4 \times 10^{-8}$ for $\gamma = \pm 0.002$ a long time after the solitons interact. The collective coordinate approximation still gives a good qualitative approximation to the behaviour of the time-integrated anomaly as we move away from the symmetric case, though the values are not exactly the same as seen in full simulations. These observations have been checked for several values of ϵ.

Conclusions for modified sine-Gordon

In this chapter we have considered the applicability of the collective coordinate approximation to a modified sine-Gordon model with two deformation parameters γ and ϵ, variation of these parameters changes the integrability properties of the system. The system is either integrable ($\epsilon = 0$), quasi-integrable ($\epsilon \neq 0$ and $\gamma = 0$) or non integrable ($\epsilon \neq 0$ and $\gamma \neq 0$).

We find that the approximation very accurately describes the trajectories and anomalies of scattering kinks when the system is either integrable or quasi-integrable (*i.e.* $\gamma = 0$) up to initial velocities of $v = 0.6$ and for values of up to $\epsilon = 1$. However, when the field configuration moves away from the symmetry necessary for quasi-integrability (*i.e.* when γ moves away from 0) the collective coordinate approximation becomes less accurate for both the trajectories and the
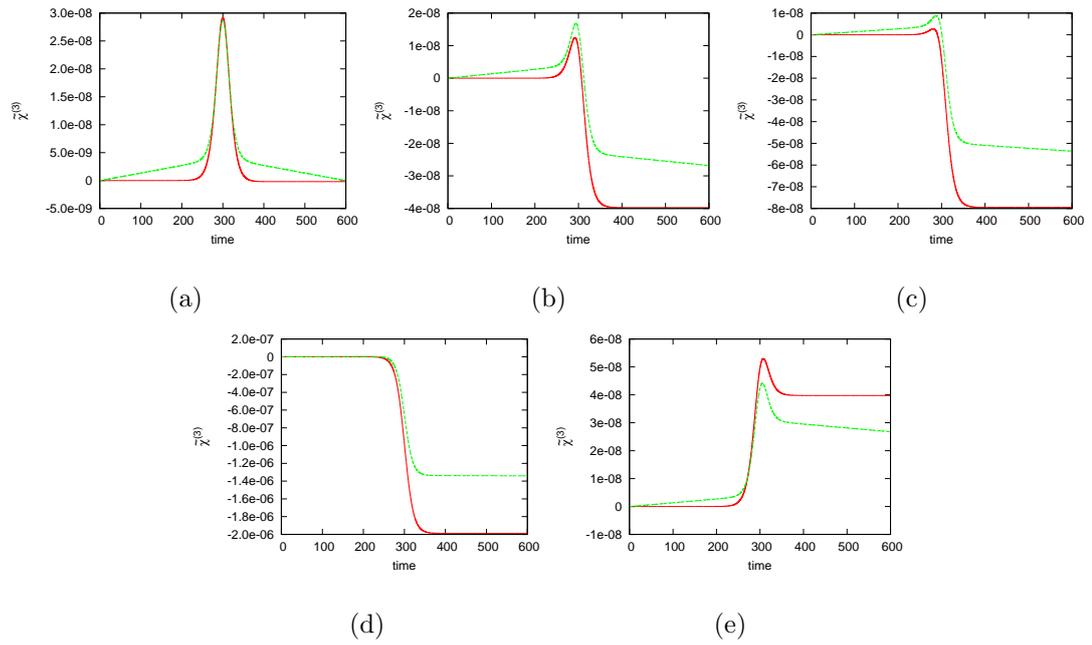
Figure 4.4: The time-integrated anomaly for solitons initially with $a = 20$ with velocity 0.05 towards the centre of mass and $\epsilon = 0.000001$. γ is chosen to be (a) $\gamma = 0.00001$, (b) $\gamma = 0.002$, (c) $\gamma = 0.004$, (d) $\gamma = 0.1$ and (e) $\gamma = -0.002$. The solid lines (red) are the results for the collective coordinate approximation and the dashed lines (green) are results for the full simulation.

anomalies. In this model the presence of the symmetries necessary for quasi-integrability seem to be a sufficient condition to ensure accuracy.

Chapter 5

The double sine-Gordon model

In the previous chapter we considered a modified sine-Gordon model with deformation parameters ϵ and γ which moved the model away from integrability in a controlled way. In this chapter we consider the double sine-Gordon model as this model allows us to vary smoothly between two integrable sine-Gordon models. Kink-antikink interactions in the double sine-Gordon model have already been considered in several papers [48], [49], [50], [51] and the collective coordinate approximation has been applied to double sine-Gordon kinks interacting with kinks [52] and with an external potential [53]. Here we have investigated the interactions between kinks in the double sine-Gordon model using the collective coordinate approximation and a full numerical method, considering a range of initial parameters and how this affects the integrability properties of the model.

Double sine-Gordon model

We consider the Lagrangian

$$\mathcal{L} = \int dx \left[\left(\frac{\partial \psi}{\partial t} \right)^2 - \left(\frac{\partial \psi}{\partial x} \right)^2 - \lambda_0^2 \sin^2(\psi) - \frac{A_0^2}{4} \sin^2(2\psi) \right], \qquad (5.1.1)$$

where λ_0 and A_0 are real parameters. When λ_0 or A_0 vanishes the model reduces to the sine-Gordon model.

The equations of motion are

$$\frac{\partial^2 \psi}{\partial t^2} - \frac{\partial^2 \psi}{\partial x^2} + \frac{\lambda_0^2}{2} \sin(2\psi) + \frac{A_0^2}{4} \sin(4\psi) = 0. \tag{5.1.2}$$

We expect a kink shaped solution so to find a one soliton solution we rewrite ψ in the form

$$\psi = 2 \tan^{-1}\left(\sqrt{u}\right), \tag{5.1.3}$$

and find that this solves the equation of motion when

$$u = \frac{e^{-2\theta}}{2\left(A_0^2 + \lambda_0^2\right)} \left(2A_0^2 e^{2\theta} + \lambda_0^2 \left(1 + e^{4\theta}\right) + \nu W\right), \tag{5.1.4}$$

where for convenience we have defined

$$W = \sqrt{-4\left(A_0^2 + \lambda_0^2\right)^2 e^{4\theta} + \left(2A_0^2 e^{2\theta} + \lambda_0^2 \left(1 + e^{4\theta}\right)\right)^2},$$
$$\theta = (x + x_0 + tv)\sqrt{A_0^2 + \lambda_0^2}. \tag{5.1.5}$$

Here $\nu = -1$ for $x < x_0 + vt$ and $\nu = 1$ for $x > x_0 + vt$. It should be noted that in the construction of this solution we have assumed that $\lambda_0 \neq 0$, so we cannot take this solution to the limit of the integrable sine-Gordon in that direction (if you take $\lambda_0 = 0$ then u loses its dependence on x). However, we can take $\lambda_0 = 0$ in the equations of motion (5.1.2) and repeat the construction to find the usual sine-Gordon kink solution). We can take $A_0 = 0$ in u directly and in this limit the solution becomes the usual sine-Gordon kink: $\psi = 2 \tan^{-1}\left(e^{(x+x_0+vt)\lambda_0}\right)$.

To demonstrate how varying the parameters A_0, λ_0 affects the system we have plotted the potential and our one-soliton solution for $x_0 = 10$ at various values of A_0 and λ_0 in figure 5.1. For $A_0 \to 0$ and $\lambda_0 = $ constant $\neq 0$ the Lagrangian (5.1.1) becomes the sine-Gordon Lagrangian whose potential has minima at $\psi = n\pi$ and the soliton becomes the sine-Gordon kink, see figures 5.1(a),(b). When A_0 and λ_0 are both non-zero and of a similar value the maxima of the potential broadens out, and as λ_0 decreases this develops into a new minima at $\psi = (n + \frac{1}{2})\pi$ and the solution starts to split into sub-kinks, see figures 5.1(c),(d). Then for $\lambda_0 \to 0$ and $A_0 = $ constant $\neq 0$ the Lagrangian becomes the sine-Gordon Lagrangian whose potential has minima at $\psi = (n + \frac{1}{2})\pi$ and kink effectively splits into two independent kinks, see figures 5.1(e),(f).
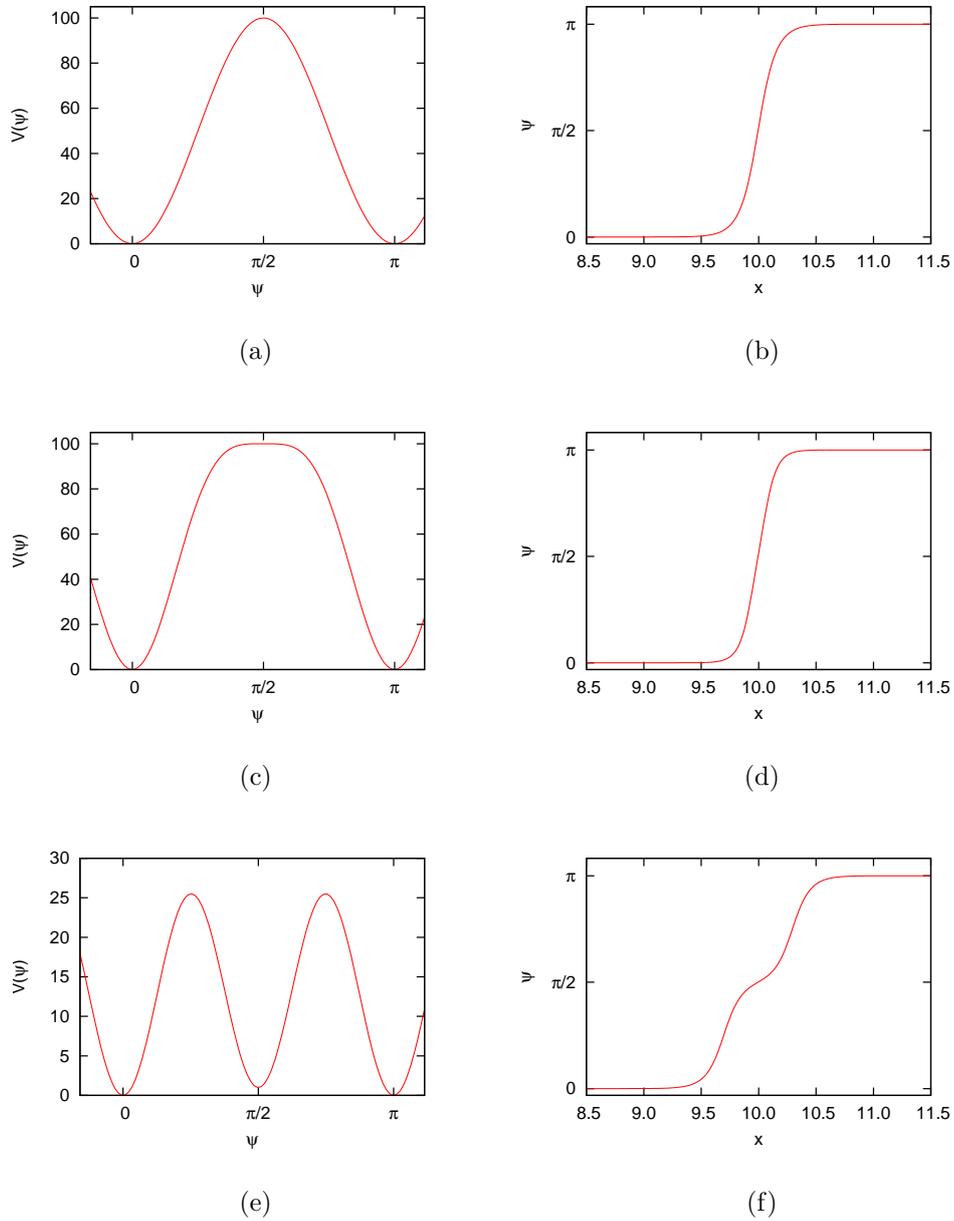
Figure 5.1: On the left the potential $V(\psi)$ for various values of the parameters A_0 and λ_0 and on the right the corresponding one double sine-Gordon kink ψ centred at $x_0 = 10$. The values are $A_0 = 1$, $\lambda_0 = 10$ for (a) and (b); $A_0 = 10$, $\lambda_0 = 10$ for (c) and (d); $A_0 = 10$, $\lambda_0 = 1$ for (e) and (f).

The double sine-Gordon model can be considered to be a modified sine-Gordon with a Lagrangian as in (4.1.1) with the potential $V = V_{DSG} = 2\lambda_0^2\sin^2(\psi) + \frac{A_0^2}{2}\sin^2(2\psi)$. We can then use the same arguments that we employed in chapter 4 to construct anomalous conserved charges for this model as given in (4.1.13), but now with the potential taken to be V_{DSG} and with different choices for the parameters ω and m contained in the anomalous conserved charges and first introduced in the connection components (4.1.7). When $\lambda_0 = 0$ the model reduces to a sine-Gordon model with $V = \frac{A_0^2}{2}\sin^2(2\psi)$, and when the parameters ω and m are chosen to be $\omega = 4$ and $m = 4A_0^2$ we find that $\tilde{X}$ (given in (4.1.10)) vanishes, then we have a zero curvature connection and therefore an infinite number of conserved charges as the model is integrable. When $A_0 = 0$ the model reduces to a sine-Gordon model with $V = 2\lambda_0^2\sin^2(\psi)$, and with the parameters chosen to be $\omega = 2$ and $m = 4\lambda_0^2$ then $\tilde{X}$ vanishes and again we have a zero curvature connection and an infinite number of conserved charges.

In a similar manner to the modified sine-Gordon, when the potential V and the field configuration ψ transform under the parity P defined in (1.2.1) as

$$P(\psi) = -\psi + \text{const.} \qquad P(V) = V, \tag{5.1.6}$$

then the anomalous charges are conserved asymptotically and the system is quasi-integrable.

For two interacting solitons we take

$$\psi = 2\tan^{-1}\left(\sqrt{u(x + x_0 + vt)}\right) + 2\tan^{-1}\left(\sqrt{u(-x + x_0 + vt)}\right) - \pi,$$

(this is discussed in more detail in the next section), and it is clear from this that the field configuration ψ does transform as in (5.1.6) under the parity P (1.2.1), (recalling that the sign dependence of W in (5.1.4) will change). From this it is also easy to see that the potential V_{DSG} transforms as in (5.1.6) under the parity P. Therefore we have the symmetries necessary for quasi-integrability and we expect the anomalous charges to be asymptotically conserved for any values of A_0 and λ_0, and completely conserved when one or other of A_0 and λ_0 is zero as the system is then integrable.

The two-soliton configuration for double sine-Gordon

We construct an appropriate two-soliton ansatz for the double sine-Gordon in the collective coordinate approximation by patching together two one-kink solutions in the following way:

$$\psi = 2\tan^{-1}\left(\sqrt{u(x+a)}\right) + 2\tan^{-1}\left(\sqrt{u(-x+a)}\right) - \pi \qquad (5.2.1)$$

where $a = x_0 + vt$ is one of our collective coordinates. When a is large (5.2.1) represents two well separated double sine-Gordon kinks centred at $\pm a$, and for energetic reasons it must be that $a > 0$ for all times.

From a previous study of kink-kink collisions in the double sine-Gordon [52] we know that the distance between the sub-kinks can change with time. Therefore, we also take A_0 and λ_0 within the solution (5.2.1) to be collective coordinates, *i.e.* we allow them to vary with time. To discriminate between these coordinates and A_0, λ_0 appearing in the Lagrangian (5.1.1) from now on we refer to them as A and λ, and naturally we always take $A(0) = A_0$ and $\lambda(0) = \lambda_0$.

Implementing the approximation in double sine-Gordon

We proceed with the collective coordinate approximation as in previous chapters by inserting our approximation ansatz (5.2.1) into the Lagrangian (5.1.1) to obtain an effective Lagrangian of the form:

$$\mathcal{L} = \left(I_a\dot{a} + I_A\dot{A} + I_\lambda\dot{\lambda}\right)^2 - V, \qquad (5.2.2)$$

where the dot denotes differentiation with respect to time; and the I's and V are functions of $a(t)$, $A(t)$, and $\lambda(t)$. Explicit expressions of $I_{a,A,\lambda}$ and V are given in appendix A.5.

From this effective Lagrangian we derive equations of motion as a set of coupled ODEs of the form:

$$\ddot{a}2I_aI_q + \ddot{A}2I_AI_q + \ddot{\lambda}2I_\lambda I_q + H_q(a, \dot{a}, A, \dot{A}, \lambda, \dot{\lambda}) = 0, \qquad (5.2.3)$$

for $q = a, A, \lambda$, and H_q a function of the coordinates and their first derivative with time. We decouple these equations and solve them using the 4th order Runge-Kutta method (for details on the numerics see section 1.4).

Results for double sine-Gordon

We consider the trajectories for double sine-Gordon kinks as they scatter, comparing the results for the full numerical simulation and the collective coordinate approximation. In each simulation we start the solitons at $x_0 = 10$ and send them towards the centre of mass with an initial velocity $\dot{a}(0) = 0.1$ so that they interact. As A_0 and λ_0 always appear squared we take, without loss of generality, $A_0 > 0$ and $\lambda_0 > 0$ throughout. When $\frac{\lambda_0}{A_0} < 1$ the initial solution for the double sine-Gordon soliton starts to separate into sub-kinks, and in this case we also investigate the trajectories of the sub-kinks and the distance between them, which we denote as d, as the solitons collide.

In figure 5.2 we have plotted the trajectories of the double sine-Gordon kinks as they collide for a range of values of A_0 and λ_0, calculated using the collective coordinate approximation and using the full numerical simulation. We find that the trajectories calculated using each method are virtually indistinguishable for all the values of A_0 and λ_0 that we have run simulations for. This can be seen by considering the plots in figure 5.2, so the collective coordinate approximation is accurate in the double sine-Gordon model. We observed in chapter 4 that in a modified sine-Gordon model the presence of the symmetries necessary for quasi-integrability are sufficient for the collective coordinate approximation to be accurate, and as we have determined that for all values of A_0 and λ_0 the double sine-Gordon system is quasi-integrable it is not surprising that we find that the approximation is accurate for all values of A_0 and λ_0.

For $\frac{\lambda_0}{A_0} \geqslant 1$ our initial two soliton solution looks like two sine-Gordon kinks, see figure 5.1, and the trajectory of the collision is similar to those of the sine-Gordon kinks, *i.e.* the kinks travel towards each other with the initial velocity $\dot{a}(0)$ and when they come close together they repel and travel away from each other with
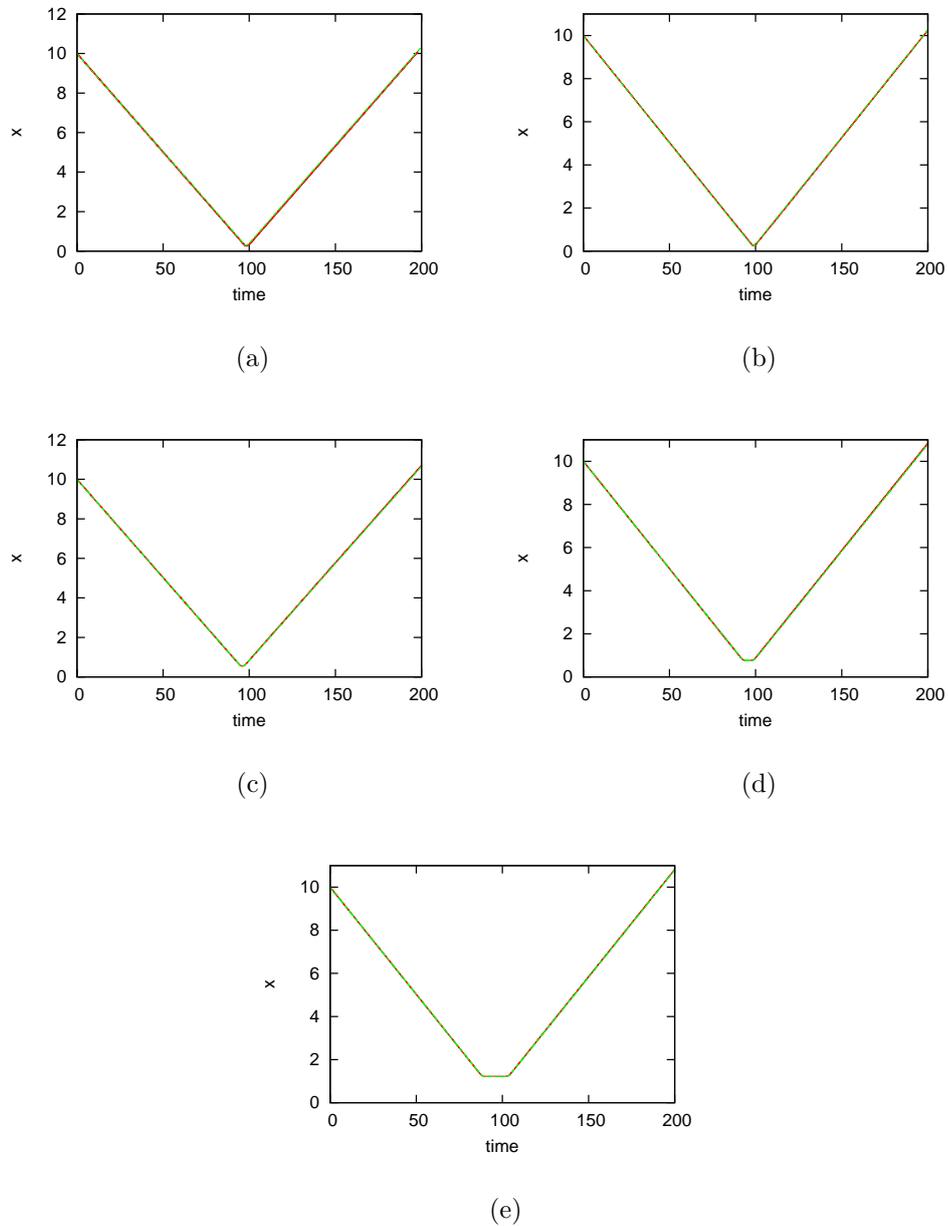
Figure 5.2: Trajectories of the colliding double sine-Gordon kinks for various values of A_0 and λ_0. The solid line (red) corresponds to the results of the collective coordinate approximation and the dashed line (green) corresponds to the results for the full numerical simulation, and the values of A_0, λ_0 are (a) $A_0 = 0$, $\lambda_0 = 10$; (b) $A_0 = 10$, $\lambda_0 = 10$; (c) $A_0 = 10$, $\lambda_0 = 1$; (d) $A_0 = 10$, $\lambda_0 = 0.1$; and (e) $A_0 = 10$, $\lambda_0 = 0.001$.

a constant velocity, see figure 5.2(a),(b). When $\frac{\lambda_0}{A_0} < 1$ each soliton in the initial solution starts to split into sub-kinks, see figure 5.1(f), and the sub-kinks become more distinct (the distance between the sub-kinks increases) as $\frac{\lambda_0}{A_0}$ decreases. The trajectory of solitons for $\frac{\lambda_0}{A_0} < 1$ shows that the solitons come together with an initial velocity $\dot{a}(0)$, then the trajectory is constant for a time before the solitons start to repel, see figure 5.2(c)-(e). The constant period in the trajectory starts when the sub-kinks that are closest to the centre of mass of the system (the inner sub-kinks) repel each other and start to travel in the opposite direction, and the sub-kinks which are furthest from the centre of mass (the outer sub-kinks) are still moving in their original direction, *i.e.* the sub-kinks within one soliton move towards each other and the position of the soliton is constant. As the sub-kinks within the soliton come together they also repel each other and both change their direction of travel, so now the inner sub-kinks travel towards the centre of mass and the outer sub-kinks travel away from it. The final interaction happens when the inner sub-kinks repel each other again and the entire soliton starts to move away from the centre of mass with constant velocity. The distance between the sub-kinks within a soliton, d, after the collision returns to the original distance between them on average; and when $0.01 \leqslant \frac{\lambda_0}{A_0} < 1$ the distance between the sub-kinks oscillates slightly after collision. These details are shown in figure 5.3 where we have plotted the trajectories of the double sine-Gordon kink and its sub-kinks, and the distance between the sub-kinks, for various values of A_0 and λ_0. In this plot we have used just used the results calculated by the collective coordinate approximation to keep the plot clear, as the results from the full simulation are essentially identical.

To further explore the double sine-Gordon model we consider the anomalous conserved charges previously discussed, and we calculate the time integrated anomaly for the first non-trivial charge $\tilde{Q}^{(3)}(t)$ defined in (4.1.14), *i.e.*

$$\tilde{\chi}^{(3)} = -\frac{1}{2} \int_{t_0}^{t} dt' \, \tilde{\beta}^{(3)} = 4 \int_{t_0}^{t} dt' \int_{-\infty}^{\infty} dx \, \partial_- \phi \, \partial_-^2 \phi \left[\frac{d^2 V}{d\phi^2} + \omega^2 V - m \right], \quad (5.3.4)$$

where $\partial_- = \partial_t - \partial_x$ and t_0 is the initial time of the simulation (in our simulations $t_0 = 0$).

As discussed in section 5.1, when the model is considered to be a deformation
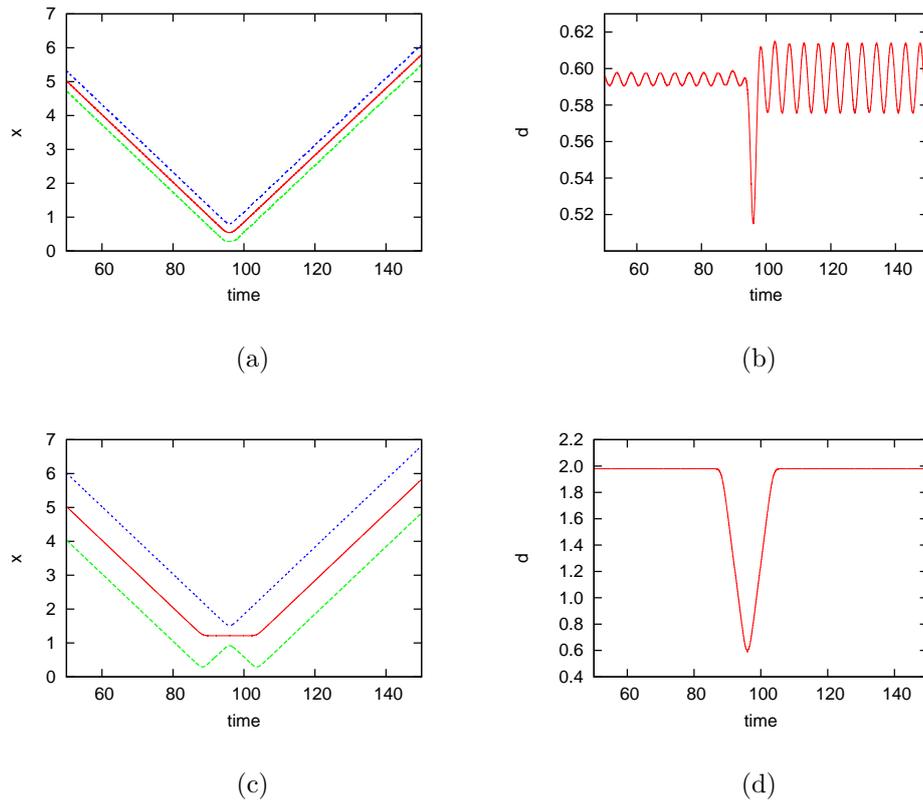
Figure 5.3: On the left the trajectories of the double sine-Gordon kink and its sub-kinks for various values of A_0 and λ_0. The solid line (red) is the kink, the dashed line (green) is the inner sub-kink and the dotted line (blue) is the outer sub-kink. On the right the corresponding distance between the sub-kinks, d. The values are $A_0 = 10$, $\lambda_0 = 1$ for (a) and (b); and $A_0 = 10$, $\lambda_0 = 0.001$ for (c) and (d).

away from the sine-Gordon model with the potential $V = \frac{A_0^2}{2} \sin^2(2\psi)$ (*i.e.* $\lambda_0 = 0$) we choose $\omega = 4$ and $m = 4A_0^2$, so whenever $\frac{\lambda_0}{A_0} < 1$ we use these values of ω and m when calculating the time integrated anomaly $\tilde{\chi}^{(3)}$ (5.3.4). Similarly when the model is considered to be a deformation away from the sine-Gordon model with the potential $V = 2\lambda_0^2 \sin^2(\psi)$ (*i.e.* $A_0 = 0$) we choose $\omega = 2$ and $m = 4\lambda_0^2$, so whenever $\frac{\lambda_0}{A_0} > 1$ we use these values of ω and m in (5.3.4). The question arises, what values of ω and m to use when $\frac{\lambda_0}{A_0} = 1$, and in this case we calculated the time integrated anomaly using both sets of values and found the results to be equivalent.

In figure 5.4 we plot the time integrated anomaly $\tilde{\chi}^{(3)}$, calculated using the full numerical simulation, for various values of A_0 and λ_0. The first thing to notice from this figure is that for all values of A_0 and λ_0 the time integrated anomaly is the same before and after the soliton collisions, *i.e.* the anomalous charge $\tilde{Q}_t^{(3)}$ is asymptotically conserved; this is expected as we have determined the system to be quasi-integrable.

In figure 5.4 we see a peak in the time integrated anomaly whenever there is an interaction between kinks, and the closer the model is to integrability (*i.e.* when $\frac{\lambda_0}{A_0} \gg 1$ or $\frac{\lambda_0}{A_0} \ll 1$) the smaller the peak is and so the closer the charge is to being conserved at all times. For the cases $\frac{\lambda_0}{A_0} \geqslant 1$, where the double sine-Gordon kinks resemble sine-Gordon kinks, there is one peak which occurs when the kinks repel, see figures 5.4(c) and (d). When $\frac{\lambda_0}{A_0} < 1$ the kinks start to split into sub-kinks and we see additional peaks which correspond to the interactions between the sub-kinks, see figures 5.4(a) and (b).

One final observation from figure 5.4 is that the time integrated anomaly oscillates throughout the interaction, this is particularly evident in figure 5.4(c), and this is probably due to the oscillations between the sub-kinks in the double sine-Gordon kink as it propagates.
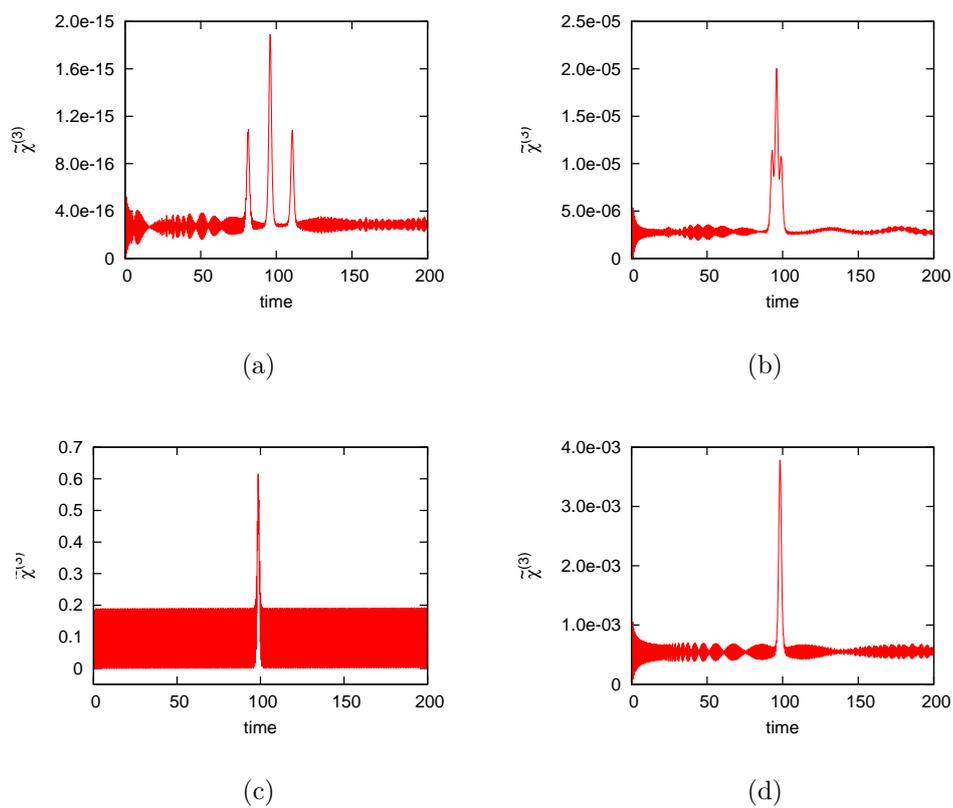
Figure 5.4: The time integrated anomaly $\tilde{\chi}^{(3)}$ for various values of A_0 and λ_0. The values are (a) $A_0 = 10$, $\lambda_0 = 0.000001$; (b) $A_0 = 10$, $\lambda_0 = 0.1$; (c) $A_0 = 10$, $\lambda_0 = 10$; and (d) $A_0 = 1$, $\lambda_0 = 10$.

Conclusions for double sine-Gordon

In this chapter we have used the collective coordinate approximation to model the scattering of double sine-Gordon kinks. We considered a range of values of the parameters A_0 and λ_0, moving between two integrable sine-Gordon models, *i.e.* when $A_0 = 0$ and $\lambda_0 \neq 0$ and when $A_0 \neq 0$ and $\lambda_0 = 0$ (though in order to construct our solution we assumed $\lambda_0 \neq 0$ so we could only get close to the integrable model in that direction by taking λ_0 very small). Whenever the model is not integrable we have shown that the field configuration does possess the symmetries necessary to be deemed quasi-integrable.

When $\frac{\lambda_0}{A_0} \geqslant 1$ our initial field configuration closely resembles two sine-Gordon kinks and the trajectories are very similar to those of two interacting sine-Gordon kinks. When $\frac{\lambda_0}{A_0} < 1$ each double sine-Gordon kink behaves as two sub-kinks, with the sub-kinks becoming more distinct and distant from each other as $\frac{\lambda_0}{A_0}$ gets smaller. In these cases the sub-kinks interact with each other and the trajectories begin to look like four sine-Gordon kinks interacting.

By comparing the soliton trajectories, calculated using the collective coordinate approximation and using a full numerical simulation, we found that the approximation accurately reproduced the scattering of the solitons for all values of A_0 and λ_0 that we considered. We also found that, as expected in a quasi-integrable system, the first non-trivial anomalous charge $\tilde{Q}^{(3)}(t)$ is asymptotically conserved for all values of A_0 and λ_0. The accuracy of the approximation in this system is therefore not a surprise, as in chapter 4 we observed that the approximation is accurate in a modified sine-Gordon model whenever that model has asymptotically conserved charges.

Chapter 6

Conclusions

We have investigated the collision of two solitons in several different nonlinear models in $(1 + 1)$ dimensions using the collective coordinate approximation. We did this initially in the integrable NLS equation where we were able to calculate the equations of motion analytically, we then evolved the system numerically using the fourth-order Runge-Kutta method. It is well known that the scattering of NLS solitons is highly dependent on the phase difference between the solitons δ, varying from greatest attraction between the solitons for $\delta = n\pi$ for odd integer n and greatest repulsion for $\delta = n\pi$ for even integer n. We compared the trajectories of the solitons found using the approximation to results gained using a full numerical simulation for a range of initial phase differences and found that the approximation works well for most values except in the most attractive cases where the phase difference between them is small. In these cases the trajectories in the full simulation show that the solitons start in an attractive channel but over time they begin to repel each other, whereas the trajectories calculated using the collective coordinate approximation show that if the solitons start in an attractive channel they continue to attract each other. This suggested that the differences may have been a result of our choice of ansatz for the collective coordinate approximation, as the ansatz we used did not allow for the phase difference to vary in time.

We then progressed to considering a modification of the NLS model with a

deformation parameter ϵ that allows us to determine the effect of changing the integrability of the model on the scattering solitons, and on the applicability of the collective coordinate approximation. We used a new approximation ansatz based on the one we used in the integrable NLS, with the new ansatz allowing the solitons to be less symmetric and also allowing the phase difference between them to vary in time. In the NLS case (*i.e.* $\epsilon = 0$) with the new ansatz the results for the trajectories of the solitons were greatly improved, with the trajectories so similar that they were frequently indistinguishable. We also compared other variables, such as the heights and phase differences of the solitons, for a greater range of initial values and saw excellent agreement between the results for the collective coordinate approximation and for the full simulation in the majority of cases. There was still some slight disagreement in the cases where the solitons come into close proximity, and we suspect that this is because the solitons deform each other away from the form assumed in the approximation ansatz as they come together, and this is not accounted for in the approximation.

In the modified NLS the two methods continued to show good agreement when the model moves away from integrability, *i.e.* for $\epsilon \neq 0$, when the solitons stay far enough apart during their interaction. Increasing ϵ decreases the accuracy of the approximation slightly, with good agreement up to at least $\epsilon = 0.3$. When the solitons come closer together than the width of one soliton the accuracy is reduced; the solitons are well modelled as they come together initially but after that the trajectories differ. In addition to the deformation the solitons experience when they are close, the solitons are also able to radiate out some energy as they come together in the non-integrable case (*i.e.* when $\epsilon \neq 0$). This is not allowed in the collective coordinate approximation which may explain why increasing ϵ reduced the accuracy of the approximation when the solitons come close together.

It is difficult to fully determine whether the collective coordinate approximation is more accurate for the fields which satisfy conditions for quasi-integrability compared to those which are completely non-integrable. This is because the quasi-integrable cases correspond to the values of the phase difference for which the solitons are most and least attractive (*i.e.* $\delta = n\pi$ for n integer) and the effect

of the soliton proximity eclipses any effect of quasi-integrability on the accuracy of the approximation.

The NLS model is integrable and therefore has an infinite number of conserved charges. The modified NLS has similar quantities - anomalous charges - which are not conserved in time, but when the fields possess additional symmetries necessary for quasi-integrability these quantities are asymptotically conserved. This gave us an additional check on our approximation by allowing us to calculate and compare the time-integrated anomaly, and we found that the approximation shows good agreement with the full simulation for the time-integrated anomaly.

Next we considered a modified sine-Gordon model to see if these effects hold in a model with topological solitons. This model has two deformation parameters γ and ϵ; when they are both zero the model is integrable, when $\epsilon \neq 0$ and $\gamma = 0$ the model maintains the symmetries necessary for quasi-integrability, and when both parameters are both not equal to zero the model is completely non-integrable. We compared the trajectories and time-integrated anomalies for a variety of initial conditions and found that there was excellent agreement between the two methods when the system was either integrable or quasi-integrable, but the accuracy was much reduced when the system was completely non-integrable.

To further explore this we then considered kink-kink collisions in a double sine-Gordon model with parameters A_0 and λ_0 which allowed us to smoothly vary between two integrable sine-Gordon models. When the double sine-Gordon model is not in the limit of an integrable sine-Gordon model (*i.e.* A_0 and λ_0 are both non zero) the field configuration possesses the necessary symmetries for the model to be considered quasi-integrable. When $\frac{\lambda_0}{A_0} > 1$ the double sine-Gordon kinks are similar to sine-Gordon kinks and the trajectories are similar to kink-kink collisions in the sine-Gordon model; but when $\frac{\lambda_0}{A_0} < 1$ the double sine-Gordon kink starts to separate into two sub-kinks and in these cases the interactions between the sub-kinks resulted in the double sine-Gordon kinks being stationary for a time before repelling. For all the values of A_0 and λ_0 that we considered, we found that the collective coordinate approximation accurately reproduces the trajectories of the double sine-Gordon kinks. We also found that, as expected,

for all values of A_0 and λ_0 the anomalous charges were asymptotically conserved.

Overall, these observations suggest that the collective coordinate approximation with a well chosen ansatz is a very useful tool to study various properties of the scatterings of solitons, topological or not, and so can be used also to investigate quasi-integrability in other perturbations of integrable models. In modified sine-Gordon models the presence of the symmetries necessary for quasi-integrability seem to be a sufficient condition to ensure accuracy, but in any model care should be taken if the solitons have the opportunity to strongly deform each other. We hope that these observations allow the collective coordinate approximation to be used with confidence in future investigations into soliton collisions in suitable modified models.

A natural extension to this work would be to use the collective coordinate approximation to investigate soliton collisions in modified models in (1+1) dimensions. A potentially interesting project would be to use the collective coordinate approximation to consider kink-antikink collisions in the double sine-Gordon, if a suitable approximation ansatz could be constructed. This would be a valuable area to explore because the double sine-Gordon system is often used to describe nonlinear phenomena in real physical systems [54] - [57], and because there is a wide range of possible soliton interactions in this system.

A more challenging open question is to define the concept of quasi-integrability in higher dimensions. The collective coordinate approximation has often been successfully used to investigate the dynamics of solitons in higher dimensional systems (for example [23], [58], [59]), so the collective coordinate approximation could be a useful tool in considering the integrability properties of systems in higher dimensions. However, in higher dimensions integrability is not as precisely defined as in 1 dimension as one cannot simply find the Lax pair of an equation (see [60], [61] for a discussion on integrability), and it would be difficult to construct quasi-conserved quantities for models in higher dimensions, but perhaps a definition could be constructed based on symmetries of the system. Despite these difficulties it would be a worthwhile area of study, as it would result in a better understanding of physical systems which, while not well described by

integrable models, still exhibit characteristics similar to integrable systems such as soliton like solutions which undergo nearly elastic collisions.

Bibliography

[1] N. S. Manton and P. M. Sutcliffe, *Topological Solitons*, CUP (2004).

[2] H. E. Baron, G. Luchini and W. J. Zakrzewski, *J. Phys. A* **47**, 265201 (2014).

[3] H. E. Baron and W. J. Zakrzewski, arXiv:1411.3620.

[4] A. Hasegawa and F. Tappert, *Appl. Phys. Lett.* **23**, 142 (1973).

[5] S. Caspi and E. Ben-Jacob, *Europhys.* **47**, 522 (1999).

[6] J. L. Hammack, *J. Fluid Mech.* **60**, 769 (1973).

[7] P. D. Lax, *Commun. Pure Appl. Math.* **21**, 467 (1968).

[8] V.E. Zakharov and A. B. Shabat, *Zh. Eksp. Teor. Fiz.* **61**, 118 (1971).

[9] C. S. Gardner, J. M. Greene, M. D. Kruskal and R. M. Miura, *Phys. Rev. Lett.* **19**, 1905 (1967).

[10] O. Babelon, D. Barnard and M. Talon, *Introduction to Classical Integrable Systems*, Cambridge University Press (2003).

[11] D. Olive and N. Turok, *Nucl. Phys. B* **257**, 277 (1985).

[12] V. G. Drinfeld and V. V. Sokolov, *J. Sov. Math.* **30**, 1975 (1985).

[13] L. A. Ferreira and W. J. Zakrzewski, *Rep. Math. Phys.* **67**, 197 (2011).

[14] L. A. Ferreira and W. J. Zakrzewski, *JHEP* **1105**, 130 (2011).

[15] L. A. Ferreira and W. J. Zakrzewski, *JHEP* **0709**, 015 (2007).

[16] L. A. Ferreira, G. Luchini and W. J. Zakrzewski, *JHEP* **1209**, 103 (2012).

[17] L. A. Ferreira and W. J. Zakrzewski, *JHEP* **058**, 01 (2014).

[18] A. A. Thiele, *Phys. Rev. Lett.* **30**, 230 (1973).

[19] O. A. Tretiakov, D. Clarke, Gia-Wei Chern, Ya. B. Bazaliy, and O. Tchernyshyov, *Phys. Rev. Lett.* **100**, 127204 (2008).

[20] N. R. Quintero, F. G. Mertens and A. R. Bishop, *Phys. Rev. E* **82**, 016606 (2010).

[21] N.S. Manton, *Nucl. Phys.* **B150**, 397 (1979).

[22] J. H. P. Dawes and H. Susanto, *Phys. Rev. E* **87**, 063202 (2013).

[23] N. S. Manton, *Phys. Lett. B* **110**, 54 (1982).

[24] P.M. Sutcliffe, *Nucl. Phys.* **393**, 211 (1993).

[25] A. Sánchez and A. R. Bishop, *SIAM Rev.* **40**, 579 (1998).

[26] F. Zou and J. Yan, *Chin. Phys. Lett.* **11**, 265 (1994).

[27] E. Tadmor, *Bull. Amer. Math. Soc. (N.S.)* **49**, 507 (2012).

[28] Y. F. Tang, L. Vázquesz, F. Zhang and V. M. Pérez-García, *Comput. Math. Appl.* **32**, 73 (1996).

[29] R. M. Caplan and R. Carretero-González, *Appl. Numer. Math.* **71**, 24 (2013)

[30] V. E. Zakharov and E. A. Kuznetsov, *Sov. Phys. JETP* **39**, 285 (1974).

[31] S. Yomosa, *J. Phys. Soc. Jpn.* **35**, 1738 (1973).

[32] P. A. Ruprecht, M. J. Holland, K. Burnett and M. Edwards, *Phys. Rev. A* **51**, 4704 (1995).

[33] A. Hasegawa, J. Sel, *Topics Quantum Electron.* **6**, 1161 (2000).

[34] M. Kunze et al, *Physica D* **128**, 273 (1999).

[35] T. Aktosun, F. Demontis and C. van der Mee, *Inverse Problems* **23**, 2171 (2007).

[36] Y. Kodama and K. Nozaki, *Optics Letters* **12**, 1038 (1987).

[37] J. E. Rothenberg, *Optics Letters* **17**, 1340 (1992).

[38] J. P. Gordon, *Optics Letters* **8**, 596 (1983).

[39] F. M. Mitschke and L. F. Mollenauer, *Optics Letters* **12**, 355 (1987).

[40] V.I. Karpman and V.V. Solov'ev, *Physica* **D 3**, 487 (1981).

[41] D. Anderson and M. Lisak, *Physica Scripta* **33**, 193 (1986).

[42] D.A. Malomed *Progress in Optics* **43**, 71 (2002).

[43] D. M. A. Stuart, *Proc. R. Soc. A* **463**, 2753 (2007).

[44] W. L. Kath, *Phys. Rev. E* **51**, 1484 (1995)..

[45] R. H. Goodman, P. J. Holmes and M. I. Weinstein *Physica D* **192**, 215 (2004).

[46] C. Adam, L. Ferreira, E. da Hora, A. Weresznzynski and W. Zakrzewski, *JHEP* **08**, 062 (2013).

[47] D. Bazeia, L. Losano, J. Malbouisson and R. Menezes, *Physica D* **237**, 937 (2008).

[48] D. K. Campbell, M. Peyrard, and P. Sodano, *Physica D* **19**, 165 (1986).

[49] V. A. Gani and A. E. Kudryavtsev, *Phys. Rev. E* **60**, 3305 (1999).

[50] S. P. Popov, *Comput. Maths. Maths. Phys.* **54**, 1876 (2014).

[51] J. Shiefman and P. Kumar, *Phys. Scr.* **20**, 435 (1979).

[52] R. Ravelo, M. El-Batanouny, C. R. Willis, and P. Sodano, *Phys. Rev. B* **38**, 4817 (1988).

[53] S. Nazifkar and K. Javidan, *Braz. J. Phys.* **40**, 102 (2010).

[54] R. K. Bullough, P. J. Caudrey and H. M. Gibbs, *Double sine-Gordon model, in: Solitons, in: Topics in Current Physics, vol. 17*, Springer Berlin (1980).

[55] M. Fabrizio, A. O. Gogolin and A. A. Nersesyan, *Nucl. Phys. B* **580**, 647 (2000)

[56] K. M. Leung, *Phys. Rev. B* **27**, 2877 (1983).

[57] O. M. Fedotova, O. K. Khasanov, G. A. Rusetsky, J. Degert and E. Freysz, *Phys. Rev. A* **90**, 053843 (2014).

[58] R. S. Ward, *Phys. Lett. B* **158**, 424 (1985).

[59] M. Peyrard, B. Piette and W. J. Zakrzewski, *Nonlinearity* **5**, 585 (1992).

[60] V. E. Zakharov (Ed.), *What is Integrability?*, Springer-Verlag (1991).

[61] B. A. Kupershmidt (Ed.), *Integrable and Superintegrable Systems*, World Scientific (1990).

Appendix A

A.1 Explicit expressions used in gauge transformation (2.2.14)

A.1.1 For NLS

The parameters $\zeta_i^{(-n)}, i = 1, 2$ used in the gauge transformation (2.2.14):

$$\zeta_1^{(-1)} = 0,$$

$$\zeta_2^{(-1)} = 2\sqrt{|\eta|}\sqrt{R},$$

$$\zeta_1^{(-2)} = \frac{i\sqrt{|\eta|}\,\partial_x R}{\sqrt{R}},$$

$$\zeta_2^{(-2)} = \sqrt{|\eta|}\,\partial_x\varphi\,\sqrt{R},$$

$$\zeta_1^{(-3)} = \frac{i\left(\sqrt{|\eta|}\,\partial_x\varphi\,\partial_x R + \sqrt{|\eta|}\,\partial_x^2\varphi\,R\right)}{\sqrt{R}},$$

$$\zeta_2^{(-3)} = \frac{16\,\sigma\,|\eta|^{3/2}\,R^3 + 3\sqrt{|\eta|}\,(\partial_x\varphi)^2\,R^2 - 6\sqrt{|\eta|}\,\partial_x^2 R\,R + 3\sqrt{|\eta|}\,(\partial_x R)^2}{6\,R^{3/2}},$$

$$\vdots$$

The components $a_x^{(3,-n)}$ as calculated in [16], (in terms of the fields R and φ

as defined in (2.2.7)) are:

$$a_x^{(3,0)} = \frac{i}{2}\partial_x\varphi,$$

$$a_x^{(3,-1)} = 2\,i\,\eta\,R,$$

$$a_x^{(3,-2)} = i\,\eta\,\partial_x\varphi\,R,$$

$$a_x^{(3,-3)} = \frac{i}{2R}\left(4\,\eta^2\,R^3 + \eta\,(\partial_x\varphi)^2\,R^2 - 2\,\eta\,\partial_x^2R\,R + \eta\,(\partial_xR)^2\right),$$

$$a_x^{(3,-4)} = \frac{i}{4R}\left(12\,\eta^2\,\partial_x\varphi\,R^3 - 6\,\eta\,R\left(\partial_x^2\varphi\,\partial_xR + \partial_x\varphi\,\partial_x^2R\right) + 3\,\eta\,\partial_x\varphi\,(\partial_xR)^2\right.$$
$$\left. + \eta\left((\partial_x\varphi)^3 - 4\,\partial_x^3\varphi\right)\,R^2\right).$$

The components $a_t^{(3,-n)}$ (in terms of the fields R and φ as defined in (2.2.7)) are:

$$a_t^{(3,0)} = \frac{i}{2}\,\partial_t\varphi,$$

$$a_t^{(3,-1)} = -2\,i\,\eta\,R\,\partial_x\varphi,$$

$$a_t^{(3,-2)} = -i\,\eta\left(2\eta\,R^2 + (\partial_x\varphi)^2\,R - \partial_x^2R + \frac{(\partial_xR)^2}{R}\right),$$

$$a_t^{(3,-3)} = -\frac{i\,\eta}{2}\left(12\,\eta\,\partial_x\varphi\,R^2 - 2\,\partial_x^2\varphi\,\partial_xR - 4\,\partial_x\varphi\,\partial_x^2R + 3\,\partial_x\varphi\frac{(\partial_xR)^2}{R}\right.$$
$$\left. + (\partial_x\varphi)^3\,R - 2\,\partial_x^3\varphi\,R\right).$$

The components $\alpha^{(3,-n)}$ introduced in (3.1.4) (in terms of the fields R and φ as defined in (2.2.7)) are:

$$\alpha^{(3,0)} = 1,$$

$$\alpha^{(3,-1)} = 0,$$

$$\alpha^{(3,-2)} = 2\,\eta\,R,$$

$$\alpha^{(3,-3)} = 2\,\eta\,\partial_x\varphi\,R,$$

$$\alpha^{(3,-4)} = 6\,\eta^2\,R^2 + \frac{3}{2}\eta\,(\partial_x\varphi)^2\,R - 2\,\eta\,\partial_x^2R + \frac{3\,\eta\,(\partial_xR)^2}{2\,R}.$$

A.1.2 For sine-Gordon

The components $\tilde{\alpha}^{(2n+1)}$ introduced in (4.1.11) (using the light cone coordinates described in (4.1.8)) are:

$$\tilde{\alpha}^{(1)} = 0,$$
$$\tilde{\alpha}^{(3)} = i\,\omega\,\partial_-^2\phi,$$
$$\tilde{\alpha}^{(5)} = i\,\omega\,\left(\frac{3\omega^2}{2}(\partial_-\phi)^2\,\partial_-^2\phi + \partial_-^4\phi\right).$$

A.2 Calculation of integrals for the effective Lagrangian in the NLS model

A.2.1 Contour for calculation of integrals
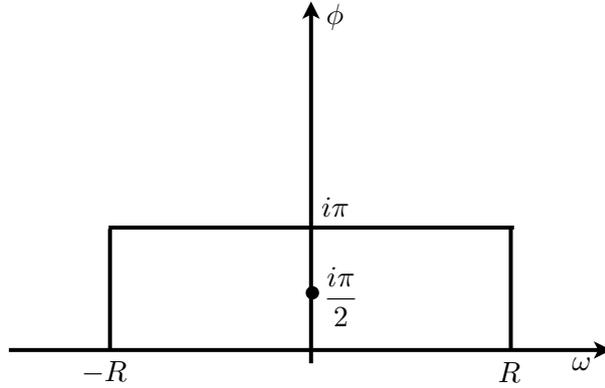
Figure A.1: Appropriate contour (called C) for all the integrals: only one of the infinitely many poles is picked.

Here we present a few details which show the way we have performed the calculations of the integrals in section 2.3.1.

A.2.2 $I = \int_{-\infty}^{+\infty} \frac{dx}{\cosh^2(b(x+\xi(t)))\cosh^2(b(x-\xi(t)))}$

Defining $\omega = b(x + \xi(t))$ we can write:

$$I = \int_{-\infty}^{+\infty} \frac{dx}{\cosh^2(b(x + \xi(t)))\cosh^2(b(x - \xi(t)))} = \frac{1}{b}\int_{-\infty}^{+\infty} \frac{d\omega}{\cosh^2(\omega)\cosh^2(\omega - 2b\xi)}.$$

Consider the following complex integral along the closed contour C (see figure A.1) in the plane $z = \omega + i\phi$

$$\oint_C f(z)dz = \oint_C \frac{z}{\cosh^2(z)\cosh^2(z - 2b\xi)}dz.$$

We have chosen our contour such that the integrand is analytic except for two second-order poles $z_1 = i\pi/2$, $z_2 = i\pi/2 + 2b\xi$, and in the limit $R \to \infty$ the integrals along the vertical paths $z = \pm R + i\phi$, $\phi \in [0, i\pi]$ vanish. From the residue theorem we have

$$\oint_C f(z)dz = -i\pi bI = 2\pi i \sum_{k=1,2} Res f(z_k),$$

where the residues can be calculated as usual:

$$Res f(z_1) = \lim_{z \to z_1} \frac{d}{dz}(z - z_1)^2 f(z) = \frac{i\pi \cosh(2b\xi)}{\sinh^3(2b\xi)} + \frac{1}{\sinh^2(2b\xi)}$$

$$\begin{aligned} Res f(z_2) &= \lim_{z \to z_2} \frac{d}{dz}(z - z_2)^2 f(z) \\ &= -\frac{(i\pi + 4b\xi)\cosh(2b\xi)}{\sinh^3(2b\xi)} + \frac{1}{\sinh^2(2b\xi)}. \end{aligned}$$

Combining these we have:

$$I = \frac{8\xi \cosh(2b\xi)}{\sinh^3(2b\xi)} - \frac{4}{b \sinh^2(2b\xi)}.$$

A.2.3 $I = \int_{-\infty}^{+\infty} \frac{\cos(2\mu x + \delta)}{\cosh(b(x+\xi))\cosh(b(x-\xi))}dx$

Rewriting this with the definition $\omega = b(x + \xi)$ we have:

$$I = \frac{1}{b} \int_{-\infty}^{+\infty} \frac{\cos(\frac{2\mu\omega}{b})\cos(\delta - 2\mu\xi) - \sin(\frac{2\mu\omega}{b})\sin(\delta - 2\mu\xi)}{\cosh(\omega)\cosh(\omega - 2b\xi)}d\omega,$$

which can be expressed as

$$\begin{aligned} I = &\frac{\cos(\delta - 2\mu\xi)}{b} Re\left[\int_{-\infty}^{+\infty} \frac{e^{i\frac{2\mu\omega}{b}}}{\cosh(\omega)\cosh(\omega - 2b\xi)}d\omega\right] \\ &- \frac{\sin(\delta - 2\mu\xi)}{b} Im\left[\int_{-\infty}^{+\infty} \frac{e^{i\frac{2\mu\omega}{b}}}{\cosh(\omega)\cosh(\omega - 2b\xi)}d\omega\right]. \end{aligned}$$

We consider the following complex function integrated around C:

$$\oint_C f(z)dz = \oint_C \frac{e^{i\frac{2\mu z}{b}}}{b\cosh(z)\cosh(z - 2b\xi)}dz.$$

Using the residue theorem we have:

$$\oint_C f(z)dz = (1 - e^{-\frac{2\mu\pi}{b}}) \int_{-\infty}^{+\infty} \frac{e^{i\frac{2\mu\omega}{b}}}{b\cosh(\omega)\cosh(\omega - 2b\xi)}d\omega = 2\pi i \sum_{k=1,2} Res f(z_k),$$

and we can calculate the residues as before to find:

$$I = \frac{2\pi\cos(\delta)\sin(2\mu\xi)}{b\sinh(\frac{\pi\mu}{b})\sinh(2b\xi)}.$$

A.3 Details for the collective coordinate approximation in the NLS

Here we present the explicit expressions for $F_{1,2}, G_{1,2}$ and $H_{1,2}$ introduced in equation 2.3.12.

$$F_1(\mu, \xi) = 0,$$

$$G_1(\mu, \xi) = \frac{\pi\cos(\delta)}{(1+\omega)\sinh(2b\xi)\sinh(\frac{\pi\mu}{b})}\left(4\mu\xi\cos(2\mu\xi)\right.$$
$$\left. - \frac{2b\xi\sin(2\mu\xi)\cosh(2b\xi)}{\sinh(2b\xi)} - \frac{\pi\mu\sin(2\mu\xi)\cosh(\frac{\pi\mu}{b})}{b\sinh(\frac{\pi\mu}{b})}\right) + w - 1,$$

$$H_1(\mu, \xi) = \frac{\pi\cos(\delta)}{\sinh(2b\xi)\sinh(\frac{\pi\mu}{b})}\left(2\xi\cos(2\mu\xi) - \frac{\pi\sin(2\mu\xi)\cosh(\frac{\pi\mu}{b})}{b\sinh(\frac{\pi\mu}{b})}\right)\left(\alpha\right.$$
$$\left. + \frac{\mu^2(\omega - 3)}{(1+\omega)} + \frac{2b^2(1-\omega)}{(1+\omega)\sinh^2(2b\xi)}\right) - \frac{8\mu\omega}{(1+\omega)} + 2\mu(1+\omega)$$
$$+ \frac{2\pi b(\omega - 1)\cos(\delta)\cosh(2b\xi)}{(1+\omega)\sinh^2(2b\xi)\sinh(\frac{\pi\mu}{b})}\left(-\mu\left(2\xi\sin(2\mu\xi) + \frac{\pi\cos(2\mu\xi)\cosh(\frac{\pi\mu}{b})}{b\sinh(\frac{\pi\mu}{b})}\right)\right.$$
$$\left. + \cos(2\mu\xi)\right) + \frac{4\pi b\cos(2\delta)}{(1+\omega)\sinh^2(2b\xi)\sinh(\frac{2\pi\mu}{b})}\left(\cos(4\mu\xi)\right.$$
$$+ \frac{\cosh(2b\xi)}{\sinh(2b\xi)}\left(\frac{\pi\sin(4\mu\xi)\cosh(\frac{2\pi\mu}{b})}{\sinh(\frac{2\pi\mu}{b})} - 2b\xi\cos(4\mu\xi)\right)$$
$$\left.\left. - 2\mu\left(2\xi\sin(4\mu\xi) + \frac{\pi\cos(4\mu\xi)\cosh(\frac{2\pi\mu}{b})}{b\sinh(\frac{2\pi\mu}{b})}\right)\right)\right),$$

$$F_2(\mu, \xi) = \frac{\pi\cos(\delta)}{(1+\omega)\sinh(2b\xi)\sinh(\frac{\pi\mu}{b})}\left(-4\mu\xi\cos(2\mu\xi)\right.$$
$$\left. + \frac{2b\xi\sin(2\mu\xi)\cosh(2b\xi)}{\sinh(2b\xi)} + \frac{\pi\mu\sin(2\mu\xi)\cosh(\frac{\pi\mu}{b})}{b\sinh(\frac{\pi\mu}{b})}\right) - w + 1,$$

$$G_2(\mu, \xi) = 0,$$

$$H_2(\mu,\xi) = \frac{2\pi\cos(\delta)}{\sinh(\frac{\pi\mu}{b})\sinh(2b\xi)}\left(\mu\cos(2\mu\xi) - \frac{b\sin(2\mu\xi)\cosh(2b\xi)}{\sinh(2b\xi)}\right)\left(\alpha\right.$$

$$+ \frac{\mu^2(\omega-3)}{(1+\omega)}\right) + \frac{4\pi b\cos(\delta)(1-\omega)}{\sinh(\frac{\pi\mu}{b})\sinh(2b\xi)(1+\omega)}\left(\frac{b}{\sinh^2(2b\xi)}\left(\mu\cos(2\mu\xi)\right.\right.$$

$$- \frac{3b\sin(2\mu\xi)\cosh(2b\xi)}{\sinh(2b\xi)}\right) - \mu\left(b\cos(2\mu\xi) - \frac{\mu\sin(2\mu\xi)\cosh(2b\xi)}{\sinh(2b\xi)}\right.$$

$$- \frac{2b\cos(2\mu\xi)\cosh^2(2b\xi)}{\sinh^2(2b\xi)}\right)\right) - \frac{8b^3}{(1+\omega)\sinh^2(2b\xi)}\left(\frac{3\cosh(2b\xi)}{\sinh(2b\xi)}\right.$$

$$+ 2\xi b\left(1 - \frac{3\cosh^2(2b\xi)}{\sinh^2(2b\xi)}\right)\right) + \frac{4\pi b\cos(2\delta)}{(1+\omega)\sinh(\frac{2\pi\mu}{b})\sinh^2(2b\xi)}\left(-b^2\sin(4\mu\xi)\right.$$

$$- \frac{2\mu b\cos(4\mu\xi)\cosh(2b\xi)}{\sinh(2b\xi)} + \frac{3b\sin(4\mu\xi)\cosh(2b\xi)}{\sinh^2(2b\xi)}$$

$$- 4\mu\left(\mu\sin(4\mu\xi) + \frac{b\cos(4\mu\xi)\cosh(2b\xi)}{\sinh(2b\xi)}\right)\right).$$

For convenience we have defined

$$\omega = \frac{\pi\sin(2\mu\xi)\cos(\delta)}{\sinh(\frac{\pi\mu}{b})\sinh(2b\xi)},$$

$$\alpha = \frac{b}{(1+\omega)}\left(-\frac{\mu^2(1+\omega)}{b} - \frac{4b\omega}{3(1+\omega)} + \frac{8\omega\mu^2}{b(1+\omega)}\right.$$

$$+ \frac{2\pi(\omega-3)\cos(\delta)}{(1+\omega)\sinh(\frac{\pi\mu}{b})\sinh^2(2b\xi)}\left(\frac{b\sin(2\mu\xi)}{\sinh(2b\xi)} - \mu\cosh(2b\xi)\cos(2\mu\xi)\right)$$

$$+ \frac{8b}{(1+\omega)\sinh^2(2b\xi)}\left(\frac{2b\xi\cosh(2b\xi)}{\sinh(2b\xi)} - 1\right)$$

$$+ \frac{4\pi\cos(2\delta)}{(1+\omega)\sinh(\frac{2\pi\mu}{b})\sinh^2(2b\xi)}\left(\frac{b\sin(4\mu\xi)\cosh(2b\xi)}{\sinh(2b\xi)} - 2\mu\cos(4\mu\xi)\right)\right).$$

A.4 Component functions for the effective Lagrangian of the modified NLS

For convenience we have defined $\omega_i = (1 + \epsilon)\, a_i(t)\, (x + \xi_i(t))$ for $i = 1, 2$, and $\theta = \theta_1 - \theta_2$.

$$I_{\xi_1} = \int_{-\infty}^{\infty} dx\, \frac{1}{4} \left(\frac{a_1\sqrt{\epsilon+2}}{\cosh(\omega_1)} \right)^{\frac{1}{\epsilon+1}} \left(4\, a_1 \sin(\theta) \tanh(\omega_1) \left(\frac{a_2\sqrt{\epsilon+2}}{\cosh(\omega_2)} \right)^{\frac{1}{\epsilon+1}} \right.$$
$$\left. + \mu_1 \left(\left(\frac{a_1\sqrt{\epsilon+2}}{\cosh(\omega_1)} \right)^{\frac{1}{\epsilon+1}} + \cos(\theta) \left(\frac{a_2\sqrt{\epsilon+2}}{\cosh(\omega_2)} \right)^{\frac{1}{\epsilon+1}} \right) \right)$$

$$I_{\xi_2} = \int_{-\infty}^{\infty} dx\, \frac{1}{4} \left(\frac{a_2\sqrt{\epsilon+2}}{\cosh(\omega_2)} \right)^{\frac{1}{\epsilon+1}} \left(-4\, a_2 \sin(\theta) \tanh(\omega_2) \left(\frac{a_1\sqrt{\epsilon+2}}{\cosh(\omega_1)} \right)^{\frac{1}{\epsilon+1}} \right.$$
$$\left. + \mu_2 \left(\cos(\theta) \left(\frac{a_1\sqrt{\epsilon+2}}{\cosh(\omega_1)} \right)^{\frac{1}{\epsilon+1}} + \left(\frac{a_2\sqrt{\epsilon+2}}{\cosh(\omega_2)} \right)^{\frac{1}{\epsilon+1}} \right) \right)$$

$$I_{\mu_1} = \int_{-\infty}^{\infty} dx\, \frac{(\xi_1+2x)}{4} \left(\frac{a_1\sqrt{\epsilon+2}}{\cosh(\omega_1)} \right)^{\frac{1}{\epsilon+1}} \left(\left(\frac{a_1\sqrt{\epsilon+2}}{\cosh(\omega_1)} \right)^{\frac{1}{\epsilon+1}} \right.$$
$$\left. + \cos(\theta) \left(\frac{a_2\sqrt{\epsilon+2}}{\cosh(\omega_2)} \right)^{\frac{1}{\epsilon+1}} \right)$$

$$I_{\mu_2} = \int_{-\infty}^{\infty} dx\, \frac{(\xi_2+2x)}{4} \left(\frac{a_2\sqrt{\epsilon+2}}{\cosh(\omega_2)} \right)^{\frac{1}{\epsilon+1}} \left(\cos(\theta) \left(\frac{a_1\sqrt{\epsilon+2}}{\cosh(\omega_1)} \right)^{\frac{1}{\epsilon+1}} \right.$$
$$\left. + \left(\frac{a_2\sqrt{\epsilon+2}}{\cosh(\omega_2)} \right)^{\frac{1}{\epsilon+1}} \right)$$

$$I_{a_1} = \int_{-\infty}^{\infty} dx\, \frac{1}{a_1} \left(\sin(\theta) \left(a_1(\xi_1+x) \tanh(\omega_1) - \frac{1}{\epsilon+1} \right) \left(\frac{a_2\sqrt{\epsilon+2}}{\cosh(\omega_2)} \right)^{\frac{1}{\epsilon+1}} \right.$$
$$\left. - 2a_1^2\, t \left(\left(\frac{a_1\sqrt{\epsilon+2}}{\cosh(\omega_1)} \right)^{\frac{1}{\epsilon+1}} + \cos(\theta) \left(\frac{a_2\sqrt{\epsilon+2}}{\cosh(\omega_2)} \right)^{\frac{1}{\epsilon+1}} \right) \right) \left(\frac{a_1\sqrt{\epsilon+2}}{\cosh(\omega_1)} \right)^{\frac{1}{\epsilon+1}}$$

$$I_{a_2} = \int_{-\infty}^{\infty} dx\, \frac{1}{a_2} \left(+\sin(\theta) \left(-a_2(\xi_2+x) \tanh(\omega_2) + \frac{1}{\epsilon+1} \right) \left(\frac{a_1\sqrt{\epsilon+2}}{\cosh(\omega_1)} \right)^{\frac{1}{\epsilon+1}} \right.$$
$$\left. - 2a_2^2\, t \left(\cos(\theta) \left(\frac{a_1\sqrt{\epsilon+2}}{\cosh(\omega_1)} \right)^{\frac{1}{\epsilon+1}} + \left(\frac{a_2\sqrt{\epsilon+2}}{\cosh(\omega_2)} \right)^{\frac{1}{\epsilon+1}} \right) \right) \left(\frac{a_2\sqrt{\epsilon+2}}{\cosh(\omega_2)} \right)^{\frac{1}{\epsilon+1}}$$

$$I_{\lambda_1} = -\int_{-\infty}^{\infty} dx \left(\frac{a_1\sqrt{\epsilon+2}}{\cosh(\omega_1)}\right)^{\frac{1}{\epsilon+1}} \left(\left(\frac{a_1\sqrt{\epsilon+2}}{\cosh(\omega_1)}\right)^{\frac{1}{\epsilon+1}} + \cos(\theta)\left(\frac{a_2\sqrt{\epsilon+2}}{\cosh(\omega_2)}\right)^{\frac{1}{\epsilon+1}}\right)$$

$$I_{\lambda_2} = -\int_{-\infty}^{\infty} dx \left(\frac{a_2\sqrt{\epsilon+2}}{\cosh(\omega_2)}\right)^{\frac{1}{\epsilon+1}} \left(\cos(\theta)\left(\frac{a_1\sqrt{\epsilon+2}}{\cosh(\omega_1)}\right)^{\frac{1}{\epsilon+1}} + \left(\frac{a_2\sqrt{\epsilon+2}}{\cosh(\omega_2)}\right)^{\frac{1}{\epsilon+1}}\right)$$

$$V = \int_{-\infty}^{\infty} dx \left(a_1^2 \left(\frac{a_1}{\cosh(\omega_1)}\right)^{\frac{2}{\epsilon+1}} \left(1 + \tanh^2(\omega_1)\right) \right.$$

$$+ a_2^2 \left(\frac{a_2}{\cosh(\omega_2)}\right)^{\frac{2}{\epsilon+1}} \left(1 + \tanh^2(\omega_2)\right)$$

$$+ \left(a_1^2 + a_2^2 + 2a_1 a_2 \tanh(\omega_1)\tanh(\omega_2)\right)\cos(\theta)\left(\frac{a_1 a_2}{\cosh(\omega_1)\cosh(\omega_2)}\right)^{\frac{1}{\epsilon+1}}$$

$$-\frac{2}{2+\epsilon}\left(\left(\frac{a_1}{\cosh(\omega_1)}\right)^{\frac{2}{\epsilon+1}} + \left(\frac{a_2}{\cosh(\omega_2)}\right)^{\frac{2}{\epsilon+1}} + 2\cos(\theta)\left(\frac{a_1 a_2}{\cosh(\omega_1)\cosh(\omega_2)}\right)^{\frac{1}{\epsilon+1}}\right)^{2+\epsilon}$$

$$\left. + \frac{1}{4}\left(\mu_1^2\left(\frac{a_1}{\cosh(\omega_1)}\right)^{\frac{2}{\epsilon+1}} + \mu_2^2\left(\frac{a_2}{\cosh(\omega_2)}\right)^{\frac{2}{\epsilon+1}}\right)\right)$$

A.5 Component functions for the effective Lagrangian of the double sine-Gordon

Here we present expressions for $I_{a,A,\lambda}$ introduced in (5.2.2). For convenience we have defined:

$$u_+ = \frac{e^{-2\theta_+}}{2\left(A_0^2 + \lambda_0^2\right)}\left(2A_0^2 e^{2\theta_+} + \lambda_0^2\left(1 + e^{4\theta_+}\right) + \nu W_+\right),$$

$$u_- = \frac{e^{-2\theta_-}}{2\left(A_0^2 + \lambda_0^2\right)}\left(2A_0^2 e^{2\theta_-} + \lambda_0^2\left(1 + e^{4\theta_-}\right) + \mu W_-\right),$$

where

$$W_\pm = \sqrt{-4\left(A_0^2 + \lambda_0^2\right)^2 e^{4\theta_\pm} + \left(2A_0^2 e^{2\theta_\pm} + \lambda_0^2\left(1 + e^{4\theta_\pm}\right)\right)^2},$$

$$\theta_\pm = (\pm x + a)\sqrt{A_0^2 + \lambda_0^2}.$$

Here $\nu = -1$ for $x < a$ and $\nu = 1$ for $x > a$; $\mu = -1$ for $x < -a$ and $\mu = 1$ for $x > -a$.

$$I_a = \frac{\partial_a u_+}{\sqrt{u_+}(1 + u_+)} + \frac{\partial_a u_-}{\sqrt{u_-}(1 + u_-)}$$

$$I_A = \frac{\partial_A u_+}{\sqrt{u_+}(1 + u_+)} + \frac{\partial_A u_-}{\sqrt{u_-}(1 + u_-)}$$

$$I_\lambda = \frac{\partial_\lambda u_+}{\sqrt{u_+}(1 + u_+)} + \frac{\partial_\lambda u_-}{\sqrt{u_-}(1 + u_-)}$$

$$V = \lambda_0^2 \sin^2\left(2\arctan(\sqrt{u_+}) + 2\arctan(\sqrt{u_-})\right)$$
$$+ \frac{A_0^2}{4} \sin^2\left(4\arctan(\sqrt{u_+}) + 4\arctan(\sqrt{u_-})\right)$$
$$+ \left(\frac{\partial_x u_+}{\sqrt{u_+}(1 + u_+)} + \frac{\partial_x u_-}{\sqrt{u_-}(1 + u_-)}\right)^2$$